Nanostructured Catalysts Based on Mesoporous Silica

Dissertation
der Mathematisch-Naturwissenschaftlichen Fakultät
der Eberhard Karls Universität Tübingen
zur Erlangung des Grades eines
Doktors der Naturwissenschaften
(Dr. rer. nat.)

vorgelegt von
Lorenz Bock
aus Freiburg i. Br.

Tübingen
2020

Gedruckt mit Genehmigung der Mathematisch-Naturwissenschaftlichen Fakultät der Eberhard Karls Universität Tübingen.

Tag der mündlichen Qualifikation:	30.07.2020
Dekan:	Prof. Dr. Wolfgang Rosenstiel
1. Berichterstatter:	Prof. Dr. Reiner Anwander
2. Berichterstatter:	Prof. Dr. Hermann A. Mayer

Nanostructured Catalysts Based on Mesoporous Silica

Synthesis and Characterization of Heterogeneous Rare-Earth-Metal Based Catalysts Accessible via Surface-Organometallic Chemistry (SOMC)

Lorenz Bock

Tübingen, 2020

Die Neugier ist die mächtigste Antriebskraft im Universum, weil sie die beiden größten Bremskräfte im Universum überwinden kann: die Vernunft und die Angst.

Walter Moers: Die Stadt der Träumenden Bücher, S. 325

Preface

The following PhD thesis consists of a short overview on the chemistry of rare-earth-metal alkoxides, the synthesis of periodic mesoporous silica nanoparticles, as well as the combination of both using the methods of surface organometallic chemistry and catalytic reactions involving the resulting hybrid materials. Furthermore, it contains a summary of the main results, and original scientific articles. It covers work conducted during the period September 2015 to December 2019 at the Institut für Anorganische Chemie in the Mathematisch-Naturwissenschaftliche Fakultät of the Eberhard Karls Universität Tübingen under the supervision of Prof. Dr. Reiner Anwander.

Parts of this thesis have been presented at national and international conferences as oral or poster presentations.

Acknowledgements

First and foremost I want to thank my supervisor, Prof. **D**r. Reiner Anw**a**nder for welcoming me into hi**s** group and providing me with a challenging and interesting topic, and for offering **s**upport, new ideas and input whenever it was ne**c**essary.

Likewise, I want to t**h**ank Dr. Yucang Liang, wh**o** introduced m**e** to to the subtle art of materials chemistry, its methods and a**n**alytical techniqu**e**s, and was always willing to give **t**ips and hints.

The work und**e**rlying this thesis wou**l**d not h**a**ve been possible as a solitary effort. I wa**n**t to thank everyone involve**d** with analyt**i**cal methods who helped me u**n**ravel many mysteries: **D**r. Klaus Eich**e**le, Dr. Wolfgang Leis and Dr. Mark**u**s Kramer for NMR, Elke Nadler for beautiful SEM images, Wolfgang Bock for Elemen**t**al Analyse**s**, Dr. Jo**c**hen Glaser for ICP-OES measurements, Dr. Doroth**e**e Wistuba for GC-MS and Dr. Cäci**l**ia M**a**ichle-Mössmer for crystal structure determi**n**ation.

I also want to thank all current and former coworkers in the Anwan**d**er Group, Denni**s**, Holli, Markus, Lars, Jakob, Eric, Theresa, Andrea, **G**ogo, Simon, T**a**ssilo, Felix, Dominic, Damir, Benni, Renita, Leilei, Jochen, Martin, Doro, Tatiana, b**u**t especially Dr. Da**n**, **D**r. Schneider, Dr. Veren**a** and Uwe, who have also become good friend**s** outs**i**de of the lab. Without all of you, thi**s** would have been a whole lo**t** less fun!

Speaking of fun, I cannot ignore my fellow B. Sc. lab rats, who shared the "a**d**venture" of being the first to enjoy **a** new curriculum in Tübingen: Alex, Rhea, Kim, Anna, Lea, Andi, Flo, **S**tuhl, Vollmer, Amiera, Maike, Oly, Oli, Hahn, Tor**b**en, Philipp **a**n**d** everyone else, tha**n**k you for making this such a fun tim**e**!

The Anwande**r** group is very **l**ucky to h**a**ve great techical a**nd** administrative staff to support them. I want to thank Elke Niquet, Jemima Birk, Sabine Ehrlich and Tobias Wolf for keeping everything running and keeping it all from descent into chaos. Special thanks to Tobi, who spent many hours with me tending to the very delicate beast that is the N_2-Physisorption machine, among others.

I also want to thank all my lab course students, especially Xuan Tran, who put an impressive amount of dedication and diligence into the optimization of the synthesis of MCM-41-type nanoparticles during her bachelor thesis work. The beautiful SEM images contained in this thesis are in no small part a result of her work.

I would never have gotten the idea of choosing materials chemistry as the topic for my PhD work on my own, so thanks to the supervisors of my master thesis, Prof. Lars Nordstierna, Dr. Alex Idström and Dr. Jonatan Bergek, for kindling my interest in this field and making my master thesis work thoroughly enjoyable.

It is impossible to express my gratitude towards Simone, who has been my closest friend since school, and her husband Christoph, for listening, talking, sharing lots of good times (and some less good), and always welcoming me to their home.

Likewise, I'm incredibly grateful for being part of the Gullideckel, who have always kept me from becoming too much of a Schwobeseckel!

To everyone who proofread parts or the whole of this thesis, especially Angie and Alex, who had to read the whole thing, thank you for every comment, nitpick and every eliminated mistake! Any remaining error is left in to test the reader's attentiveness.

I am immensely grateful to my family, especially my parents, who have not only enabled me to study, but have supported all of my plans and ideas throughout my whole life.

Contents

A. Introduction 1
- Cerium(IV) Silylamide Chemistry . . . 3
- Rare-Earth-Metal Alkoxides . . . 5
  - Trivalent Alkoxides . . . 5
  - Tetravalent Alkoxides of Cerium . . . 6
- Surface Organometallic Chemistry . . . 7
  - Support materials . . . 8
  - Periodic Mesoporous Silica . . . 9
  - Immobilization Strategies . . . 11
  - Surface Binding Modes / Podality . . . 12
- The Meerwein-Ponndorf-Verley-Oppenauer Reaction . . . 13
  - The Meerwein-Ponndorf-Verley Reduction . . . 13
  - The Oppenauer Oxidation . . . 13

B. Summary of the Main Results 17
- Organometallic Chemistry . . . 19
  - Cerium Silylamide Chemistry . . . 19
  - Ce(IV) Alkoxide Chemistry . . . 22
- Mesoporous Silica Nanoparticles . . . 27
- Surface Organometallic Chemistry . . . 28
- Homogeneous and Heterogeneous Catalysis . . . 35

C. Unpublished Results 39
- Oppenauer Oxidation . . . 41
  - Experimental Details . . . 45

D. Bibliography 49

Bibliography 51

E. Publications 61

List of Abbreviations

12-crown-4	1,4,7,10-Tetraoxacylododecane
BET	Brunauer-Emmett-Teller
BJH	Barrett-Joyner-Halenda
CMC	Critical Micelle Concentration
CP	Cross Polarization
DFT	Density Functional Theory
DME	Dimethoxyethane
do	Donor
DOSY	Diffusion Ordered Spectroscopy
DRIFTS	Diffuse Reflectance Infrared Fourier Transform Spectroscopy
equiv.	Equivalents
GC	Gas Chromatography
HPDEC	High Power Decoupling
ICP-OES	Inductively Coupled Plasma – Optical Emission Spectroscopy
*i*Pr	Isopropyl ($CH(CH_3)_2$)
Ln	Rare-Earth Metal (Sc, Y, La-Lu)
MAS	Magic Angle Spinning
MCM	Mobil Composition of Matter
MEK	Methyl-Ethyl Ketone (2-butanone)
MPV	Meerwein-Ponndorf-Verley
MPVO	Meerwein-Ponndorf-Verley-Oppenauer
MSN	Mesoporous Silica Nanoparticles
NMR	Nuclear Magnetic Resonance
PMS	Periodic Mesoporous Silica
PXRD	Powder X-ray Diffraction
SBA	Santa Barbara Amorphous
SEM	Scanning Electron Microscopy
SOMC	Surface Organometallic Chemistry
*t*Bu	*tert*-Butyl ($C(CH_3)_3$)
THF	Tetrahydrofuran
TMEDA	Tetramethylethylenediamine

Summary

The classical Meerwein-Ponndorf-Verley-Oppenauer redox system describes the conversion of a ketone or aldehyde into an alcohol (Meerwein-Ponndorf-Verley reduction) or vice versa (Oppenauer Oxidation) catalyzed by $Al(O\mathit{i}Pr)_3$. In practical application, both reactions suffer from the relative inactivity of the catalyst, necessitating the use of large (stoichiometric instead of catalytic) amounts of catalyst. It has been shown in several earlier works, that rare-earth-metal alkoxide-based catalysts as well as careful control of the reaction conditions with respect to O_2 and H_2O are ways to greatly increase catalytic efficiency.

In order to further this research, and furthermore to investigate the effects of immobilized (heterogenized) rare-earth-metal alkoxide-based catalysts, surface organometallic chemistry was employed to graft several rare-earth-metal alkoxides onto the surface of a carefully optimized periodic mesoporous silica nanomaterial to generate a hybrid material able to perform well as a heterogeneous catalyst.

This involved the synthesis of a hitherto unknown homoleptic Ce(IV) isopropoxide, that was consequently fully characterized. During the course of this synthesis, the synthesis of an important precursor complex for Ce(IV) chemistry, $Ce(N\{SiHMe_2\}_2)_4$, was investigated in detail and could be optimized. Furthermore, significant insights into the structural chemistry of the donor-induced transfer of the cerous ate-complex $Ce(N\{SiHMe_2\}_2)_4Li(thf)$ into a solvent-separated ion pair of the type $[Ce(N\{SiHMe_2\}_2)_4][Li(do)_n]$ could be gained.

As the Ce(III)/(IV) redox couple offers unique possibilities to investigate the effect of electronical differences between closely related rare-earth-metal complexes, a series of immobilized Ce(III) and Ce(IV) based immobilized alkoxides was screened towards their performance in the MPVO reaction system, and after establishing the superiority of the Ce(III) based catalysts, La(III) alkoxides were similarly tested. All rare-earth-metal alkoxide-based catalysts showed greatly improved performance over $Al(O\mathit{i}Pr)_3$.

Zusammenfassung

Das klassische Meerwein-Ponndorf-Verley-Oppenauer Redox-System beschreibt die durch Al(O*i*Pr)$_3$ katalysierte Umwandlung eines Ketons oder Aldehyds in einen Alkohol (Meerwein-Ponndorf-Verley-Reduktion) oder die umgekehrte Reaktion (Oppenauer-Oxidation). In der praktischen Anwendung leiden diese Reaktionen unter der relativen Inaktivität des Katalysators, dessen Einsatz in großen Mengen (stöchiometrisch statt katalytisch) nötig ist. Mehrere frühere Arbeiten konnten zeigen, dass Seltenerdmetall-Alkoxid basierte Katalysatoren sowie die genaue Kontrolle der Reaktionsbedingungen in Bezug auf O_2 und H_2O in der Lage waren, die katalytische Effizienz deutlich zu verbessern.

Um diese Forschungen weiter voran zu bringen und gleichzeitig die Effekte immobilisierter (heterogenisierter) Seltenerdmetall-Alkoxid basierter Katalysatoren zu untersuchen, wurden die Methoden der Oberflächen-Organometallchemie angewendet um mehrere Seltenerdmetall-Alkoxide auf sorgfältig optimierte periodisch-mesoporöse Silica-Nanomaterialien zu graften, um Hybridmaterialien für den Einsatz als heterogene Katalysatoren zu generieren.

Dies beinhaltete die Synthese eines bis dato unbekannten, homoleptischen Ce(IV)-Isopropoxids, das vollständig charakterisiert werden konnte. Während dieser Synthese wurde außerdem die Synthese einer wichtigen Ausgangsverbindung für die Ce(IV)-Chemie, Ce(N{SiHMe$_2$}$_2$)$_4$, detailliert untersucht und konnte auch optimiert werden. Dabei wurden signifikante Erkenntnisse über den Donor-induzierten Übergang des at-Komplexes Ce(N{SiHMe$_2$}$_2$)$_4$Li(thf) in ein Solvens-separiertes Ionenpaar der Form Ce(N{SiHMe$_2$}$_2$)$_4$][Li(do)$_n$] gewonnen.

Da das Ce(III)/(IV)-Redox-Paar die einzigartige Möglichkeit bietet, die Auswirkungen elektronischer Unterschiede zwischen eng verwandten Seltenerdmetallkomplexen zu untersuchen, wurde eine Reihe immobilisierter Ce(III)- und Ce(IV)-basierter Alkoxide auf ihre katalytische Leistungsfähigkeit im MPVO-Reaktionssystem überprüft, wobei, nachdem die Überlegenheit der Ce(III)-basierten Katalysatoren deutlich wurde, La(III)-Alkoxide ebenfalls getestet wurden. Alle Seltenerdmetall-basierten Katalysatoren zeigten gegenüber Al(O*i*Pr)$_3$ eine deutlich gesteigerte Leistungsfähigkeit.

Publications

Publications Incorporated in this Thesis

Publications where I am (one of) the principal author(s):

Paper I A Facile Route toward Ceric Silylamide [Ce{N(SiHMe$_2$)$_2$}$_4$]
U. Bayer, L. Bock, C. Maichle-Mössmer and R. Anwander
Eur. J. Inorg. Chem., **2020**, 101-106.

Paper II SOMC @ Periodic Mesoporous Silica Nanoparticles: Meerwein-Ponndorf-Verley Reduction Promoted by Immobilized Rare-Earth-Metal Alkoxides
L. Bock, X. Tran, Y. Liang, M. Kramer, C. Maichle-Mössmer and R. Anwander
Organometallics, **2020**, 39, 7, 1046-1058.

Publications containing contributions by myself:

Paper III Cerium(IV) Neopentoxide Complexes
J. Friedrich, D. Schneider, L. Bock, C. Maichle-Mössmer and R. Anwander
Inorg. Chem., **2017**, 56, 14, 8114-8127.

Oral and Poster Presentations

Poster I Exchange of Donor Influences the Oxidation Susceptibility of ate-Complex [Ce(N{SiHMe$_2$}$_2$)$_4$Li(thf)]
U. Bayer, L. Bock, C. Maichle-Mössmer and R. Anwander
XXVIII. Tage der Seltenen Erden, Tübingen, Germany, *October 4-6*, **2017**

Presentation I A Facile Route toward Ceric Precursor [Ce(N{SiHMe$_2$}$_2$)$_4$]
U. Bayer, L. Bock, C. Maichle-Mössmer and R. Anwander
ICOMC, Florence, Italy, *July 15-20*, **2018**

Personal Contribution

Paper I: A Facile Route toward Ceric Silylamide $Ce(N\{SiHMe_2\}_2)_4$

All planning of experiments, reactions and analyses described, except the ones mentioned below, were conducted by myself and Uwe Bayer in close cooperation. The article was written cooperatively by myself and Uwe Bayer and revised by Reiner Anwander.

Elemental analyses (CHN) were performed by Wolfgang Bock. The structural solutions of the single crystal X-ray diffraction experiments were performed by Dr. Cäcilia Maichle-Mössmer. ^{1}H-PGSE-NMR experiments were performed by Dr. Wolfgang Leis.

Paper II: SOMC @ Periodic Mesoporous Silica Nanoparticles: Meerwein-Ponndorf-Verley Reduction Promoted by Immobilized Rare-Earth-Metal Alkoxides

All planning of experiments, reactions and analyses described, except the ones mentioned below, were conducted by myself. The article was written by myself and revised by Reiner Anwander.

Elemental analyses (CHN) were performed by Wolfgang Bock, elemental analyses (ICP-OES) were performed by Dr. Jochen Glaser. The structural analyses by single crystal X-ray diffraction were performed by Dr. Cäcilia Maichle-Mössmer. ^{1}H-PGSE-NMR experiments were performed and interpreted by Dr. Markus Kramer. Optimization of the synthesis of the MCM-41-type MSN was done by Xuan Tran during the course of her B. Sc. thesis work supervised by myself. SEM images were recorded by Elke Nadler.

Paper III: Cerium(IV) Neopentoxide Complexes

A reproduction and optimization of the synthesis of $[Ce(OCH_2tBu)_4]_3$ as well as sublimation experiments on the same complex were contributed by myself.

Objective of the Thesis

The aim of the work underlying this thesis was to explore the possibilities afforded by SOMC-derived heterogeneous catalysts in the Meerwein-Ponndorf-Verley-Oppenauer reaction system, with particular focus on the performance of redox active Ce-based compounds and the effects of employing third generation periodic mesoporous silica nanoparticulate carrier materials.

Part A of this thesis provides an overview over rare-earth metal alkoxides with a special focus on cerium, a view into the history, synthesis, and use of mesoporous silica materials, and a brief outline of the Meerwein-Ponndorf-Verley-Oppenauer reaction system and specifically the use of mesoporous silica-based heterogeneous catalysts therein.

Part B of this thesis gives a summary of the main results published in papers **I & II**

Part C of this thesis describes further results hitherto not published in scientific articles.

Part E is a compilation of published articles.

Part A.

Introduction

The work that forms the basis of this thesis lies at the intersection of several different fields of chemistry: The goal that informed most decisions and choices was the improvement of the Meerwein-Ponndorf-Verley-Oppenauer (MPVO) reaction system, and as such belongs to the field of organic chemistry. The methods used, and angles chosen from which to approach this, are, however, those of organometallic and surface organometallic chemistry as well as materials chemistry, and thus belong mostly to the field of inorganic chemistry.

The following introduction tries to illuminate all fields necessary for a thorough understanding of the results presented in the next section, as well as in the appended scientific articles (**Papers I & II**), starting with the organometallic chemistry of cerium and other lanthanides, and continuing with an overview over periodic mesoporous silica materials and surface organometallic chemistry, before closing with a short description of the MPVO reaction system. Due to the breadth of topics that need to be addressed, this introduction avoids an exhaustive discussion of each of these topics and refers the reader to the more specialized works used as references and listed in the bibliography (Part D).

Cerium(IV) Silylamide Chemistry

Cerium has long held a unique position among the rare-earth metals, being the only one of which molecular complexes with the metal in the formal oxidation state +IV were known.[1] Only very recently, terbium and praseodymium have joined this group and opened the perspective for even more Ln(IV) complexes.[2–5] Still, as of yet, only Ce(IV) complexes are known in relative abundance, and there are several synthesis protocols to access them.[6]

In order to realize the full potential of organometallic Ce(IV) chemistry, easily accessible precursor complexes are of paramount importance. Early works by Bradley et al. drew on $(py)_2CeCl_6$ as a precursor,[7] while later ceric ammonium nitrate (CAN, $[(NH_4)_2Ce(NO_3)_6]$) and ceric ammonium chloride (CAC, $[(NH_4)_2Ce(Cl_3)_6]$) as well as ceric triflate ($Ce(OTf)_4$, Tf = $SO_2CF_3^-$) played an important role.[8,9]

The development of rare-earth-metal silylamides with the general formula $Ln(N\{SiMe_3\}_2)_3$ gave the field of organo-rare-earth-metal chemistry a further boost, as with their high pK_a values (ca. 26 in THF[10]) they made reaction protocols based on protonolysis reactions feasible for a large number of less basic ligand systems (e.g alcohols[11] or pyrazolates[12]). In Ce(IV) chemistry however, the

high steric demand of this ligand prevents the formation of $Ce(N\{SiMe_3\}_2)_4$. To overcome this limitation, and make a similar kind of chemistry based on Ce(IV) available, we and others have actively explored the possibilities offered by the less sterically demanding $N(SiHMe_2)_2$ ligand. $Ce(N\{SiHMe_2\}_2)_4$, that our group was able to present a few years ago,[13] provided a convenient starting point for this kind of chemistry, and enabled the synthesis of several new complexes.[14–18]

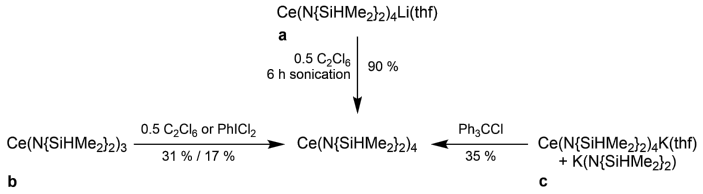

Scheme 1. Different synthesis routes to access tretravalent precursor $Ce(N\{SiHMe_2\}_2)_4$.

Scheme 1 shows the available routes to access $Ce(N\{SiHMe_2\}_2)_4$ with corresponding overall yields. The fact that this complex is predominantly used as a precursor to access further ceric complexes highlights the necessity of optimizing its synthesis and making it available in an easy, straightforward manner with good yield.

The formation of this precursor complex, however, starting from trivalent $Ce(N\{SiHMe_2\}_2)_3(thf)_2$ as well as from ate complexes $Ce(N\{SiHMe_2\}_2)_4K(thf)$ and $Ce(N\{SiHMe_2\}_2)_4Li(thf)$ (see Scheme 1), is rather inefficient due to several problems: When using route **b**, the yield is intrinsically limited to 75 % due to the consumption of starting material in a ligand rearrangement process, but in reality reports show only yields of 31 % (when oxidized with C_2Cl_6) with a rather long reaction time of 18 h, or even 17 % (when oxidized with $PhICl_2$).[13] Route **c**, utilizing the potassium-ate complex in the presence of $K[N(SiHMe_2)_2]$ and Ph_3CCl as an oxidant, while offering more intrinsic efficiency, still only affords an overall yield of 35 % of the tetravalent silylamide overall.[16] Route **a**, oxidizing the lithium-ate complex with C_2Cl_6 under sonication is currently the route with the best published yield (ca. 90 %),[15] but requires a prolonged reaction time and proved difficult to reproduce.

Our own attempts at improving this synthesis along with the results and structural insights gained are described in part B as well as **Paper I**.

Rare-Earth-Metal Alkoxides

Due to the high oxophilicity of rare-earth-metal ions, alkoxides are, compared to other organometallic complexes, relatively easy to obtain, and have thus been under investigation for over half a century, when Bradley and coworkers first reported the synthesis of several examples.[7,19,20] Their isolation and handling require, however, still sophisticated setups to guarantee moisture- and oxygen-free conditions as they are easily hydrolyzable and have a high tendency to form oxo-complexes in the presence of H_2O and, in the case of tetravalent cerium alkoxides, O_2. Today, rare-earth-metal alkoxide and aryloxide chemistry covers a large and varied number of complexes. Their role has shifted on one hand towards that of precursor complexes for other applications, e. g. in organometallic chemistry, or as volatile precursors for the production of highly pure rare-earth-metal oxides,[21] and on the other hand to applications in catalysis.[22–26]

Owing to the breadth of this field, and the fact that the work on rare-earth-metal alkoxides only constituted a relatively smart part of the work underlying this thesis, the following will focus on homoleptic alkoxide complexes that were the focus of the described efforts of improving the MPVO reaction system, and exclude aryloxides and heteroleptic complexes involving other functional groups (e.g. nitrato, cyclopentadienido).

Trivalent Alkoxides

Given the high oxophilicity of rare-earth-metal cations, their alkoxides are relatively stable compared to organometallic compounds featuring, e.g., Ln–C bonds. Several different synthetic protocols to access alkoxide complexes have been established. These are summarized in Scheme 2 and include the synthesis directly from the elemental rare-earth metals (**a**), which needs to be catalyzed by $HgCl_2$ to activate the metal, the reaction of rare-earth-metal halides and pseudohalides with alkali-metal alkoxides in salt metathesis reactions (**b**), where the formation of insoluble alkali-metal halides is an additional driving force for the reaction, a transalcoholysis (**c**), where an alkoxide ligand with a higher pK_a value is replaced by one with a lower pK_a value, and protonolysis reactions (**d**), where rare-earth-metal complexes bearing ligands with high proligand pK_a values are used as starting materials and are exchanged with the desired alcohol under liberation of the protonated ligand (e.g., amine or alkane).

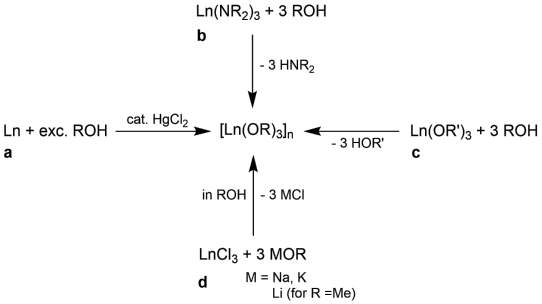

Scheme 2. Different synthesis routes to access homoleptic trivalent rare-earth-metal alkoxides.

Tetravalent Alkoxides of Cerium

As mentioned above, cerium is the only rare-earth metal of which a significant number of molecular tetravalent complexes are known, and the only one of which alkoxides exist. Recently, the first tetravalent complexes of terbium and praseodymium bearing sterically demanding siloxy ligands $OSi(O\mathit{t}Bu)_3$ and $OSiPh_3$ have been isolated and characterized.[2–4] In comparison to those compounds, the synthesis of Ce(IV) complexes, while far from trivial, is much more straightforward. Generally speaking, similar synthesis strategies as for trivalent rare-earth metal alkoxides can be employed (cf. Scheme 2, routes **b** and **c**), with the exception of route **a** (synthesis directly from the metal) and route **d** (synthesis from rare-earth metal halides). The main difference to the synthesis of trivalent alkoxides is the employment of tetravalent cerium precursors, which can be classified as inorganic precursors (comprising e.g. $[(NH_4)_2Ce(NO_3)_6]$ (CAN), or $Ce(OTf)_4$ (cerium triflate)) and (pseudo-)organometallic precursors like alkoxides and silylamides. The accessibility of tetravalent Ce alkoxides has thus always been dependent on the availability of those precursors, and new structural motifs have often resulted from new synthesis routes, even when using the same alkoxy ligands (cf. $[Ce(O\mathit{i}Pr)_4(\mathit{i}PrOH)]_2$[27] vs. $[Ce(O\mathit{i}Pr)_4]_3$ in **Paper II**). Scheme 3 depicts the different synthesis routes and corresponding tetravalent precursors in cerium alkoxide chemistry.

In 1992, Rheingold et al. demonstrated the oxidation of $Ce(OC\mathit{t}Bu_3)_3$ with several different oxygen-containing oxidants, and were able to tentatively identify

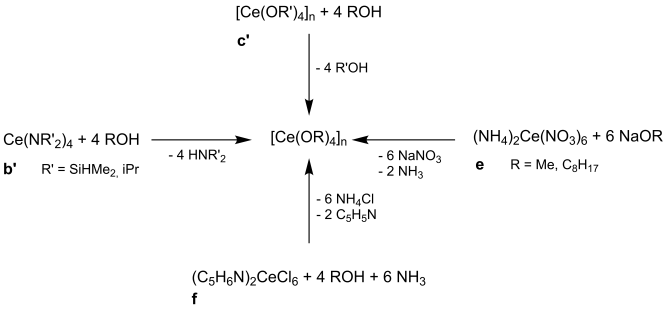

Scheme 3. Different synthesis routes to access homoleptic tetravalent Ce alkoxides.

$[Ce(OCtBu_3)_2(OtBu)_2]$ as the product of the oxidation with *t*BuOO*t*Bu.[28] The identification was done based on NMR data indicative of a diamagnetic Ce(IV) species and the X-ray structural characterization of $[Ce(OCtBu_3)_2(OtBu)]_2$ as a possible trivalent degradation product. A direct oxidation of a trivalent Ce alkoxide resulting in a homoleptic tetravalent alkoxide (i.e. bearing only alkyl moieties on the alkoxy ligands), however, has not been published as of yet.

Surface Organometallic Chemistry

Surface organometallic chemistry (SOMC), a term first coined by Jean-Marie Basset,[29] aims to adopt methods used in classical organometallic chemistry to obtain hybrid materials where organometallic species are covalently immobilized on the surface of a suitable carrier material. SOMC enables the generation of single-site heterogeneous catalysts, where, through the control of all sythesis steps and site isolation of the individual catalyst molecules on a surface, ideally the exact surface species is known and reactions between catalyst molecules are suppressed by covalently grafting them to the surface, thus avoiding any mobility.

With respect to classical heterogeneous catalysts (e.g. Raney-Ni; iron-based catalysts in the Haber-Bosch process), SOMC-derived heterogenized catalysts have the advantage that there are few to no catalytically active centers that are

inaccessible to the reactants due to their position within the bulk of the solid catalyst. Thus, the amount of catalyst, often featuring rare or expensive metals, that is needed for an efficient catalytic reaction can be minimized. This optimizes economic aspects while minimizing environmental impact, from mining as well as from disposal of the used catalyst. Furthermore, the more controlled synthesis pathways facilitate the characterization of the catalyst and thus enable a deeper understanding of the whole catalytic process.[30]

Compared to homogeneous catalysis, on the other hand, the advantages of SOMC-derived catalysts are mostly the same as those of heterogeneous catalysts in general, first and foremost a much easier separation of the catalyst from the reaction mixture after a catalytic reaction. Only in terms of thermal stability do classical heterogeneous catalysts clearly outperform SOMC-derived catalysts. Since heterogeneous catalysts can be separated by filtration or centrifugation, they remove the need of more elaborate purification protocols including solvent extraction, fractional crystallization, or distillation, all of which are energy or labor intensive or require potentially hazardous substances.

The possibility to design the support materials for SOMC-derived heterogeneous catalysts on a nanoscale level furthermore provides opportunities to influence the course of the projected catalytic reaction favorably. Having the reaction take place in suitably sized pores might, via confinement effects, increase the contact time between the reactants or the reactants and the catalytic center, while at the same time introducing geometric strain, thus selectively weakening bonds involved in the reaction.[11]

Support materials

For surface organometallic chemistry to yield meaningful results, the support materials and their surface properties need to be chosen with care and with the designated goal in mind. To achieve this, factors like the specific surface area, the nature and number of reactive surface moieties, acidity of the surface, and, where applicable, size and configuration of pores need to be taken into account.

Silica materials have proven themselves as versatile and reliable support materials for SOMC applications. They combine good chemical resistance with the availability of reactive surface groups, and an extremely high variability in terms of particle morphology, ranging from films, via solid particles of various sizes and materials with high, but morphologically undefined surfaces (fumed silica) to materials with regular/periodic porosity on different length scales. These

latter materials encompass especially zeolites, with pores in the microporous regime below 2 nm diameter, and periodic mesoporous silica materials (PMSs), with pores in the range of 2 – 50 nm. As support materials for the heterogeneous catalysts investigated in this thesis work, PMSs were chosen, and thus need to be discussed in greater detail.

Periodic Mesoporous Silica

The term "Periodic Mesoporous Silica" describes an amorphous silica material with a topology with regularly organized pores with diameters in the range of 2 – 50 nm that is often termed "semicrystalline".[31] PMS materials were discovered in 1992 by scientists at the Mobil Oil Company during their works on zeolites.[32,33] Originally, they envisaged molecular sieves similar to zeolites but with larger pores, and the great versatility of these novel larger-pore-size materials soon became apparent.

Today, PMSs are used in a variety of fields from column materials in chromatography applications[34] to drug delivery[35] and, indeed, SOMC. Periodic mesoporous silica materials have a high specific surface area (up to more than 1700 m^2g^{-1}, depending on the pore configuration and size[36]), and tunable pore size, are thermally stable and chemically relatively inert while bearing reactive moieties on the surface.[11] These include strained siloxane bridges as well as surface-terminating silanol groups, whose amount can be controlled by thermal treatment, thus influencing the reactivity of the material as a whole as well as the coordination environment for SOMC-derived surface species via site isolation of neighboring silica surface moieties and between neighboring organometallic entities (cf. also Scheme 2 in **Paper II**).[11]

In comparison to zeolites, with whom they share several common traits, e.g. the thermal stability or variety of pore configurations, PMSs display significantly larger pores and a much wider range of accessible pore sizes (spanning the whole definition of mesoporosity, with pore diameters between 2 nm and 50 nm and even to some extent above) as well as a concentration of reactive surface moieties that is controllable post-synthesis via thermal treatment in vacuum.[37] Purely siliceous PMSs lack, however, the Lewis-acidic Al centers present in zeolites.

Specifically the larger possible pore sizes are predestined to enable a large swathe of SOMC, as many organometallic complexes, even ones considered to be rather small, are too large to be introduced into the micropores present in zeolites.[11]

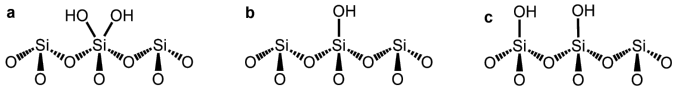

Scheme 4. Schematic depiction of geminal (a), isolated (b) and vicinal (c) silanol groups on the surface of a silica material.

The synthesis of PMSs is usually done using a liquid crystal templating approach, where the silica matrix is synthesized in a solution of surface active molecules (surfactants) above the critical micelle concentration (CMC). Depending on the specific surfactant and concentration, different pore geometries can thus be obtained with the same general method. The exact formation mechanism depends on the type of surfactant, the silica source, the pH of the reaction mixture and the interaction of all these factors and has been the subject of several original research or review articles.[33,38–43] The as-synthesized product is an organic-inorganic hybrid material with the surfactant micelles embedded in the silica matrix. Further treatment, either by solvent extraction or by calcination, is used to remove the organic components and gives the purely inorganic PMS material.

The most common geometries generated in this way are: (a) a hexagonal array of cylindrical pores (*P6mm* in e.g. MCM-41[33] and SBA-15[44]); (b) an entwined network of cylindrical pores displaying cubic symmetry (e.g. $Pm\bar{3}n$ in SBA-1 with a cage-like structure, $Ia\bar{3}d$ in MCM-48[33]); and (c) lamellar layers (e.g. MCM-50[33]).[45] Only the first two of those are of interest for use as support materials for SOMC as the materials consisting of lamellar layers are basically non-porous and thermally unstable.

The surface of silica materials generated this way is terminated with Si–OH moieties, whose number is dependent on the degree of hydrolyzation and can be post-synthetically controlled by thermal treatment in vacuum.[37] The number and distribution of those silanol groups is crucial for SOMC applications, as it determines the amount of organometallic molecules that can be grafted onto the surface and possible interactions between them, but also for the hydrothermal stability of the silica material itself.[46] The possible types of surface silanol groups are shown in Scheme 4.

PMSs with a nanoparticulate, uniform morphology have emerged as a third generation support material, enabling further control over the conditions in which

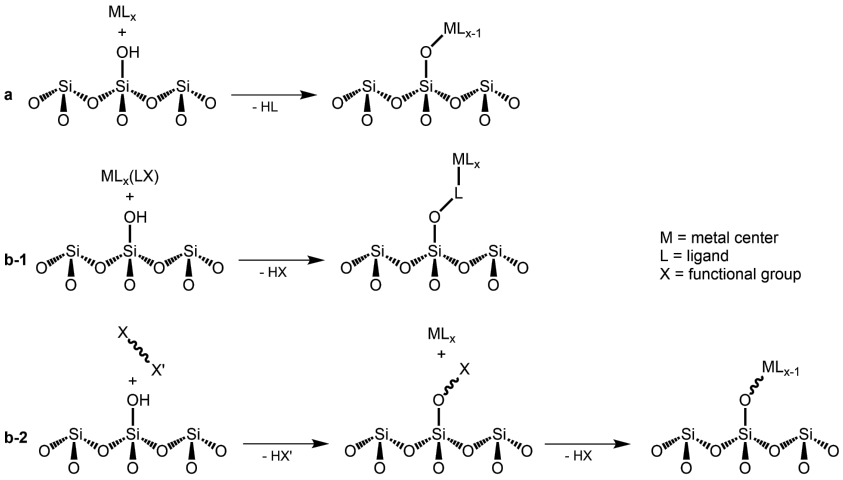

Scheme 5. Schematic representation of three possible immobilization strategies for organometallic complexes on a silica surface with isolated silanol groups.

catalytic reactions take place. By limiting the length of the pores in the material via a uniform "small" particle size, meaning spherical nanoparticles of uniform size, the influence of diffusion on the generated results can be controlled, making those materials especially suitable as model systems to gain further insights into the mechanisms underlying these kinds of heterogenized, SOMC-derived catalysts.

Immobilization Strategies

There are several possible routes to achieve an immobilization of organometallic complexes on the surface of PMSs, the two most important ones are (a) a direct approach (SOMC), where the precursor complex directly reacts with reactive surface moieties, and (b) a tethered approach, where a functionalized tether reacts with the surface to form a flexible linker between the surface and the metal ion. Approach (b) can be further subdivided in (b-1) reactions where the linker is present in the precursor complex as a ligand, and (b-2) stepwise reactions where

a bi-functional linker reacts with the surface first and in a second step reacts with the precursor complex, immobilizing it (see also Figure 5).

For other materials, other immobilization strategies can be employed, e. g. a "ship-in-a-bottle" approach for zeolites with cage-like pore morphology, where a molecule is synthesized, assembled in a manner of speaking, within the pores, with the resulting molecule being physically entrapped within the larger compartments.[11] This strategy plays a minor roll for PMSs, where the pores are generally channel-like, with similar diameter over their entire length.

Surface Binding Modes / Podality

When organometallic complexes undergo immobilization reactions with surface-Si–OH groups of siliceous carrier materials, there are several binding modes possible that influence the resulting surface species and can consequently have implications for the reactivity behavior of the resulting hybrid species.[47]

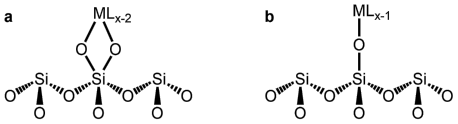

Scheme 6. Two possible binding modes of a organometallic complex on a silica surface where there are no vicinal Si–OH groups present (i. e. dehydroxylated above 400 °C).

The binding modes for rare-earth metal based organometallic complexes have been investigated experimentally[48–53] as well as theoretically,[52,54] and it was shown that the binding modes are independent of the used rare-earth metal, but heavily influenced by the amount and distribution of the silanol groups present on the silica surface. These, in turn, are controlled by the dehydroxylation treatment prior to grafting which comprises the application of vacuum at elevated temperatures to force a removal of physisorbed water from the surface at lower temperatures. At higher temperatures, the condensation of silanol groups happens under formation of siloxane bridges and water. It has been shown that after such treatment at temperatures above 400 °C, vicinal silanol groups are basically fully condensed and thus play no more role for SOMC.[37]

The Meerwein-Ponndorf-Verley-Oppenauer Reaction

The Meerwein-Ponndorf-Verley Reduction

The Meerwein-Ponndorf-Verley (MPV) reduction is a long known reaction that has first been reported in the 1920s independently by Meerwein and Schmitt[55] as well as Verley,[56] and refined to the still established version shortly after by Ponndorf.[57]

In it, an aldehyde or ketone is reduced to the corresponding alcohol, using the solvent (usually *i*PrOH) as reductant. The catalyst in the original MPV reduction is $Al(O\textit{i}Pr)_3$, and the most viable hypothesis of the reaction mechanism, that is also supported by DFT calculations, is one where the substrate as well as the reductant coordinate to the Lewis-acidic Al center and hydride transfer takes place via a six-membered transition state (see Scheme 7).[58,59] The progression of this reaction is thus influenced on one hand by the Lewis acidity of the metal center, governing its ability to coordinate the alkoxy ligands, and on the other hand on its tendency to exchange ligands, liberating the formed product and the oxidized reductant.

Since the catalyst established by Meerwein, Schmitt, Ponndorf and Verley, $Al(O\textit{i}Pr)_3$, shows very low activities, requiring the use of catalyst in stoichiometric or even superstoichiometric amounts,[60] plenty of work has been done to investigate the use of other metals as catalysts.[25,58,61–65] It could be shown that not only Al, but a host of main group as well as transition metals can be used as catalytically active centers for the MPV reduction, but that in terms of activity, rare-earth metals show some of the best performances.[24,25,61,64–67]

It has further been shown that it is not only possible to perform this catalytic reaction with heterogenized catalysts, but that SOMC-derived heterogeneous catalysts can in some cases even outperform their homogeneous counterparts, especially when taking into account factors like reusability and ease of separation.[49,50,68,69]

The Oppenauer Oxidation

The Oppenauer Oxidation, while offering in theory a mild catalytic one-electron oxidation route for primary and secondary alcohols utilizing cheap oxidizing agents, is hampered by the same shortcomings as the Meerwein-Ponndorf-Verley reduction, especially the necessity of using stoichiometric amounts of the metal

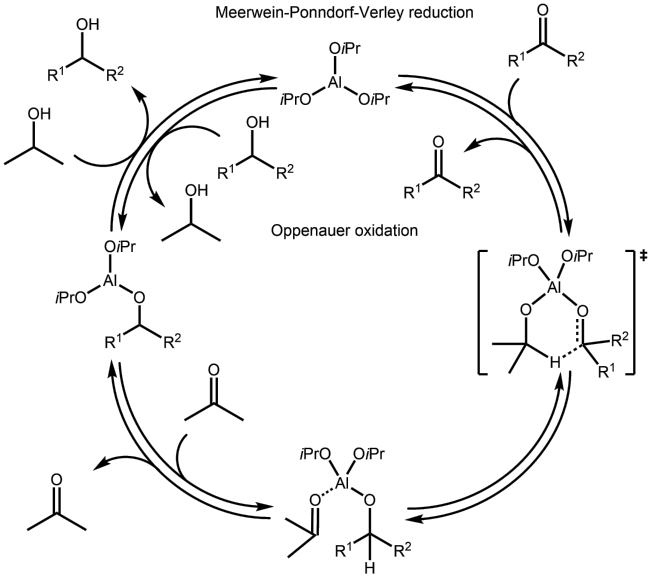

Scheme 7. Catalytic cycle of the Meerwein-Ponndorf-Verley-Oppenauer reaction system.

alkoxide catalyst. It has, however, the advantage that it accomplishes the oxidation of alcohols to ketones without the hazard of overoxidizing to the corresponding carboxylic acid.[61] Thus, it sees some niche use on a laboratory scale, mainly in the synthesis of steroids and other terpenoids or the oxidation of nitrogen-containing alcohols, where other oxidation protocols show less satisfactory results (e.g. in the total synthesis of natural products[70]).

In the classical understanding of this system, the Oppenauer oxidation is simply achieved by inverting the catalytic cycle seen in Scheme 7. By exchanging the isopropanol used as solvent and hydride source with acetone, the equilibrium of all steps involving the solvent is inverted, resulting in an oxidation of the respective substrate.

While this method works when employing $Al(O\mathit{i}Pr)_3$ as a catalyst, using rare-earth-metal based catalysts requires a different approach, as those tend to prefer-

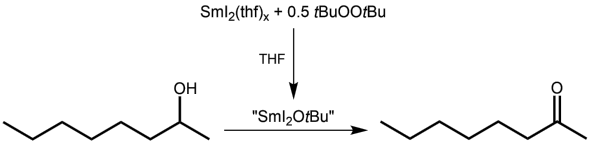

Scheme 8. The reaction setup used by Kagan *et al.* to achieve a Sm-catalyzed oxidation of 1-octanol to 1-octanone with 2-butanone as the oxidant.

entially catalyze aldol-type reactions in a competing pathway. The latter often lead to catalyst deactivation through condensation of alkoxy ligands with acetone and formation of rare-earth metal aldolates and enolates.[71]

Kagan et al. showed, however, that the Oppenauer oxidation can be performed with a samarium-based catalyst they designated "SmI_2O*t*Bu" in THF using different ketones stoichiometrically or in excess (1 to 8 equivalents) as oxidants on a variety of substrates. However, they did not elucidate the catalytically active species. They rather employed a solution obtained from the reaction of SmI_2 with *t*BuOO*t*Bu in THF, where they titrated the metal content afterwards to determine the amount of catalyst in the reaction mixture and be able to assess the catalytic performance (see Scheme 8).[64]

The obvious assumption for an active species in this reaction would indeed be SmI_2O*t*Bu, especially since this compound could be isolated and crystallographically analyzed by Barbier-Baudry and coworkers as a THF-adduct,[72] and since Kagan's reaction setup avoids a solvent that could undergo aldol-type reactions. Unfortunately, a full elucidation of the catalytically active species and a mechanistic investigation of this reaction has hitherto not been published.

Part B.

Summary of the Main Results

Organometallic Chemistry

Cerium Silylamide Chemistry

With $Ce(N\{SiHMe_2\}_2)_4$ being a crucial precursor for the synthesis of several Ce(IV) complexes, a reliable and efficient route to access it is of great importance. Earlier synthesis strategies using the ate complex $Ce(N\{SiHMe_2\}_2)_4Li(thf)$ ($\mathbf{1^{thf}}$) or $Ce(N\{SiHMe_2\}_2)_3(thf)_2$ as precursors were hampered by low yields or the necessity of extensive purification processes.[13,15,16] By adding additional donating THF in $Ce(N\{SiHMe_2\}_2)_4Li(thf)$ or exchanging it with other donor molecules (DME, TMEDA, pyridine, 12-crown-4), complexes $\mathbf{2^{thf}}$, $\mathbf{2^{dme}}$, $\mathbf{2^{tmeda}}$, $\mathbf{2^{py}}$, and $\mathbf{2^{12\text{-}crown\text{-}4}}$ could be generated, which adopt the structure of a solvent-separated ion pair of the type $[Ce(N\{SiHMe_2\}_2)_4][Li(do)_n]$, where n varied based on the amount of solvent necessary to saturate the Li cation's coordination sphere (i.e. n = 3 for do = DME* , 2 for TMEDA, 4 for pyridine and THF and 1 with one additional molecule of THF for 12-crown-4) (**Paper I**).

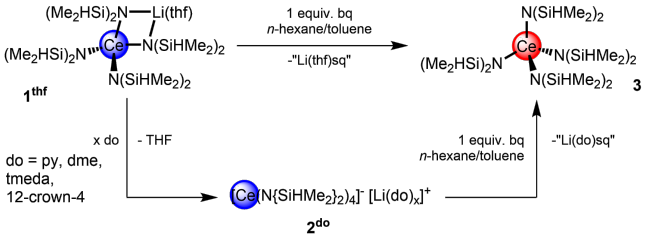

Scheme 9. Formation of $Ce(N\{SiHMe_2\}_2)_4$ (**3**) via direct oxidation of ate complex $Ce(N\{SiHMe_2\}_2)_4Li(thf)$ ($\mathbf{1^{thf}}$) with 1,4-benzoquinone (bq) or by preceding donor exchange and subsequent oxidation of the formed solvent-separated ion pair $[Ce(N\{SiHMe_2\}_2)_4][Li(do)_x]$ ($\mathbf{2^{do}}$) (sq = 1,4-benzosemiquinolato). Blue spheres denote Ce(III) species, red spheres Ce(IV).

For all separated ion pair-type complexes, except for $\mathbf{2^{dme}}$, it was possible to obtain crystal structures by X-ray crystallography, confirming the separation of the $Ce(N\{SiHMe_2\}_2)_4$ anion from the $Li(do)_n$ cations (see Figure 1). Comparing the Ce–N bond lengths of those separated ion pairs with the ones in

*Based on results from elemental analysis; a crystal structure could not be obtained.

$Ce(N\{SiHMe_2\}_2)_4Li(thf)$ shows the effect of this separation on the molecular geometries: While in $Ce(N\{SiHMe_2\}_2)_4Li(thf)$ there are two shorter and two longer Ce – N bonds (2.386(4)/2.388(5) Å vs. 2.523(4)/2.532(5) Å), with the longer ones involved in Ce – N– Li linkages, the Ce – N bond lengths in all separated ion pair type complexes are all very similar to each other (e.g. 2.397(4) – 2.417(4) Å in $\mathbf{2^{py}}$), reflecting the fact that the $Ce(N\{SiHMe_2\}_2)_4$ anionic moiety is nearly uninfluenced by the lithium cation.

These different donor exchanged complexes were screened for their oxidizability by 1,4-benzoquinone, and it was found that $[Ce(N\{SiHMe_2\}_2)_4][Li(py)_4]$ underwent the cleanest oxidation with high yield. The oxidation of the complexes with do = TMEDA and do = 12-crown-4 showed even higher yields in NMR-experiments, but at the expense of more impurities, rendering the oxidation of the pyridine complex the superior one in terms of ease of access to the desired product.

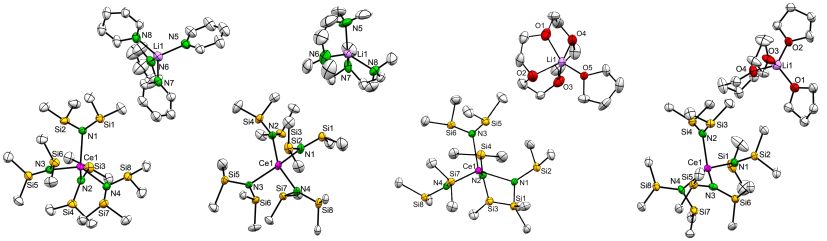

Figure 1. Crystal structures of donor-separated ion-pair type complexes $[Ce(N\{SiHMe_2\}_2)_4][Li(py)_4]$ ($\mathbf{2^{py}}$, left), $[Ce(N\{SiHMe_2\}_2)_4][Li(tmeda)_2]$ ($\mathbf{2^{tmeda}}$, center left), $[Ce(N\{SiHMe_2\}_2)_4][Li(12\text{-crown-}4)(thf)]$ ($\mathbf{2^{12\text{-}crown\text{-}4}}$, center right) and $[Ce(N\{SiHMe_2\}_2)_4][Li(thf)_4]$ ($\mathbf{2^{thf}}$, right).

Due to the paramegnetism of the Ce(III) ion and the strong signal broadening for nuclei in close proximity to the cerium ion arising from it, ^{1}H-NMR spectroscopy is of limited use in examining trivalent cerium complexes. We could show, however, that that same phenomenon could be exploited for the transition from ate complexes to separated ion pairs. Since the ^{7}Li-NMR spectra are considerably less complex than the corresponding ^{1}H-NMR spectra, showing only one resonance for the lithium cation, these spectra could be used to differentiate between the ate complex and the separated ion pair. As the lithium cation in

the ate complex is strongly influenced by the paramagnetic Ce(III) center, its signal is strongly shifted downfield ($\delta = 84$ ppm for $\mathbf{1^{thf}}$). Conversely, in the separated ion pair-type complexes, the lithium cation is nearly uninfluenced by the cerium anion, which is reflected in the strongly reduced deshielding, giving a chemical shift range of $\delta = -1.44$–2.45 ppm for the separated ion pairs, with much narrower resonances. It was thus possible to follow the transition from the ate complex to a separated ion pair by ^{7}Li-NMR spectroscopy, by following the shift from a broad, strongly shifted signal to a sharp one with a much smaller chemical shift (see Figure 2).

^{7}Li-NMR spectroscopy further revealed that the original ate complex $\mathbf{1^{thf}}$ contains a small amount of separated ion pair $\mathbf{2^{thf}}$ (ca. 3 %, see Figure 2). This can be explained from the synthesis protocol used to generate $\mathbf{1^{thf}}$, where the reactivity of $CeCl_3$ was increased by activating it through Soxhlet-extraction with THF, giving statistically $CeCl_3(thf)_{1.04}$. This slightly superstoichiometric amount of THF matches well with the amount of $\mathbf{2^{thf}}$ in $\mathbf{1^{thf}}$.

After examining the available options for the oxidation of these separated ion pair-type complexes, 1,4-benzoquinone was chosen as the oxidant, as it best fits the set goal of the most straightforward oxidation protocol. This is mainly due to the fact that the oxidation of either the ate complex or a separated ion pair should only lead to insoluble, easy-to-separate byproducts in non-polar solvents, which would greatly simplify the purification process. Earlier attempts at oxidizing $\mathbf{1^{thf}}$ with 1,4-benzoquinone always resulted in low yields,[15,18,73] so a re-investigation seemed appropriate. The oxidation attempts were monitored by ^{1}H-NMR spectroscopy, as the product, $Ce(N\{SiHMe_2\}_2)_4$ (**3**), shows a clean spectrum with two signals at 0.34 and 6.01 ppm, making it easy to quickly estimate the amount of side products. The first attempt with 0.5 equivalents of the oxidant, assuming a complete reduction of each molecule of 1,4-benzoquinone, gave unsatisfactory results and it became apparent that only a Li-semiquinolate was formed, making the usage of 1 equivalent of oxidant necessary (see Scheme 9).

After the implementation of this revised oxidation protocol, all oxidation reactions proceeded to completion, with varying yields and varying amounts of side products (see Figure 2). In terms of yield, the reactions involving $\mathbf{2^{py}}$, $\mathbf{2^{tmeda}}$, and $\mathbf{2^{12\text{-}crown\text{-}4}}$ showed the best results, with yields determined by NMR spectroscopy as high as 75 % for $\mathbf{2^{tmeda}}$. In terms of purity, however, the oxidation of $\mathbf{2^{py}}$ gave the best result with nearly no impurities visible in the ^{1}H-NMR spectrum, while $\mathbf{2^{tmeda}}$ and $\mathbf{2^{12\text{-}crown\text{-}4}}$ showed some significant impurities and thus required additional recrystallization steps to obtain the desired product.

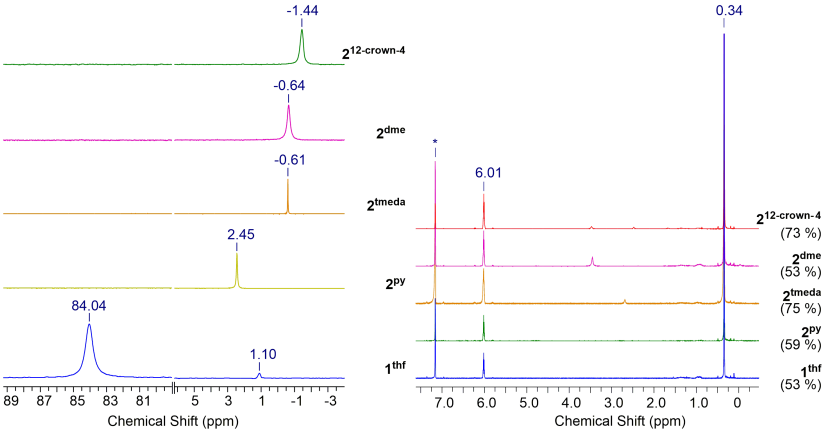

Figure 2. Left: ^{7}Li-NMR spectra of the ate complex $\mathbf{1^{thf}}$, as well as all four synthesized separated ion pair-type complexes ($\mathbf{2^{py}}$, $\mathbf{2^{tmeda}}$, $\mathbf{2^{dme}}$, and $\mathbf{2^{12\text{-}crown\text{-}4}}$).
Right: ^{1}H-NMR spectra of the crude products of the oxidation reactions of $\mathbf{1^{thf}}$ and $\mathbf{2^{do}}$ with one equivalent of 1,4-benzoquinone with the yields given in parentheses. The product peaks are those at 6.01 and 0.34 ppm, the solvent signal is marked with an asterisk.

Thus, the oxidation of $\mathbf{2^{py}}$ was deemed the superior approach to receive clean $Ce(N\{SiHMe_2\}_2)_4$ (**3**) in good yield and with a simple and non-time-consuming reaction protocol.

Ce(IV) Alkoxide Chemistry

Ce(IV) Isopropoxide

For the Meerwein-Ponndorf-Verley (MPV) reduction, Ce(IV) isopropoxide was chosen as a promising Ce(IV) alkoxy-based catalyst, since the ligand exchange during the catalytic reaction causes a replacement of any alkoxy ligands with isopropoxy ligands, substantially reducing the impact of other alkoxy ligands. Hitherto, the only known Ce(IV) isopropoxide reported and structurally characterized was $[Ce(O\mathit{i}Pr)_4(\mathit{i}PrOH)]_2$,[74] a dimer where the coordination sphere of each Ce(IV) ion is saturated by one molecule of *i*PrOH acting as a donor. The structure is further characterized by hydrogen-bridge bonds between the donat-

ing alcohol molecules and neighboring isopropoxy ligands. When attempting to synthesize this complex from a different precursor, via a protonolysis reaction of $Ce(N\{SiHMe_2\}_2)_4$ (**3**) with *i*PrOH, this complex was not formed, instead homoleptic complex $[Ce(O\textit{i}Pr)_4]_3$ (**4**) was obtained and could be fully characterized, marking the first homoleptic cerium isopropoxide (**Paper II**). By using a significant excess of *i*PrOH (up to 8 equiv.), it was tried to force the formation of $[Ce(O\textit{i}Pr)_4(\textit{i}PrOH)]_2$, but even then only the homoleptic complex was obtained. The unexpected advantage of this was that the synthesis protocol could be simplified, since it was possible to use the marked color difference between $Ce(N\{SiHMe_2\}_2)_4$ (dark red) and $[Ce(O\textit{i}Pr)_4]_3$ (yellow) to judge the completion point of the reaction, which removed the necessity of controlling the exact stoichiometric amount of *i*PrOH.

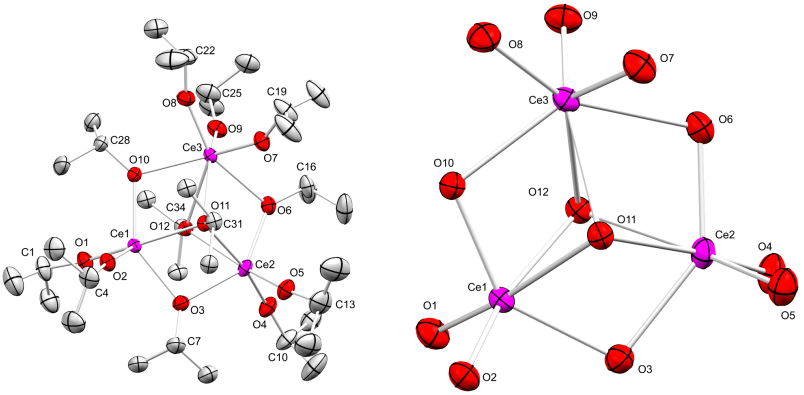

Figure 3. Left: Crystal structure of one of the four independent molecules of $[Ce(O\textit{i}Pr)_4]_3$ in the unit cell. Ellipsoids are shown at the 50 % level, hydrogen atoms and disorder in the isopropyl groups are omitted for clarity.
Right: The core of the structure without *i*Pr-groups.

Contrary to the structure of $[Ce(O\textit{i}Pr)_4(\textit{i}PrOH)]_2$, **4** is trimeric in nature, adopting an unprecedented variation on a common structural motif (for examples, cf. the textbook on alkoxides by Bradley et al.[58]). Where the core structure of this motif usually displays a C_3 symmetry with the threefold rotation axis defined by two μ_3-bridging ligands, this symmetry in **4** is broken by one of the

cerium centers accepting three instead of two terminal alkoxy ligands, leading to a heptacoordination at Ce3, while Ce1 and Ce2 are hexacoordinated.

Table 1. Selected interatomic distances and bond angles for $[Ce(OiPr)_4]_3$ (**4**).

Distance/Å		**Angle**/°	
Ce1 – O1	2.061(3)	Ce1 – O1 – C1	165.7(3)
Ce1 – O2	2.071(3)	Ce1 – O2 – C4	174.7(3)
Ce1 – O3	2.337(3)	Ce1 – O3 – C7	129.6(8)
Ce1 – O10	2.237(3)	Ce1 – O10 – C28	132.0(3)
Ce1 – O11	2.480(3)	Ce1 – O11 – C31	123.8(2)
Ce1 – O12	2.362(3)	Ce1 – O12 – C34	130.2(3)
Ce1 – O3	2.357(3)	Ce1 – O3 – C7	127.1(7)
Ce1 – O4	2.070(3)	Ce1 – O4 – C10	166.6(3)
Ce1 – O5	2.06(1)	Ce1 – O5 – C13	169(1)
Ce1 – O6	2.184(3)	Ce1 – O6 – C16	138.8(3)
Ce1 – O11	2.446(3)	Ce1 – O11 – C31	121.7(2)
Ce1 – O12	2.462(3)	Ce1 – O12 – C34	117.9(2)
Ce1 – O6	2.558(3)	Ce1 – O6 – C16	117.2(3)
Ce1 – O7	2.100(3)	Ce1 – O7 – C19	149.0(9)
Ce1 – O8	2.087(3)	Ce1 – O8 – C22	159.0(3)
Ce1 – O9	2.092(3)	Ce1 – O9 – C25	146.9(7)
Ce1 – O10	2.497(3)	Ce1 – O10 – C28	123.7(3)
Ce1 – O11	2.517(3)	Ce1 – O11 – C31	116.6(2)
Ce1 – O12	2.721(3)	Ce1 – O12 – C34	116.8(2)

This difference in the coordination environments can also be seen in the interatomic distances between cerium and the corresponding ligand-O-atoms: The Ce3 – O_{μ_2} bonds as well as the Ce3 – O_{μ_3} bonds are markedly elongated in comparison to their Ce1/2 – $O_{\mu_{2/3}}$ counterparts (Ce3 – O6/O10 2.558(3)/2.497(3) Å, Ce1 – O10 2.237(3) Å, Ce2 – O6 2.184(3) Å; Ce3 – O11/12 2.517(3)/2.721(3) Å, Ce1 – O11/12 2.480(3)/2.362(3) Å, Ce2 – O11/12 2.446(3)/2.462 Å). The equally trimeric, albeit linear Ce(IV) neopentoxide discussed later in this section and in **Paper III** shows similar bond lengths for its terminal and μ_2-bridging Ce – O bonds.[75]

The same structural motif with one cerium center showing similarly lengthened bonds can be found in $Ce_3(OtBu)_{11}$,[27,73] where those increased bond lengths are due to the complex displaying mixed valence for the Ce centers, with two being

tetravalent and one being trivalent with increased ionic radius and consequently greater Ce – O interatomic distances. To rule out any mixed valent complex and prove that the increased bond lengths in **4** are solely due to the increased coordination number of Ce3, a magnetic susceptibility study using the Evans method was carried out and, in combination with the absence of paramagnetic line broadening in the ^{1}H-NMR spectra, confirmed a diamagnetic complex with $\mu_{\text{eff}} = 0.70\,\mu_{\text{B}}$.

In order to gain insight into the grafting process of **4** onto MSN-MCM-41, a crucial piece of information was its molecular structure in solution, as a trimeric structure similar to the solid-state structure would induce a noticeably different surface species as a result of the grafting process. To elucidate this, ^{1}H-DOSY NMR studies were undertaken comparing the diffusion coefficient, which is inversely proportional to the hydrodynamic radii, of **4** with that of a complex of similar molecular weight, whose structure in solution was known. For this role, $Ce(N\{SiHMe_2\}_2)_4$ was chosen, as it is monomeric in the solid state and does not partake in ligand exchange processes with **4**. The ratio of diffusion coefficients of the standard and that measured for **4** could thus be compared with the ratio between the standard and a hypothetical monomeric structure "$Ce(OiPr)_4$" and the standard and the trimeric solid-state structure, thus giving a clear indication to the solution-state structure of **4**.

Table 2. Molecular radii and ratios of the two possible species of $[Ce(OiPr)_4]_n$ and $Ce(N\{SiHMe_2\}_2)_4$

Compound	$\mathbf{r_{calc}}$[a] / Å	$\mathbf{r_{meas}}$[b] / Å	**ratio vs. $Ce[N(SiHMe_2)_2]_4$**
$[Ce(OiPr)_4]_3$ (**4**)	6.35	6.35	1.15
$Ce(OiPr)_4$	4.85	n/a	0.88
$Ce(N\{SiHMe_2\}_2)_4$	5.5	5.5[13]	

[a] From energy-optimized structures (Chem3D). [b] From X-ray crystal structures.

Table 2 shows the calculated, and, where known, measured molecular radii and their ratios for all involved species. For **4** and $Ce(N\{SiHMe_2\}_2)_4$, the molecular radii calculated from an energy-optimized structure were in excellent agreement with the values measured in the solid-state structure, lending significant credibility to the calculated value for the hypothetical monomer.

The ^{1}H-DOSY measurements gave a ratio of hydrodynamic radii between $[Ce(OiPr)_4]_n$ and $Ce(N\{SiHMe_2\}_2)_4$ of 1.13, thus confirming a trimeric structure

for **4** in solution (calculated ratio: 1.15) and ruling out a monomeric structure (calculated ratio: 0.88).

While the ^{1}H-DOSY measurements showed the trimeric structure of **4** to be stable in solution, variable temperature NMR studies between -80 and $+27\,^\circ$C showed some mobility in the O*i*Pr-ligands, as only below $-40\,^\circ$C there was decoalescence of their signals into two distinct signal sets with an integral ratio of 2:10, indicating a loss of mobility for the two μ_3-bridging alkoxide ligands, while the μ_2-bridging and terminal ligands could still undergo fast exchange. On further cooling to $-80\,^\circ$C, there was no further signal decoalescence or change of integral ratio, and thus no further loss of ligand mobility.

Ce(IV) Neopentoxide

In a further effort to revisit and expand established Ce(IV) alkoxide chemistry,[19] a collaborative study on Ce(IV) neopentoxide complexes was undertaken (**Paper III**). According to literature reports, the neopentoxide complex of tetravalent cerium assumes a singular position among the smaller alkoxides as it was reported to be the only one that could be sublimated without decomposition.[19] With $Ce(N\{SiHMe_2\}_2)_4$ as an excellent entry point into Ce(IV) alkoxide chemistry, it seemed promising not only to try to replicate the results from the earlier study, but also to fill in gaps, as, e.g., an X-ray crystal structure for this complex had never been reported.

And indeed, the tetravalent cerium neopentoxide could successfully be synthesized from $Ce(N\{SiHMe_2\}_2)_4$ and was structurally characterized as the trimeric $[Ce(OCH_2tBu)_4]_3$ shown in Figure 4. Contrary to $[Ce(OiPr)_4]_3$ described above, which also forms a trimer, the trimetallic core of this complex adopts a linear structure, with one central cerium being connected to the other two by two μ_2-bridging neopentoxy ligands each and bearing one additional terminal alkoxy ligand, while the two peripheral Ce(IV) ions both bear three terminal ligands in addition tho the two bridging ones.

The claim that $[Ce(OCH_2tBu)_4]_3$ could be sublimated at 260 °C at a pressure of 0.05 mmHg ($= 6.66 \cdot 10^{-2}$ mbar) could further be confirmed and sublimation was performed at 150 °C and $5 \cdot 10^{-5}$ mbar.

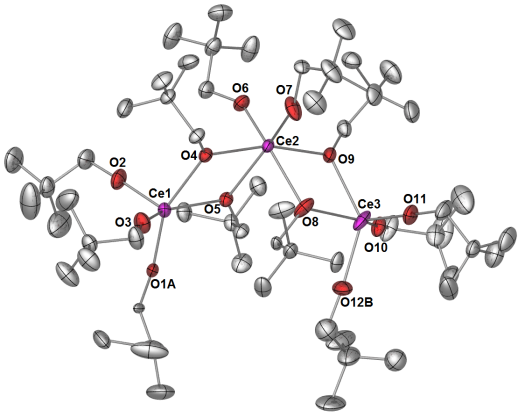

Figure 4. Crystal structure of $[Ce(OCH_2tBu)_4]_3$. Ellipsoids are shown at the 50 % level, H atoms are omitted for clarity.

Mesoporous Silica Nanoparticles

The synthesis of mesoporous silica nanoparticles of the MCM-41 type (MSN-MCM-41), while well established and described in detail in literature,[35,39,76,77] still leaves room for optimization and adaption to specific fields of application. In this work, the aim was to establish a third-generation-support platform for SOMC with clearly defined and reproducible properties. To this end, monodisperse mesoporous silica nanoparticles (MSN) with MCM-41-type porosity and spherical morphology were envisaged. Closely following a reported procedure[41] yielded particles with the desired mesoporous structure, while the particle morphology was not satisfactory. Parameters investigated on their influence on the particle morphology included reaction time, pH-value, stirring rate, and the type of stir bar used.[78] This extensive investigation led to a synthesis protocol that reliably yielded close-to-spherical particles of the desired periodic mesoporous structure, with high specific surface area and reproducible pore diameters between 2.6 and 2.7 nm (see Table 3 and Figure 5 as well as **Paper II**).

The resulting MSN were characterized with PXRD and SEM measurements to confirm their periodic mesoporous structure, as well as N_2-physisorption

to characterize their specific surface area and pore size. DRIFT spectroscopy measurements as well as surface silylation experiments with $HN(SiHMe_2)_2$ were undertaken to glean insight into the characteristics of the silica surface with respect to terminating silanol groups. The results for the used MSN materials are summarized in Table 3.

Table 3. Characterization data of three individual batches of MSN-MCM-41_{500} used to generate the SOMC-derived hybrid materials in **Paper II**

Material	a_{BET} [a] / $m^2\,g^{-1}$	V_{pore} [b] / $cm^3\,g^{-1}$	d_{pore} [c] / nm	$c_{surface\ Si–OH}$ [d] / $mmol\,g^{-1}$
MSN-MCM-41-a	1062	0.72	2.6	1.11
MSN-MCM-41-b	1134	0.89	2.6	1.04
MSN-MCM-41-c	1107	0.77	2.6	1.11

[a] BET surface calculated between p/p_0 0.07 and 0.15.
[b] BJH desorption cumulative pore volume between 1.5 and 4.5 nm.
[c] Maximum pore diameter from the BJH desorption branch.
[d] Calculated according to published procedures.[79]

N_2-physisorption measurements of the activated parent materials showed reversible type IV isotherms that are typical for mesoporous MCM-41-type materials. From those isotherms, the specific surface area and pore size distribution were calculated according to the BET and BJH methods, respectively.[80,81] The specific surface area lay reproducibly in the range of 1000–1200 m^2g^{-1}, with a monomodal pore size distribution narrowly centered around a pore diameter of 2.6 nm (see Table 3 and Figure 8, as well as the supporting information of **Paper II**).

Surface Organometallic Chemistry

Using the methods of surface organometallic chemistry, it was possible to generate several hybrid materials Ln_xL_y@MSN-MCM-41_{500} suitable for use as heterogeneous catalysts for the MPV reduction. To this end, two different strategies, illustrated in Scheme 10, were employed, viz, a direct and a sequential approach. In the direct approach, the desired alkoxide precursor was synthesized first, and later immobilized on the surface of the MCM-41-type MSN in a protonolysis-type grafting reaction, while in the sequential approach the immobilized complex was a precursor molecule to the desired catalyst, e.g. a silylamide, that was

transformed to the envisioned alkoxy surface complex in a second, protonolytic ligand-exchange step by exposing the hybrid precursor material to the desired alcohol. Both approaches were successfully employed to obtain hybrid materials, with the direct approach yielding $[Ce(O\mathit{i}Pr)_4]_3$@MSN-MCM-41_{500}-a (**H1**) and the sequential approach yielding all other hybrid materials. The prevalence of hybrid materials generated through the sequential approach is explained by the low solubility of Ln(III)-based alkoxides that precluded a formation of those materials via the direct approach.

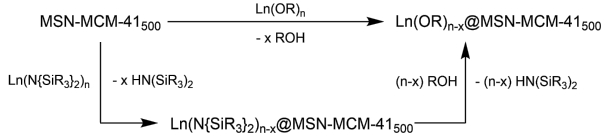

Scheme 10. Direct and sequential approaches toward catalytically active hybrid materials.

The resulting hybrid materials generally showed metal contents of ca. 10 %, which seems to be the limit for this specific combination of parent material and similarly sized cerium-based complexes, with the one exception being material **H2** ($Ce(N\{SiHMe_2\}_2)_4$@MSN-MCM-41_{500}-c), where only half of that amount was reached (see Table 4). A likely explanation for this reduced amount of surface grafted complex and thus metal content lies in the protonolytic grafting process, where one $N(SiHMe_2)_2$ ligand is replaced by an Si–O surface moiety, liberating one molecule of $HN(SiHMe_2)_2$. It has been shown not only that $HN(SiHMe_2)_2$ undergoes surface reactions with a silica surface itself (see Scheme 11), but in doing so achieves a near-complete surface coverage.[48] It is thus an obvious assumption that this liberated proligand competitively binds to the silica surface and reduces the amount of available reactive sites for the desired grafting reaction with $Ce(N\{SiHMe_2\}_2)_4$.

To find further support for this hypothesis, material **H1** was suspended in *n*-hexane and exposed to $HN(SiHMe_2)_2$. DRIFT spectroscopy could be employed to gain qualitative insight into the amount of non-interacting surface silanol groups. Figure 6b shows this DRIFTS study, comparing the spectra of **H1** before and after treatment with $HN(SiHMe_2)_2$ with that of hybrid material **H2**, where $Ce(N\{SiHMe_2\}_2)_4$ was directly grafted onto MSN-MCM-41_{500}-c. The Si–OH stretching vibration at 3740 cm^{-1} that is still clearly visible in **H1** entirely vanished

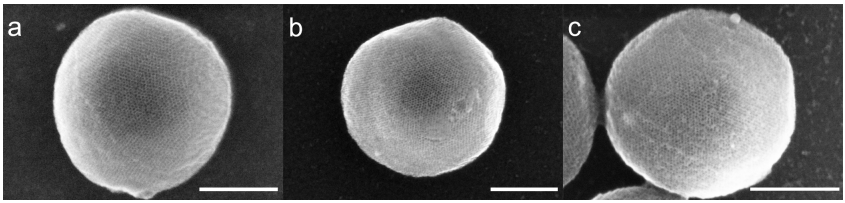

Figure 5. SEM micrographs of one particle each of the parent material MSN-MCM-41_{500} (a) and the corresponding hybrid material La[$N(SiMe_3)_2$]$_3$@MSN-MCM-41_{500} before (b) and after (c) use in MPV catalysis. The scale bars correspond to 100 nm.

upon treatment with $HN(SiHMe_2)_2$, while the spectrum of **H2** only shows a small and broadened band, indicating that a much larger number of surface silanol groups than in **H1** has been consumed despite the lower metal content.

Scheme 11. Surface silylation of an activated silica surface with $HN(SiHMe_2)_2$ by grafting of $SiHMe_2$ groups.

Success of the grafting reactions was further corroborated by DRIFT spectroscopy, where the sharp band of the OH-stretching vibrations of the surface-isolated Si–OH at 3740 cm^{-1} provides a convenient spectroscopic probe to monitor the grafting process and judge its successful completion. Figure 6a shows the DRIFT spectra of parent material MSN-MCM-41_{500}-a, complex **4**, and the hybrid material resulting from the grafting reaction of both. The spectrum of the hybrid material shows bands stemming from the parent material as well as those arising from the organometallic complex. The remaining band from Si–OH groups still visible in the hybrid material's spectrum shows that not all silanol groups on the parent material's surface were consumed in the grafting reaction.

To confirm the stability of the hybrid materials, and rule out mere adsorption of the organometallic complexes into the pores, leaching experiments were performed, and analysis of the supernatant by ICP-OES showed the absence of any

traces of metal. Furthermore, the hybrid materials were stored at −35 °C for prolonged periods of time (up to several weeks), and showed little to no decrease in activity. Only in the case of immobilized Ce(III) species, some problems with storage became apparent, with slight color changes in the regions of the powder exposed most to the atmosphere even at low temperatures, and within hours if left openly exposed to the glovebox atmosphere.*

Table 4. N_2 physisorption and ICP-OES characterization data of all of $Ln(L)_n$@MSN-MCM-41_{500} hybrid materials before and after use in MPV catalysis.

Material	a_{BET}[a] /$m^2\,g^{-1}$	V_{pore}[b] /$cm^3\,g^{-1}$	d_{pore}[c] /nm	**wt% metal**[d] /$mmol\,g^{-1}$
[Ce(O*i*Pr)$_4$]$_3$@MSN-MCM-41_{500}-a (**H1**)	786	0.47	1.8	9.8
[Ce(O*i*Pr)$_4$]$_3$@MSN-MCM-41_{500}-a (**H1'**)[e]	791	0.48	1.8	
Ce(N{SiMe$_3$}$_2$)$_3$@MSN-MCM-41_{500}-a (**H3**)	824	0.41	1.8	10.8
HO*i*Pr@Ce(N{SiMe$_3$}$_2$)$_3$@MSN-MCM-41_{500}-a (**H3a**)[f]				11.3
La(N{SiMe$_3$}$_2$)$_3$@MSN-MCM-41_{500}-b (**H4**)	903	0.54	2.0	10.2
HO*i*Pr@La(N{SiMe$_3$}$_2$)$_3$@MSN-MCM-41_{500}-a (**H4a**)	754	0.47	1.8	10.0
Ce(N{SiHMe$_2$}$_2$)$_4$@MSN-MCM-41_{500}-c (**H2**)	758	0.43	1.7	5.0
HO*i*Pr@Ce(N{SiHMe$_2$}$_2$)$_4$@MSN-MCM-41_{500}-c (**H2a**)[f]				7.1

[a] BET surface area calculated between p/p_0 0.07 and 0.15.
[b] BJH desorption cumulative pore volume between 1.5 and 4.5 nm. [c] Maximum pore diameter from the BJH desorption branch. [d] Determined by ICP-OES. [e] The hybrid material denoted **H1'** has been used in catalysis once before. [f] N_2-physisorption data could not be acquired due to volatile compounds stemming from catalysis experiments that were not removable from the pores without destroying surface-grafted complexes.

While the immobilization of the catalyst on a solid support yields several advantages for application in catalysis, as stated in the introductory section, it limits the application of liquid-state NMR spectroscopy as one of the most important and versatile analytic techniques available. Even though more sophisticated

*That this was not a problem with excessive O_2 or H_2O within the glovebox was checked by leaving some NaK-alloy exposed to the atmosphere for some time, which showed no signs of matting.

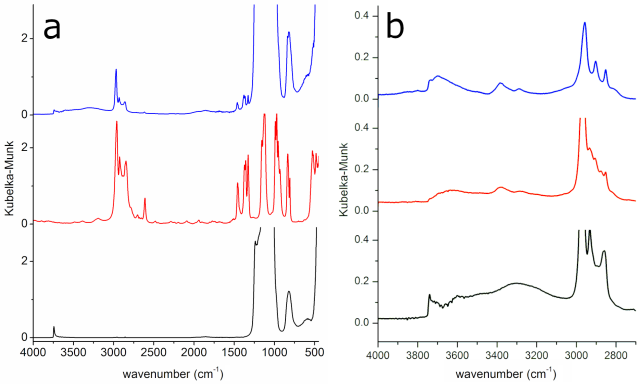

Figure 6. a: DRIFT spectra of parent material MSN-MCM-41$_{500}$-a (bottom), complex **4** (middle), and hybrid material [Ce(O*i*Pr)$_4$]$_3$@MSN-MCM-41$_{500}$ (**H1**) (top). **b**: DRIFT spectra of [Ce(O*i*Pr)$_4$]$_3$@MSN-MCM-41$_{500}$ (**H1**) before (bottom) and after (middle) silylation with HN(SiHMe$_2$)$_2$, as well as of Ce(N{SiHMe$_2$}$_2$)$_4$@MSN-MCM-41$_{500}$ (**H2**).

experiments are not available, and the general sensitivity is reduced requiring increased acquisition times, there are still important insights available from the results of solid-state NMR spectroscopy studies. Furthermore, as Ce(III) is paramagnetic, which leads to significant line broadening as well as a concentration dependence of resonances from nuclei in proximity to the Ce(III) nucleus, only materials involving Ce(IV) species were investigated.

The ^{1}H MAS NMR spectra of parent and hybrid materials revealed several interesting facts that generally supported the underlying hypotheses concerning the grafting process, and confirmed the success of post-synthetic ligand exchange from silylamide to alkoxide complexes. Figure 7 shows the obtained spectra for the parent material as well as those of a hybrid material generated by directly grafting a Ce(IV) alkoxide ([Ce(O*i*Pr)$_4$]$_3$) and those of a hybrid material generated post-synthetically by grafting a silylamide (Ce(N{SiHMe$_2$}$_2$)$_4$) and later exposing it to *i*PrOH to achieve a protonolytic ligand exchange (the post-synthetic ligand exchange was performed in situ in the reaction mixture for a catalysis experiment).

The spectrum obtained from the parent material (Figure 7, left, a) shows two major peaks that are attributable to the surface-isolated Si–*OH* groups (1.1 ppm)

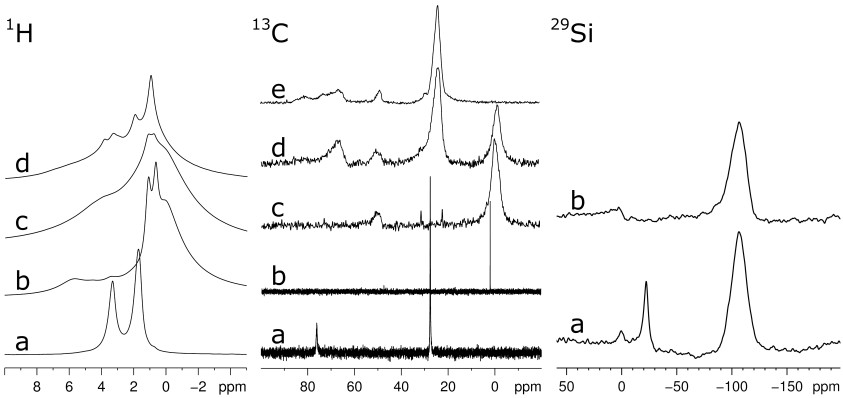

Figure 7. Solid-state NMR spectra of parent and hybrid materials. Left: ^{1}H-MAS solid-state NMR spectra of parent material MSN-MCM-41$_{500}$ (a), Ce(N{SiHMe$_2$}$_2$)$_4$@MSN-MCM-41$_{500}$ (**H2**) (b), *i*PrOH@Ce(N{SiHMe$_2$}$_2$)$_4$@MSN-MCM-41$_{500}$ (**H2a**) (c), and [Ce(O*i*Pr)$_4$]$_3$@MSN-MCM-41$_{500}$ (**H1**) (d). Middle: liquid-state ^{13}C{^{1}H} NMR spectra of [Ce(O*i*Pr)$_4$]$_3$ (a) and Ce(N{SiHMe$_2$}$_2$)$_4$ (b), as well as ^{13}C{^{1}H} CPMAS NMR spectra of Ce(N{SiHMe$_2$}$_2$)$_4$@MSN-MCM-41$_{500}$ (**H2**) (c), *i*PrOH@Ce(N{SiHMe$_2$}$_2$)$_4$@MSN-MCM-41$_{500}$ (**H2a**) (d), and [Ce(O*i*Pr)$_4$]$_3$@MSN-MCM-41$_{500}$ (**H1**) (e). Right: ^{29}Si HPDEC solid-state NMR spectra of Ce(N{SiHMe$_2$}$_2$)$_4$@MSN-MCM-41$_{500}$ (**H2**) (a) and *i*PrOH@Ce(N{SiHMe$_2$}$_2$)$_4$@MSN-MCM-41$_{500}$ (**H2a**) (b).

and to surface grafted methoxy groups stemming from the solvent extraction process in the material synthesis (3.3 ppm; see also experimental section in **Paper II**).[82] That these methoxy groups persist even after the grafting process can be seen in the ^{13}C CP/MAS NMR spectra of the hybrid materials (Figure 7, middle, c-e), where they are visible as a peak around 50 ppm, while their peaks in the ^{1}H spectra are more difficult to identify due to the large linewidth and overlap between the signals.

The ^{1}H NMR spectrum of material **H1** revealed several new signals, but also shows that the consumption of surface Si–*OH* groups was incomplete, as the signal at 1.1 ppm is still clearly visible, while it has vanished completely in the case of materials **H2** and **H2a**, indicating complete consumption of those groups. The spectrum of **H2** further shows a new signal at 5.7 ppm, attributable to the Si–*H* groups of the grafted Ce(N{SiHMe$_2$}$_2$)$_4$ that has vanished in the spectrum for **H2a**, confirming successful ligand exchange.

The $^{13}C\{^1H\}$ CP/MAS NMR spectra also showed very broad signals, due to the much greater chemical shift range in ^{13}C spectra, however, there was no significant overlap between the signals, much simplifying peak assignment and interpretation of the spectra. Figure 7 (middle) shows a comparison of the liquid-state spectra of $[Ce(O\mathit{i}Pr)_4]_3$ and $Ce(N\{SiHMe_2\}_2)_4$ with the solid state spectra of **H1**, **H2**, and **H2a**. As mentioned above, the peak at ca. 50 ppm in the solid state spectra stems from surface grafted methoxy groups from the material synthesis. The spectra of $Ce(N\{SiHMe_2\}_2)_4$, **H2**, and **H2a** (Figure 7, middle, b-d) all show the methyl resonance of $SiH\mathit{Me}_2$ at -2 ppm, lending further credibility to the hypothesis that during the ligand exchange of the silylamido ligands in **H2** for alkoxo ligands to form **H2a**, significant surface silylation by the liberated $HN(SiHMe_2)_2$ takes place.

Comparison of the spectra of **H1** and **H2a** with the solution-state spectrum of $[Ce(O\mathit{i}Pr)_4]_3$ indicated that both hybrid materials indeed contain Ce(IV) isopropoxide species, as both show the same signal set also present in the liquid-state spectrum (signal for $OCH(CH_3)_2$ at ca. 67 ppm and signal for $OCH(CH_3)_2$ at 23.5 ppm) in addition to the methoxy signal mentioned earlier, and, in the case of **H2a**, the methyl signal stemming from surface silylation.

Since surface silylation involves the fragmentation of $HN(SiHMe_2)_2$ into NH_3 and two $SiHMe_2$ moieties, which show a significant chemical shift difference from the parent compound in the ^{29}Si NMR spectrum (δ (^{29}Si) for $HN(\mathit{Si}HMe_2)_2$ in C_6D_6: -22.8 ppm), ^{29}Si HPDEC solid-state NMR spectroscopy could be used to confirm the ligand surface silylation in both **H2** and **H2a** as well as the successful ligand exchange (see Figure 7, right). While **H2** shows both the resonance of the $N(SiHMe_2)_2$ ligand at ca. -22 ppm and the $SiHMe_2$ surface moiety at 0.6 ppm, the spectrum of **H2a** only shows the latter.

N_2-physisorption measurements of the hybrid materials largely gave the expected results: The specific surface area a_{BET} and pore volume V_{pore}, as well as the pore diameter d_{pore} all decreased due to the newly formed layer of grafted complex molecules on the silica surface. Surprisingly, material **H2** showed a bimodal pore-size distribution, with one set of pores with strongly reduced diameter, and one set of pores where the reduction was only very minor (see Figure 8). A possible explanation for this is that the trimeric precursor complex **4**, after being grafted near the pore entrances, blocks the inner volume of the pores, making it inaccessible for further precursor molecules. Even though the molar amount of grafted complex is thus reduced, the metal content of **H1** is in the same range as that of the other hybrid materials due to its trimeric nature.

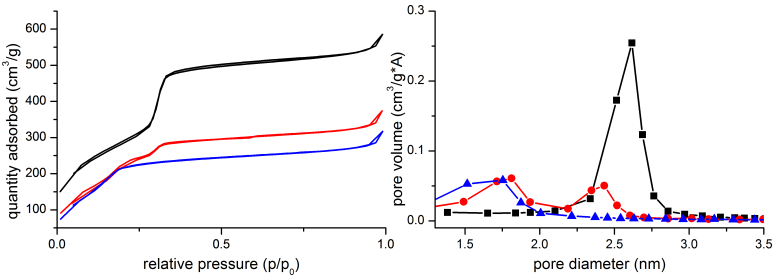

Figure 8. N_2-physisorption isotherms (left) and dV/dD pore size distributions (right) of parent material MSN-MCM-41$_{500}$-a (black) and hybrid materials **H1** (red) and **H3** (blue). The bimodal pore-size distribution in **H1** is clearly visible in the isotherm as two separate adsorption steps between p/p$_0$ 0.0 and 0.3.

Homogeneous and Heterogeneous Catalysis

All rare-earth metal derived complexes and hybrid materials were able to act as homogeneous and heterogeneous catalysts in the MPV reduction (ca. 5 mol% metal). Even AlO*i*Pr$_3$, however, whose performance was used as a baseline against which all rare-earth-metal based catalysts were measured, showed markedly increased performance when compared to the literature reports stating the necessity of using superstoichiometric amounts of catalyst. As some earlier records have already indicated,[49] this can likely be attributed to the rigorous exclusion of O_2 and H_2O from the reaction system, which prevented inactivation of the catalyst. At a metal loading of 5 mol% aluminum, the classical MPV catalyst was able to completely catalyze the reduction of 4-*t*Bu-cyclohexanone to the corresponding *cis*- and *trans*-4-*t*Bu-cyclohexanol within 24 h (see Table 5, entry 1).

All rare-earth metal complexes that were used as homogeneous catalysts in the same reaction and under the same conditions, however, were able to significantly outperform the aluminum-based catalyst, and of the hybrid materials there was only one that did not reach the benchmark set by the reaction with AlO*i*Pr$_3$. Among the rare-earth-metal based catalysts, however, there were clear trends observable: All Ce(IV)-based catalysts showed inferior performance compared to their Ce(III)-based counterparts, and all heterogeneous catalysts showed slightly reduced activity in comparison to homogeneous catalysis with the respective

precursor. While the latter difference can be explained with restricted diffusion of substrate within the pores of the parent material, the former demands a closer look into the MPV reaction system and the factors influencing the catalytic cycle. Since the MPV reduction depends on the formation and subsequent disbanding of a six-membered, cyclic transition state (ref. Scheme 7), several, sometimes conflicting, factors are involved: For the activation of the substrate, a highly Lewis-acidic metal center is desirable, while on the other hand the metal center should not be too oxophilic, in order to enable a fast ligand exchange and thus a fast turnover rate. The results for the Ce(IV)-based catalysts show how these factors can counteract each other, with the higher Lewis-acidity of Ce(IV) compared to Ce(III) also leading to a higher oxophilicity, thus reducing the ligand exchange ability and ultimately the catalytic activity of the corresponding complexes and heterogeneous catalysts based on them.

Using Ce(III)-based catalysts in the MPV reduction gave better results, however, due to the high surface area and site isolation of the heterogeneous catalysts, those were exceedingly sensitive against exposure to oxygen and water, showing a color change even under Ar atmosphere with <1 ppm of O_2 and H_2O present, respectively. This resulted in a reduced recyclability in catalytic reactions (see Table 5, entries 6 and 7).

To counteract this, and make the heterogeneous catalysts more resilient, La(III) alkoxides and silylamides were used as (pre-)catalysts, as La(III) can not be oxidized chemically. Not only did this indeed increase the recyclability of the respective heterogeneous catalysts, but the base activity of the catalysts was also increased (see Table 5, entries 11–13).

Heterogenizing the organometallic catalysts also had a noticeable effect on the configuration of the resulting alcohols, and significantly increased the amount of *trans*-4-*t*Bu-cyclohexanol in the product mixture (*trans*:*cis* 2.9-3.7:1 vs. ca. 2:1 for homogeneous catalysts, see Table 5). This seems to be an effect of the pore confinement in the hybrid materials, as the variations were only tied to whether a homogeneous or heterogeneous catalyst was used, while the specifics of the catalysts themselves (metal center and ligand environment) played a negligible role. Space restrictions imparted by the pore geometry of the hybrid materials thus seem to favor the generation of the *trans*-alcohol, most likely by favoring the corresponding transition state over that leading to the *cis*-alcohol.

Table 5. Catalytic activities of Ln-based catalysts in the MPV reduction of 4-*t*Bu-cyclohexanone at ambient temperature

Entry	(Pre-)catalyst	mol% M	Conversion/% (*trans:cis*)	
			1 h	24 h
1	$Al(OiPr)_3$	5.1	<1	>99 (2.0)
2	MSN-MCM-41_{500}-c	n/a[a]	0	0
3	$[Ce(OiPr)_4]_3$ (**1**)	5.1	29 (1.9)	>99 (2.2)
4	$[Ce(OCH_2tBu)_3]_4$[b]	5.0	>99 (2.2)	n/a
5	$La(N\{SiMe_3\}_2)_3$	5.0	>99[c] (2.2)	n/a
6[d]	$[Ce(OiPr)_4]_3$@MSN-MCM-41_{500}-a (**H1**)	5.3	n/a	>99 (2.9)
7[d]	$[Ce(OiPr)_4]_3$@MSN-MCM-41_{500}-a (**H1′**)[e]	5.0	n/a	84 (3.1)
8	$Ce(N\{SiHMe_2\}_2)_4$@MSN-MCM-41_{500}-c (**H2**)	5.0	18 (3.4)	65 (3.7)
9	$Ce(N\{SiMe_3\}_2)_3$@MSN-MCM-41_{500}-a (**H3**)	5.0	84 (3.1)	>99 (3.0)
10	$Ce(N\{SiMe_3\}_2)_3$@MSN-MCM-41_{500}-a (**H3′**)[e]	5.0	70 (3.2)	>99 (3.1)
11	$La(N\{SiMe_3\}_2)_3$@MSN-MCM-41_{500}-b (**H4**)	5.0	97 (2.8)	>99 (3.0)
12	$La(N\{SiMe_3\}_2)_3$@MSN-MCM-41_{500}-b (**H4′**)[e]	5.0	70 (3.6)	>99 (3.1)
13	$La(N\{SiMe_3\}_2)_3$@MSN-MCM-41_{500}-b (**H4″**)[e]	5.0	55 (3.2)	n/a[f]
14[g]	$Nd(OCtBu_3)_3$	1.4	95 (2.7)	>99 (2.6)
15[g]	$Nd(N\{SiMe_3\}_2)_3$@MSN-MCM-41_{100}[h]	1.9	30 (3.3)	>99 (3.3)

[a] 96 mg, calculated as 5.3 % Si–OH. [b] $[Ce(OCH_2tBu)_3]_4$ was chosen as a cerous alkoxide due to its better solubility compared to $[Ce(OiPr)_3]_n$. [c] >99 % already after 15 min. [d] Performed at 60 °C due to the low activity of the Ce(IV)-based catalyst. [e] Hybrid materials denoted **HX′** have been used in catalysis once before and those denoted **HX″** two times. [f] 83 % conversion after 5 h. [g] Values taken from earlier reports.[50] [h] The parent material was dehydroxylated at 100 °C and $1 \cdot 10^{-3}$ mbar for 3 h.

Part C.

Unpublished Results

Oppenauer Oxidation

After successfully exploring the use of heterogenized rare-earth-metal alkoxides in MPV-reduction catalysis, the obvious next goal was their application in the Oppenauer oxidation. In the classical form with $Al(OiPr)_3$, this simply requires an exchange of substrate and solvent to shift the equilibrium and reverse the direction of the reaction shown in Scheme 7. Similarly to the benchmark reaction of the MPV reduction (Table 5, entry 1), this was achieved with catalytic amounts of $Al(OiPr)_3$ when performing the reaction under an inert atmosphere (see Table 6, entry 1).

In a series of exploratory experiments, it was attempted to replicate this reaction using rare-earth-metal based homogeneous catalysts with the same reaction conditions. The use of acetone as solvent and oxidant, however, proved to be impossible due to a competing catalytic pathway involving aldol-type coupling reactions between acetone molecules that result in the formation of several addition and condensation products up to phorone (see Scheme 12). This type of coupling reaction, and the formation of trivalent rare-earth-metal complexes involving diacetone alkoxy ligands had been described in 1992 by Teuben et al.[71]

Especially in the reactions involving heterogeneous catalysts (**H1** and **H4**), it was possible to identify (using GC/MS) all intermediate stages during the condensation of three molecules of acetone to give phorone as the end product (diacetone alcohol, mesityl oxide, semiphorone and phorone). The fact that the reactions with heterogeneous catalysts yielded the largest amounts of semiphorone and phorone might hint at an involvement of residual Si–OH groups on the silica surface that might play a role as acidic catalyst for the condensation step depicted in scheme 12.

To circumvent this problem while at the same time retaining the use of the reaction solvent as a sacrificial oxidant, and thus keeping the catalytic equilibrium favorable, the possibility of utilizing non-enolizable solvents bearing a keto or aldehyde functionality was examined. Based on toxicological as well as availability considerations, benzaldehyde and hexachloroacetone were identified as possible candidates for this role. When used in a catalytic setup, however, both led to failed attempts, with the reactions involving benzaldehyde showing no reaction at all. It can be assumed that benzaldehyde, bearing a large phenyl ring in place of a methyl group in acetone, might be too sterically demanding to be able to participate in the transition state necessary for the Oppenauer oxidation.

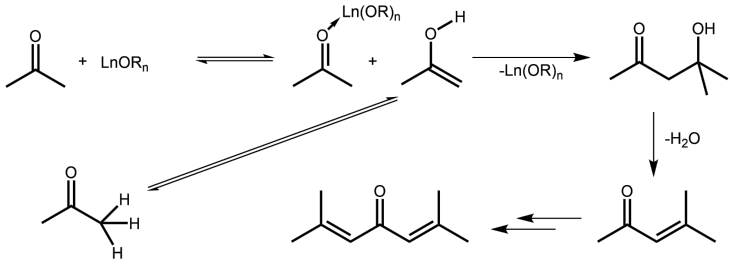

Scheme 12. Reaction scheme for the rare-earth metal-catalyzed aldol addition and subsequent condensation of acetone.

The reactions involving hexachloroacetone, on the other hand, showed an immediate strong color change to a very dark blue upon addition of the catalyst ($Ce(N\{SiMe_3\}_2)_3$), and aldol-type reaction products similar to the reactions involving acetone after some time. The compound responsible for the dark color could be identified as the ceric $Ce(N\{SiMe_3\}_2)_3Cl$, revealing hexachloroacetone as another possible chlorinating oxidant for use in Ce(III)/(IV) chemistry. In a further, albeit non-optimized attempt at this oxidation reaction, $Ce(N\{SiMe_3\}_2)_3Cl$ could be obtained in 56 % crystalline yield.

Literature research on rare-earth-metal based Oppenauer oxidation led to a report by Kagan et al.[64] about the use of samarium iodo-alkoxides as catalysts in the Oppenauer oxidation of several alcohols of different molecular complexity. Owing to this article's focus on the organic chemistry of this reaction system, the catalyst was neither isolated nor directly identified, and the reaction mechanism was not elucidated. Crucially, the catalyst, termed "SmI_2O*t*Bu", was used as-is after synthesis without any workup procedure (see Scheme 8), which was acknowledged by the authors as such.

Directly recreating this reaction, and using the resulting mixture in the Oppenauer oxidation of *n*-octanol with 8 equivalents of methyl-ethyl ketone (MEK) in THF, gave the expected results, driving the oxidation to completion in under 1 h (see Table 6, entry 11). It was also possible, however, to isolate the proposed catalyst, and crystallographically identify it as SmI_2O*t*$Bu(thf)_4$, which had been structurally described by Barbier-Baudry et al. in 2001.[72]

Interestingly, when this compound was isolated, purified and used under otherwise identical conditions as a catalyst for the Oppenauer oxidation, it showed

no catalytic activity at all, ruling it out as the catalytically active species in the original reaction. So far, however, the identification of the catalytic species in this reaction was not possible, nor even to ascertain if a single species or a combination of partial reactions is responsible for the successful catalytic oxidation.

Table 6. Catalytic activities of Ln-based catalysts in the Oppenauer oxidation of 4-*t*Bu-cyclohexanol at ambient temperature.

(Pre-)catalyst	mol% M	Solvent	Substrate	Oxidant	T	Conversion/%	
						1 h	24 h
$Al(OiPr)_3$	5.12	Acetone	4-*t*Bu-cyclohexanol	Acetone	rt	<1	3[a]
$Ce(N\{SiMe_3\}_2)_3$	4.96	Acetone	4-*t*Bu-cyclohexanol	Acetone	rt	<1	<1[b]
$Ce(N\{SiMe_3\}_2)_3$	4.93	Acetone-Cl_6	4-*t*Bu-cyclohexanol	Acetone-Cl_6	rt	<1	<1
$Ce(OCH_3tBu)_3$	5.04	Acetone	4-*t*Bu-cyclohexanol	Acetone	rt	<1	<1
$Ce(OCH_3tBu)_3$	5.01	THF	4-*t*Bu-cyclohexanol	MEK[c]	rt	<1	<1
$[Ce(OiPr)_4]_3$	4.96	Benzaldehyde	4-*t*Bu-cyclohexanol	Benzaldehyde	rt	<1	<1
$[Ce(OiPr)_4]_3$@ MSN-MCM-41_{500} (**H1**)	5.00	Acetone	4-*t*Bu-cyclohexanol	Acetone	rt	<1	<1
$La(N\{SiMe_3\}_2)_3$@ MSN-MCM-41_{500} (**H4**)	2.55	Acetone	4-*t*Bu-cyclohexanol	Acetone	rt	<1	<1[d]
$SmI_2OtBu(thf)_4$	4.12	THF	2-octanol	MEK[e]	65 °C	<1	<1
"$SmI_2OtBu(thf)_4$"	5.02	THF	2-octanol	MEK[c]	65 °C	24	30
"$SmI_2OtBu(thf)_4$"	10.00	THF	2-octanol	MEK[c]	65 °C	86	91
$LaI_3(thf)_{3.7}$	10.00	THF	2-octanol	MEK[c]	rt	<1	<1

[a] Conversion after 25 h. [b] Conversion after 3 h. [c] 8 equiv. based on the amount of substrate.
[d] Conversion after 22 h. [e] 6.7 equiv. based on the amount of substrate.

Experimental Details

General Considerations. All experiments were conducted under rigorous exclusion of air and moisture in an argon atmosphere, using Schlenk and glovebox (MBraun MB150B-G-II) techniques. Acetone was dried by stirring over $CaSO_4$ over night and distilling it afterwards. It was stored in a Schlenk flask over molecular sieve (4 Å). THF was dried with a Grubbs-type column (MBraun MB SPS-800) and stored in a glovebox over molecular sieve. All other liquids were dried by storing them over a generous amount of molecular sieve for at least one week. Solid chemicals were stored in a glovebox and used as received.

SmI_2O*t*Bu. $SmI_2(thf)_{1.97}$ (209.9 mg, 0.384 mmol) was dissolved in THF (ca. 5 ml), di-*tert*-butyl-peroxide ($C_8H_{18}O_2$, 28.1 mg, 0.192 mmol, 0.50 eq.) was likewise mixed with THF (ca. 5 ml). The peroxide solution was slowly added to the solution of $SmI_2(thf)_{1.97}$. After being stirred over night, the solution had changed its color from green to pale yellow. The solvent was removed in vacuo, 286.5 mg SmI_2O*t*Bu$(thf)_4$ (0.374 mmol, 97 %) was received as yellow crystals. Anal. calcd. for $C_{20}H_{41}I_2O_5Sm$ (765.71 g mol^{-1}): C, 31.37; H, 5.40. Found: C, 30.84; H, 5.13.

Ce(N{SiMe$_3$}$_2$)$_3$Cl. Ce(N{SiMe$_3$}$_2$)$_3$ ($C_{18}H_{54}CeN_3Si_6$, 270.4 mg, 0.435 mmol) was dissolved in 8 ml *n*-hexane in a Schlenk flask. Via a septum, ca. 0.1 ml acetone-Cl_6 ($CO(CCl_3)_2$, ca. 0.66 mmol) was added and briefly mixed by shaking. After being left standing over night, the solvent was removed in vacuo to yield a dark solid the turned out to be two mixed compounds. Ce(N{SiMe$_3$}$_2$)$_3$Cl could be removed from this mixture by dissolving it in *n*-hexane, which left a brown solid that was only soluble in THF and was not investigated further. From the *n*-hexane fraction, the solvent was evaporated again to give 160.2 mg (56 %) Ce(N{SiMe$_3$}$_2$)$_3$Cl as a dark purple, crystalline solid. ^{1}H NMR (C_6D_6, 400.16 MHz, 299 K): δ 0.41 (s, I = 1.0 a.u.), 0.43 (s, I = 2.5 a.u.) ppm. ^{13}C NMR (C_6D_6, 100.6 MHz, 298 K): δ 4.61 (Si*Me*$_3$) ppm.

Catalysis. For a typical catalysis reaction done as a reversal of the MPV reactions, the catalyst together with a stir bar and the substrate were placed in 50 ml Schlenk flasks each inside the glovebox. Outside the glovebox, 5 ml of dry acetone were added to each Schlenk flask with a syringe. The substrate solution was then transferred to the flask containing the catalyst with a steel cannula and the reaction mixture was stirred for the course of the reaction. For GC analysis, samples of 0.1 ml each were taken with syringes at set intervals (usually 15 min, 1 h, 2 h, 3 h and, where required, 24 h). Identification of side products was done using GC-MS analyses provided by the mass-spectrometry department of the department for organic chemistry.

Catalytic reaction with Al(O*i*Pr)$_3$ in acetone. Al(O*i*Pr)$_3$ (20.9 mg, 0.102 mmol. 5 %) and 312.1 mg 4-*t*Bu-cyclohexanone (1.997 mmol) were dissolved in 5 ml acetone in a 25 ml Schlenk flask inside a glovebox each. Outside the glovebox, the substrate solution was added to the catalyst solution via a steel cannula, and the resulting reaction mixture was stirred for several days. Samples for GC analysis of 0.1 ml each were taken via syringe at 15 min, 1 h, 2 h, 3 h, 25 h and 122 h.

Catalytic reaction with Ce(N{SiMe$_3$}$_2$)$_3$ in acetone. Ce(N{SiMe$_3$}$_2$)$_3$ (60.2 mg, 0.097 mmol, 4.98 %) and 304.0 mg 4-*t*Bu-cyclohexanone (1.945 mmol) were dissolved in 5 ml acetone in a 25 ml Schlenk flask inside a glovebox each. Outside the glovebox, the substrate solution was added to the catalyst solution via a steel cannula, and the resulting reaction mixture

was stirred for several days. Samples for GC analysis of 0.1 ml each were taken via syringe at 15 min, 1 h, 2 h, 3 h and 123 h.

Catalytic reaction with Ce(N{SiMe$_3$}$_2$)$_3$ in acetone-Cl$_6$. Ce(N{SiMe$_3$}$_2$)$_3$ (61.2 mg, 0.099 mmol, 4.93 %) and 312.0 mg 4-*t*Bu-cyclohexanone (1.997 mmol) were dissolved in 5 and 11 ml acetone-Cl$_6$, respectively, in a 25 ml Schlenk flask inside a glovebox each. When adding the solvent to the catalyst, an immediate color change from bright yellow to dark cherry-red was observed. Outside the glovebox, the substrate solution was added to the catalyst solution via a steel cannula, and the resulting reaction mixture was stirred for 24 h. During the first hour, the colour changed from deep red to a translucent orange. Samples for GC analysis of 0.1 ml each were taken via syringe at 15 min, 1 h, 2 h and 24 h.

Catalytic reaction with Ce(OCH$_3$*t*Bu)$_3$ in acetone. Ce(OCH$_3$*t*Bu)$_3$ (42.1 mg, 0.105 mmol, 5.04 %) and 325.8 mg 4-*t*Bu-cyclohexanone (2.085 mmol) were dissolved in 5 ml acetone in a 25 ml Schlenk flask inside a glovebox each. Outside the glovebox, the substrate solution was added to the catalyst solution via a steel cannula, and the resulting reaction mixture was stirred for 3 h. Immediately after addition of the substrate solution, a color change from nearly colorless to yellow was observed. Samples for GC analysis of 0.1 ml each were taken via syringe at 15 min, 1 h, 2 h and 3 h.

Catalytic reaction with Ce(OCH$_3$*t*Bu)$_3$ in THF with MEK as oxidant. Ce(OCH$_3$*t*Bu)$_3$ (20.1 mg, 0.050 mmol, 5.01 %) was dissolved in 2 ml THF in a screw-cap vial inside a glovebox. 155.8 mg 4-*t*Bu-cyclohexanone (0.997 mmol) and 580.1 mg MEK (8.044 mmol, 8.07 equiv.) were dissolved in 3 ml THF in a screw-cap vial inside a glovebox each. The MEK solution was added to the catalyst solution, the resulting solution became turbid and peach colored. After 5 min, the substrate solution was added and the resulting reaction mixture was stirred for 4 days. Samples for GC analysis of 0.1 ml each were taken with glass pasteur pipettes at 15 min, 1 h, 2 h, 3 h, 24 h and 96 h.

Catalytic reaction with [Ce(O*i*Pr)$_4$]$_3$ in benzaldehyde. [Ce(O*i*Pr)$_4$]$_3$ (37.3 mg, 0.099 mmol, 4.96 %) and 311.8 mg 4-*t*Bu-cyclohexanone (1.995 mmol) were dissolved in 5 ml acetone in a 25 ml Schlenk flask inside a glovebox each. Upon addition of benzaldehyde to the catalyst dissolved and a colour change from yellow to dark orange was observed. Outside the glovebox, the substrate solution was added to the catalyst solution via a steel cannula, and the resulting reaction mixture was stirred for several days. Samples for GC analysis of 0.1 ml each were taken via syringe at 15 min, 1 h, 2 h and 24 h.

Catalytic reaction with [Ce(O*i*Pr)$_4$]$_3$@MSN-MCM-41$_{500}$ (H1) in acetone. H1 (100.6 mg, 0.070 mmol Ce, 4.95 %) and 220.6 mg 4-*t*Bu-cyclohexanone (1.412 mmol) were suspended and dissolved in 5 ml acetone in a 25 ml Schlenk flask inside a glovebox, respectively. Outside the glovebox, the substrate solution was added to the catalyst suspension via a steel cannula, and the resulting reaction mixture was stirred for 24 h. Samples for GC analysis of 0.1 ml each were taken via syringe at 15 min, 1 h, 2 h, 22 h and 24 h.

Catalytic reaction with La(N{SiMe$_3$}$_2$)$_3$@MSN-MCM-41$_{500}$ (H4) in acetone. H4 (69.5 mg, 0.051 mmol La, 2.55 %) and 312.1 mg 4-*t*Bu-cyclohexanone (1.997 mmol) were suspended and dissolved in 5 ml acetone in a 25 ml Schlenk flask inside a glovebox, respectively. Upon addition of acetone to the catalyst, development of smoke as well as a transient discoloration to yellow was observed. Outside the glovebox, the substrate solution was added to the catalyst suspension via a steel cannula, and the resulting reaction mixture was

stirred for several days. Samples for GC analysis of 0.1 ml each were taken via syringe at 15 min, 1 h and 22 h.

Catalytic reaction with isolated $SmI_2OtBu(thf)_4$. $SmI_2OtBu(thf)_4$. (27.8 mg, 0.036 mmol, 4.12 %) and 426.5 mg MEK (5.91 mmol, 6.72 equiv.) were dissolved in 3 ml THF each, then combined in a 25 ml Schlenk flask. 2-octanol (114.5 mg, 0.879 mmol) was dissolved in 2 ml THF inside a 25 ml Schlenk flask. Outside the glovebox, the oxidant solution was added to the catalyst-substrate mixture via a steel cannula. Upon addition of the oxidant, a color change from colorless to yellow was observed. The mixture was heated to 65 °C and stirred for 48 h. Samples for GC analysis of 0.1 ml each were taken via syringe at 15 min, 1 h, 19 h, 24 h and 48 h.

Preparation of catalyst solution 1. A stock solution of 11.77 mg ml^{-1} di-*tert*-butyl-peroxide was prepared. To 1 ml of this stock solution (11.77 mg, 0.080 mmol, 0.5 equiv.), a solution of 87.4 mg $SmI_2(thf)_{1.97}$ (0.160 mmol) in 2 ml THF was added. Immediately upon addition, a color change from deep blue-green to light yellow was observed. The mixture was left standing for 2 h and then used in the catalytic reaction in its entirety as **catalyst solution 1**.

Catalytic reaction with catalyst solution 1. 2-octanol (208.4 mg, 1.600 mmol) and 927.9 mg MEK (12.868 mmol, 8.04 equiv.) were mixed in 7 ml THF in a 25 ml Schlenk flask inside a glovebox. Outside the glovebox, **catalyst solution 1** was added via a steel cannula (3 ml, 0.160 mmol Sm, 10.00 %). The mixture was heated to 65 °C and stirred for 1 h. Samples for GC analysis of 0.1 ml each were taken via syringe at 15 min and 1 h.

Preparation of catalyst solution 2. To 0.5 ml of the stock solution from the synthesis of **catalyst solution 1** (5.89 mg, 0.040 mmol, 0.5 equiv.), a solution of 43.8 mg $SmI_2(thf)_{1.97}$ (0.080 mmol) in 2.5 ml THF was added. Immediately upon addition, a color change from deep blue-green to light yellow was observed. The mixture was left standing for 2 h and then used in the catalytic reaction in its entirety as **catalyst solution 2**.

Catalytic reaction with catalyst solution 2. 2-octanol (208.2 mg, 1.599 mmol) and 930.5 mg MEK (12.904 mmol, 8.07 equiv.) were mixed in 7.5 ml THF in a 25 ml Schlenk flask inside a glovebox. Outside the glovebox, **catalyst solution 2** was added via a steel cannula (2.5 ml, 0.080 mmol Sm, 5.02 %). The mixture was heated to 65 °C and stirred for 1 h. Samples for GC analysis of 0.1 ml each were taken via syringe at 15 min, 1 h, 2.5 h and 24 h.

Part D.

Bibliography

Bibliography

(1) Anwander, R.; Dolg, M.; Edelmann, F. T. The difficult search for organocerium(iv) compounds. *Chem. Soc. Rev.* **2017**, DOI: 10.1039/c7cs00147a.

(2) Palumbo, C. T.; Zivkovic, I.; Scopelliti, R.; Mazzanti, M. Molecular Complex of Tb in the +4 Oxidation State. *J. Am. Chem. Soc.* **2019**, *141*, 9827–9831, DOI: 10.1021/jacs.9b05337.

(3) Willauer, A. R.; Palumbo, C. T.; Zivkovic, I.; Fadaei Tirani, F.; Douair, I.; Maron, L.; Mazzanti, M. Accessing the + IV Oxidation State in Molecular Complexes of Praseodymium. *J. Am. Chem. Soc.* **2020**, DOI: 10.1021/jacs.0c01204.

(4) Willauer, A. R.; Palumbo, C. T.; Scopelliti, R.; Zivkovic, I.; Douair, I.; Maron, L.; Mazzanti, M. Stabilization of the Oxidation State +IV in Siloxide-Supported Terbium Compounds. *Angew. Chem. Int. Ed.* **2020**, *59*, 3549–3553, DOI: 10.1002/anie.201914733.

(5) Rice, N. T.; Popov, I. A.; Russo, D. R.; Bacsa, J.; Batista, E. R.; Yang, P.; Telser, J.; La Pierre, H. S. Design, Isolation, and Spectroscopic Analysis of a Tetravalent Terbium Complex. *J. Am. Chem. Soc.* **2019**, *141*, 13222–13233, DOI: 10.1021/jacs.9b06622.

(6) So, Y.-M.; Leung, W.-H. Recent advances in the coordination chemistry of cerium(IV) complexes. *Coord. Chem. Rev.* **2017**, *340*, 172–197, DOI: 10.1016/j.ccr.2016.12.009.

(7) Bradley, D. C.; Chatterjee, A. K.; Wardlaw, W. 671. Structural chemistry of the alkoxides. Part VII. Secondary alkoxides of quadrivalent cerium and thorium. *J. Chem. Soc.* **1956**, 3469–3472, DOI: 10.1039/jr9560003469.

(8) Nair, V.; Deepthi, A. Cerium(IV) ammonium nitrate–a versatile single-electron oxidant. *Chem. Rev.* **2007**, *107*, 1862–91, DOI: 10.1021/cr068408n.

(9) Nair, V.; Deepthi, A. Recent advances in CAN mediated reactions in organic synthesis. *Tetrahedron* **2009**, *65*, 10745–10755, DOI: 10.1016/j.tet.2009.10.083.

(10) Fraser, R. R.; Mansour, T. S.; Savard, S. Acidity measurements on pyridines in tetrahydrofuran using lithiated silylamines. *J. Org. Chem.* **1985**, *50*, 3232–3234, DOI: 10.1021/jo00217a050.

(11) Anwander, R. SOMC@PMS. Surface Organometallic Chemistry at Periodic Mesoporous Silica. *Chem. Mater.* **2001**, *13*, 4419–4438, DOI: 10.1021/cm0111534.

(12) Werner, D.; Bayer, U.; Rad, N. E.; Junk, P. C.; Deacon, G. B.; Anwander, R. Unique and contrasting structures of homoleptic lanthanum(iii) and cerium(iii) 3,5-dimethylpyrazolates. *Dalton Trans.* **2018**, *47*, 5952–5955, DOI: 10.1039/c8dt00338f.

(13) Crozier, A. R.; Bienfait, A. M.; Maichle-Mössmer, C.; Törnroos, K. W.; Anwander, R. A homoleptic tetravalent cerium silylamide. *Chem. Commun.* **2013**, *49*, 87–9, DOI: 10.1039/c2cc37404h.

(14) Schneider, D.; Spallek, T.; Maichle-Mössmer, C.; Törnroos, K. W.; Anwander, R. Cerium tetrakis(diisopropylamide)–a useful precursor for cerium(IV) chemistry. *Chem. Commun.* **2014**, *50*, 14763–6, DOI: 10.1039/c4cc06228k.

(15) Werner, D.; Deacon, G. B.; Junk, P. C.; Anwander, R. Cerium(III/IV) formamidinate chemistry, and a stable cerium(IV) diolate. *Chemistry* **2014**, *20*, 4426–38, DOI: 10.1002/chem.201304582.

(16) Williams, U. J.; Schneider, D.; Dorfner, W. L.; Maichle-Mössmer, C.; Carroll, P. J.; Anwander, R.; Schelter, E. J. Variation of electronic transitions and reduction potentials of cerium(IV) complexes. *Dalton Trans.* **2014**, *43*, 16197–206, DOI: 10.1039/c4dt01386g.

(17) Levin, J. R.; Dorfner, W. L.; Dai, A. X.; Carroll, P. J.; Schelter, E. J. Density Functional Theory as a Predictive Tool for Cerium Redox Properties in Nonaqueous Solvents. *Inorg. Chem.* **2016**, *55*, 12651–12659, DOI: 10.1021/acs.inorgchem.6b01779.

(18) Werner, D.; Deacon, G. B.; Junk, P. C.; Anwander, R. Pyrazolates advance cerium chemistry: a Ce(III)/Ce(IV) redox equilibrium with benzoquinone. *Dalton Trans.* **2017**, *46*, 6265–6277, DOI: 10.1039/c7dt00635g.

(19) Bradley, D. C.; Chatterjee, A. K.; Wardlaw, W. Primary alkoxides of quadrivalent cerium and thorium. *J. Chem. Soc.* **1956**, 2260–2264, DOI: 10.1039/JR9560002260.

(20) Bradley, D. C.; Chatterjee, A. K.; Wardlaw, W. 506. Structural chemistry of the alkoxides. Part IX. tert.-Alkoxides of quadrivalent cerium. *J. Chem. Soc.* **1957**, 2600–2604, DOI: 10.1039/jr9570002600.

(21) Ozaki, Y.; Kaneko, K.; Mitachi, S. Process for the production of a rare earth metal alkoxide, 4507245, 1985.

(22) Groth, U.; Jeske, M. Diastereoselective Ce(OiPr)3-Catalyzed Pinacol Couplings of Aldehydes. *Angew. Chem. Int. Ed.* **2000**, *39*, 574–576, DOI: 10.1002/(sici)1521-3773(20000204)39:3<574::aid-anie574>3.0.co;2-o.

(23) Sasai, H.; Suzuki, T.; Arai, S.; Arai, T.; Shibasaki, M. Basic character of rare earth metal alkoxides. Utilization in catalytic carbon-carbon bond-forming reactions and catalytic asymmetric nitroaldol reactions. *J. Am. Chem. Soc.* **1992**, *114*, 4418–4420, DOI: 10.1021/ja00037a068.

(24) Okano, T.; Matsuoka, M.; Konishi, H.; Kiji, J. Meerwein-Ponndorf-Verley Reduction of Ketones and Aldehydes Catalyzed by Lanthanide Tri-2-propoxides. *Chem. Lett.* **1987**, *16*, 181–184, DOI: 10.1246/cl.1987.181.

(25) Huskens, J.; de Graauw, C. F.; Peters, J. A.; van Bekkum, H. Chiral induction in lanthanide(III)-alkoxide-catalysed Meerwein-Ponndorf-Verley reductions. *Recl. Trav. Chim. Pays-Bas* **2010**, *113*, 488–491, DOI: 10.1002/recl.19941131014.

(26) Gromada, J.; Chenal, T.; Mortreux, A.; Carpentier, J.; Ziller, J. W.; Leising, F. Rare earth alkoxides as inorganic precursors for olefin polymerization: an alternative to traditional lanthanocene chemistry. *Chem. Commun.* **2000**, 2183–2184, DOI: 10.1039/b006941h.

(27) Schläfer, J.; Tyrra, W.; Mathur, S. Octakis(tert-butoxo)dicerium(IV) [Ce2(O-(t)Bu)8]: synthesis, characterization, decomposition, and reactivity. *Inorg. Chem.* **2014**, *53*, 2751–3, DOI: 10.1021/ic4025876.

(28) Sen, A.; Stecher, H. A.; Rheingold, A. L. Synthesis, structure, and reactivity of homoleptic cerium(IV) and cerium(III) alkoxides. *Inorg. Chem.* **1992**, *31*, 473–479, DOI: 10.1021/ic00029a025.

(29) Basset, J. M.; Choplin, A. Surface organometallic chemistry: A new approach to heterogeneous Catalysis? *J. Mol. Catal.* **1983**, *21*, 95–108, DOI: 10.1016/0304-5102(93)80113-9.

(30) Samantaray, M. K.; Pump, E.; Bendjeriou-Sedjerari, A.; D'Elia, V.; Pelletier, J. D. A.; Guidotti, M.; Psaro, R.; Basset, J. M. Surface organometallic chemistry in heterogeneous catalysis. *Chem. Soc. Rev.* **2018**, DOI: 10.1039/c8cs00356d.

(31) Campos, J. M.; Lourenço, J. P.; Cramail, H.; Ribeiro, M. R. Nanostructured silica materials in olefin polymerisation: From catalytic behaviour to polymer characteristics. *Progress in Polymer Science* **2012**, *37*, 1764–1804, DOI: 10.1016/j.progpolymsci.2012.02.006.

(32) Kresge, C. T.; Leonowicz, M. E.; Roth, W. J.; Vartuli, J. C.; Beck, J. S. Ordered mesoporous molecular sieves synthesized by a liquid-crystal template mechanism. *Nature* **1992**, *359*, 710–712, DOI: 10.1038/359710a0.

(33) Beck, J. S.; Vartuli, J. C.; Roth, W. J.; Leonowicz, M. E.; Kresge, C. T.; Schmitt, K. D.; Chu, C. T. W.; Olson, D. H.; Sheppard, E. W.; McCullen, S. B.; Higgins, J. B.; Schlenker, J. L. A new family of mesoporous molecular sieves prepared with liquid crystal templates. *J. Am. Chem. Soc.* **1992**, *114*, 10834–10843, DOI: 10.1021/ja00053a020.

(34) Gallis, K. W.; Araujo, J. T.; Duff, K. J.; Moore, J. G.; Landry, C. C. The Use of Mesoporous Silica in Liquid Chromatography. *Adv. Mater.* **1999**, *11*, 1452–1455, DOI: 10.1002/(sici)1521-4095(199912)11:17<1452::aid-adma1452>3.0.co;2-r.

(35) Lai, C. Y.; Trewyn, B. G.; Jeftinija, D. M.; Jeftinija, K.; Xu, S.; Jeftinija, S.; Lin, V. S. A mesoporous silica nanosphere-based carrier system with chemically removable CdS nanoparticle caps for stimuli-responsive controlled release of neurotransmitters and drug molecules. *J. Am. Chem. Soc.* **2003**, *125*, 4451–9, DOI: 10.1021/ja028650l.

(36) Thahir, R.; Wahab, A. W.; Nafie, N. L.; Raya, I. Synthesis of high surface area mesoporous silica SBA-15 by adjusting hydrothermal treatment time and the amount of polyvinyl alcohol. *Open Chem.* **2019**, *17*, 963–971, DOI: 10.1515/chem-2019-0106.

(37) Zhuravlev, L. T. The surface chemistry of amorphous silica. Zhuravlev model. *Colloids and Surfaces A: Physicochemical and Engineering Aspects* **2000**, *173*, 1–38, DOI: 10.1016/s0927-7757(00)00556-2.

(38) Wang, Y.; Zhang, F.; Wang, Y.; Ren, J.; Li, C.; Liu, X.; Guo, Y.; Guo, Y.; Lu, G. Synthesis of length controllable mesoporous SBA-15 rods. *Materials Chemistry and Physics* **2009**, *115*, 649–655, DOI: 10.1016/j.matchemphys.2009.01.027.

(39) Huh, S.; Wiench, J. W.; Yoo, J.-C.; Pruski, M.; Lin, V. S. Y. Organic Functionalization and Morphology Control of Mesoporous Silicas via a Co-Condensation Synthesis Method. *Chem. Mater.* **2003**, *15*, 4247–4256, DOI: 10.1021/cm0210041.

(40) Kim, T.-W.; Chung, P.-W.; Lin, V. S. Y. Facile Synthesis of Monodisperse Spherical MCM-48 Mesoporous Silica Nanoparticles with Controlled Particle Size. *Chem. Mater.* **2010**, *22*, 5093–5104, DOI: 10.1021/cm1017344.

(41) Radu, D. R.; Lai, C. Y.; Jeftinija, K.; Rowe, E. W.; Jeftinija, S.; Lin, V. S. A polyamidoamine dendrimer-capped mesoporous silica nanosphere-based gene transfection reagent. *J. Am. Chem. Soc.* **2004**, *126*, 13216–7, DOI: 10.1021/ja046275m.

(42) Gu, J.; Huang, K.; Zhu, X.; Li, Y.; Wei, J.; Zhao, W.; Liu, C.; Shi, J. Sub-150 nm mesoporous silica nanoparticles with tunable pore sizes and well-ordered mesostructure for protein encapsulation. *J. Colloid Interface Sci.* **2013**, *407*, 236–42, DOI: 10.1016/j.jcis.2013.06.028.

(43) Asefa, T.; Tao, Z. Mesoporous silica and organosilica materials — Review of their synthesis and organic functionalization. *Canad. J. Chem.* **2012**, *90*, 1015–1031, DOI: 10.1139/v2012-094.

(44) Zhao, D.; Feng, J.; Huo, Q.; Melosh, N.; Fredrickson, G. H.; Chmelka, B. F.; Stucky, G. D. Triblock copolymer syntheses of mesoporous silica with periodic 50 to 300 angstrom pores. *Science* **1998**, *279*, 548–52, DOI: 10.1126/science.279.5350.548.

(45) Ciesla, U.; Schüth, F. Ordered mesoporous materials. *Micropor. Mesopor. Mat.* **1999**, *27*, 131–149, DOI: 10.1016/s1387-1811(98)00249-2.

(46) Taguchi, A.; Schüth, F. Ordered mesoporous materials in catalysis. *Microporous and Mesoporous Materials* **2005**, *77*, 1–45, DOI: 10.1016/j.micromeso.2004.06.030.

(47) Anwander, R. In *Handbook of Heterogeneous Catalysis*, Ertl, G., Knözinger, H., Schüth, F., Weitkamp, J., Eds.; Wiley-VCH: Weinheim, 2008; Chapter 2.4.9, pp 583–614, DOI: 10.1002/9783527610044.hetcat0029.

(48) Anwander, R.; Nagl, I.; Widenmeyer, M.; Engelhardt, G.; Groeger, O.; Palm, C.; Röser, T. Surface Characterization and Functionalization of MCM-41 Silicas via Silazane Silylation. *J. Phys. Chem. B* **2000**, *104*, 3532–3544, DOI: 10.1021/jp993108d.

(49) Anwander, R.; Gerstberger, G.; Palm, C.; Groeger, O.; Engelhardt, G. Enhanced catalytic activity of MCM-41-grafted aluminium isopropoxide in MPV reductions. *Chem. Comm.* **1998**, 1811–1812, DOI: 10.1039/a802996b.

(50) Anwander, R.; Palm, C. Meerwein-Ponndorf-Verley reductions mediated by lanthanide-alkoxide-functionalized mesoporous silicates. *Stud. Surf. Sci. Catal.* **1998**, *117*, 413–420, DOI: 10.1016/s0167-2991(98)81019-7.

(51) Anwander, R.; Görlitzer, H. W.; Gerstberger, G.; Palm, C.; Runte, O.; Spiegler, M. Grafting of bulky rare earth metal complexes onto mesoporous silica MCM-41†. *J. Chem. Soc., Dalton Trans.* **1999**, 3611–3615, DOI: 10.1039/a903096d.

(52) Vancompernolle, T.; Valente, A.; Chenal, T.; Zinck, P.; Del Rosal, I.; Maron, L.; Taoufik, M.; Harder, S.; Gauvin, R. M. Silica-Grafted Lanthanum Benzyl Species: Synthesis, Characterization, and Catalytic Applications. *Organometallics* **2017**, DOI: 10.1021/acs.organomet.7b00538.

(53) Gauvin, R. M.; Chenal, T.; Hassan, R. A.; Addad, A.; Mortreux, A. Grafted lanthanide amides: Versatile catalysts for various transformations. *J. Mol. Catal. A: Chemical* **2006**, *257*, 31–40, DOI: 10.1016/j.molcata.2006.04.022.

(54) Del Rosal, I.; Yahia, A.; Maron, L. Effects of the Grafting of Lanthanum Complexes on a Silica Surface on the Reactivity: Influence on Ethylene, Propylene, and 1,3-Butadiene Homopolymerization. *Inorg. Chem.* **2016**, *55*, 10024–10033, DOI: 10.1021/acs.inorgchem.6b01238.

(55) Meerwein, H.; Schmidt, R. Ein neues Verfahren zur Reduktion von Aldehyden und Ketonen. *Liebigs Ann. Chem.* **1925**, *444*, 221–238, DOI: 10.1002/jlac.19254440112.

(56) Verley, A. Sur l'échange des groupements fonctionelles entre deux molécules. Passage de la fonction alcool à la fonction aldéhyde et inversement. *Bull. Soc. Chim. Fr.* **1925**, *37*, 537–542.

(57) Ponndorf, W. Der reversible Austausch der Oxydationsstufen zwischen Aldehyden oder Ketonen einerseits und primären oder sekundären Alkoholen anderseits. *Angew. Chem.* **1926**, *39*, 138–143, DOI: 10.1002/ange.19260390504.

(58) Bradley, D. C.; Mehrotra, R.; Rothwell, I.; Singh, A., *Alkoxo and Aryloxo Derivatives of Metals*; Academic Press: London, San Diego, 2001.

(59) Cohen, R.; Graves, C. R.; Nguyen, S. T.; Martin, J. M.; Ratner, M. A. The mechanism of aluminum-catalyzed Meerwein-Schmidt-Ponndorf-Verley reduction of carbonyls to alcohols. *J. Am. Chem. Soc.* **2004**, *126*, 14796–803, DOI: 10.1021/ja047613m.

(60) Wilds, A. L. Reduction with Aluminum Alkoxides. *Org. React.* **2011**, *2*, 178–223, DOI: 10.1002/0471264180.or002.05.

(61) De Graauw, C. F.; Peters, J. A.; van Bekkum, H.; Huskens, J. Meerwein-Ponndorf-Verley Reductions and Oppenauer Oxidations: An Integrated Approach. *Synthesis* **1994**, *1994*, 1007–1017, DOI: 10.1055/s-1994-25625.

(62) Cha, J. S. Recent Developments In Meerwein-Ponndorf-Verley and Related Reactions for the Reduction of Organic Functional Groups Using Aluminum, Boron, and Other Metal Reagents: A Review. *Org. Process Res. Dev.* **2006**, *10*, 1032–1053, DOI: 10.1021/op068002c.

(63) Ruiz J. R.; Jiménez-Sanchidrián, C. Heterogeneous Catalysis in the Meerwein-Ponndorf-Verley Reduction of Carbonyl Compounds. *Curr. Org. Chem.* **2007**, *11*, 1113–1125, DOI: 10.2174/1385272077816.

(64) Namy, J. L.; Souppe, J.; Collin, J.; Kagan, H. B. New preparations of lanthanide alkoxides and their catalytical activity in Meerwein-Ponndorf-Verley-Oppenauer reactions. *J. Org. Chem.* **1984**, *49*, 2045–2049, DOI: 10.1021/jo00185a053.

(65) Evans, D. A.; Nelson, S. G.; Gagne, M. R.; Muci, A. R. A chiral samarium-based catalyst for the asymmetric Meerwein-Ponndorf-Verley reduction. *J. Am. Chem. Soc.* **1993**, *115*, 9800–9801, DOI: 10.1021/ja00074a057.

(66) Nakano, Y.; Sakaguchi, S.; Ishii, Y. Meerwein–Ponndorf–Verley-type reductive acetylation of carbonyl compounds to acetates by lanthanide complexes in the presence of isopropenyl acetate. *Tetrahedron Lett.* **2000**, *41*, 1565–1569, DOI: 10.1016/s0040-4039(00)00012-5.

(67) Fukuzawa, S.; Nakano, N.; Saitoh, T. Reduction of Carbonyl Compounds by Lanthanide Metal/2-Propanol: In-situ Generation of Samarium Isopropyloxide for Stereoselective MeerweinPonndorfVerley Reduction. *Eur. J. Org. Chem.* **2004**, *2004*, 2863–2867, DOI: 10.1002/ejoc.200400030.

(68) Uysal, B.; Oksal, B. S. New heterogeneous B(OEt)3-MCM-41 catalyst for preparation of α,β-unsaturated alcohols. *Res. Chem. Intermed.* **2013**, *41*, 3893–3911, DOI: 10.1007/s11164-013-1498-0.

(69) Uysal, B.; Oksal, B. S. Catalytic activity of SBA-15-grafted indium tri-isopropoxide in chemoselective MPV reductions. *J. Porous Mater.* **2015**, *22*, 1053–1064, DOI: 10.1007/s10934-015-9980-2.

(70) Bagal, S. K.; Adlington, R. M.; Baldwin, J. E.; Marquez, R.; Cowley, A. Biomimetic synthesis of biatractylolide and biepiasterolide. *Org. Lett.* **2003**, *5*, 3049–52, DOI: 10.1021/ol035022f.

(71) Heeres, H. J.; Maters, M.; Teuben, J. H.; Helgesson, G.; Jagner, S. Organolanthanide-induced carbon-carbon bond formation. Preparation and properties of monomeric lanthanide aldolates and enolates. *Organometallics* **1992**, *11*, 350–356, DOI: 10.1021/om00037a059.

(72) Barbier-Baudry, D.; Heiner, S.; Kubicki, M. M.; Vigier, E.; Visseaux, M.; Hafid, A. An Easy Synthetic Route to Heteroleptic Samarium Monoalkoxides for Ring-Opening Polymerization Initiators. Molecular Structures of [(C5Hi-Pr4)SmI(THF)2]2, SmI2Ot-Bu(THF)4, and (C4Me4P)2SmOt-Bu(THF). *Organometallics* **2001**, *20*, 4207–4210, DOI: 10.1021/om010423p.

(73) Arnold, P. L.; Casely, I. J.; Zlatogorsky, S.; Wilson, C. Organometallic Cerium Complexes from Tetravalent Coordination Complexes. *Helv. Chim. Acta* **2009**, *92*, 2291–2303, DOI: 10.1002/hlca.200900152.

(74) Toledano, P.; Ribot, F.; Sanchez, C. Structure du bis(2-propanol)-bis-μ-(2-propanolato)-hexakis(2-propanolato)dicérium(IV).
Acta Crystallogr. Sect. C: Cryst. Struct. Commun. **1990**, *46*, 1419–1422, DOI: 10.1107/s0108270189012564.

(75) Friedrich, J.; Schneider, D.; Bock, L.; Maichle-Mössmer, C.; Anwander, R. Cerium(IV) Neopentoxide Complexes. *Inorg. Chem.* **2017**, *56*, 8114–8127, DOI: 10.1021/acs.inorgchem.7b00828.

(76) Liang, Y.; Anwander, R. Nanostructured catalysts via metal amide-promoted smart grafting. *Dalton Trans.* **2013**, *42*, 12521–45, DOI: 10.1039/c3dt51346g.

(77) Büchel, G.; Unger, K. K.; Matsumoto, A.; Tsutsumi, K. A Novel Pathway for Synthesis of Submicrometer-Size Solid Core/Mesoporous Shell Silica Spheres. *Adv. Mater.* **1998**, *10*, 1036–1038, DOI: 10.1002/(sici)1521-4095(199809)10:13<1036::aid-adma1036>3.0.co;2-z.

(78) Tran Vi Le, X. Synthese und Charakterisierung von periodisch mesoporösen Silica-Nanopartikeln des MCM-41-Typs, B. Sc. Thesis, 2017.

(79) König, S. Manganese, Chromium, and Cobalt Surface-Functionalized Cubic Mesoporous Silica KIT-6 and MCM-48, Thesis, 2009.

(80) Brunauer, S.; Emmett, P. H.; Teller, E. Adsorption of Gases in Multimolecular Layers. *J. Am. Chem. Soc.* **1938**, *60*, 309–319, DOI: 10.1021/ja01269a023.

(81) Barrett, E. P.; Joyner, L. G.; Halenda, P. P. The Determination of Pore Volume and Area Distributions in Porous Substances. I. Computations from Nitrogen Isotherms. *J. Am. Chem. Soc.* **1951**, *73*, 373–380, DOI: 10.1021/ja01145a126.

(82) Hara, K.; Akahane, S.; Wiench, J. W.; Burgin, B. R.; Ishito, N.; Lin, V.-S. Y.; Fukuoka, A.; Pruski, M. Selective and Efficient Silylation of Mesoporous Silica: A Quantitative Assessment of Synthetic Strategies by Solid-State NMR. *J. Phys.l Chem. C* **2012**, *116*, 7083–7090, DOI: 10.1021/jp300580f.

Part E.

Publications

Paper I

ChemPubSoc Europe

DOI: 10.1002/ejic.201901023

EurJIC European Journal of Inorganic Chemistry

Full Paper

Cerium(III) Oxidation | *Very Important Paper* |

A Facile Route toward Ceric Silylamide [Ce{N(SiHMe$_2$)$_2$}$_4$]

Uwe Bayer,[a][‡] Lorenz Bock,[a][‡] Cäcilia Maichle-Mössmer,[a] and Reiner Anwander*[a]

Abstract: Treatment of the ate complex [Ce{N(SiHMe$_2$)$_2$}$_4$Li(thf)] with neutral donor molecules (do) gave several solvent(do)-separated ion-pair complexes of the composition [Ce{N(SiHMe$_2$)$_2$}$_4$][Li(do)$_n$] (do = thf, pyridine, tmeda, dme, 12-crown-4). Their solid-state structures have been analyzed by X-ray diffraction and DRIFTS. Displacement of the [Li(do)$_n$] entity, resulting in a solvent-separated ion pair with a symmetric environment around the Ce(III) center, was also revealed in solution by ^{7}Li NMR spectroscopy. The oxidation of [Ce{N(SiHMe$_2$)$_2$}$_4$]-[Li(do)$_n$] with 1,4-benzoquinone to afford homoleptic ceric [Ce{N(SiHMe$_2$)$_2$}$_4$] has been investigated and screened. Overall, the separated ion pairs [Ce{N(SiHMe$_2$)$_2$}$_4$][Li(do)$_n$] performed better than the intramolecular ate complex [Ce{N(SiHMe$_2$)$_2$}$_4$-Li(thf)], with pyridine as donor giving the best results.

Introduction

Molecular cerium chemistry is currently experiencing a veritable boom, which is documented by a number of review articles.[1] This is mainly due to the unique cerium redox chemistry featuring +3 and +4 as stable oxidation states of molecular compounds in many polar and apolar solvents.[1] Although ceric derivatives have long been a focus of scientific interest in metal-organic chemistry as well,[2] many of these compounds could only be fully characterized in recent years, because of their high sensitivity toward oxygen and moisture.[3]

With respect to the synthesis of molecular Ce(IV) compounds, ceric ammonium nitrate (CAN), $(NH_4)_2Ce(NO_3)_6$, has long been the precursor of choice.[1d,3a,4] More recently, synthesis protocols have also drawn on alternative ceric precursors such as triflate Ce(OTf)$_4$[5] or various alkoxides Ce(OR)$_4$.[1c,6] We and others have embarked on the silylamide [Ce{N(SiHMe$_2$)$_2$}$_4$] as a more versatile precursor en route to unprecedented Ce(IV) chemistry.[7,8] Solely judged by the proligand pK_a values, the more basic organoamides are supposed to display enhanced reactivity compared to, e.g. alkoxides,[2c,9] thus markedly extending the scope of potentially accessible Ce(IV) complexes.[7–10] The synthesis of the tetravalent homoleptic silylamide itself, however, has so far been impaired by several problems: the synthesis from [Ce{N(SiHMe$_2$)$_2$}$_3$(thf)$_2$] afforded only unsatisfactory yields (ca. 31 %) after a reaction time of 18 h, when oxidized with C_2Cl_6 or even 17 % for the oxidation with $PhICl_2$ respectively;[7] moreover, ca. 35 % of [Ce{N(SiHMe$_2$)$_2$}$_4$] (based on employed $CeCl_3$) were obtained in the presence of K[N(SiHMe$_2$)$_2$] via the potassium ate complex and oxidation with Ph_3CCl,[8b] and a still time-consuming synthesis (6 h sonication) was involved when accessed more directly from $CeCl_3(thf)_{1.04}$ via the ate complex [Ce{N(SiHMe$_2$)$_2$}$_4$Li(thf)] and oxidized with C_2Cl_6.[8a]

We found that by adjusting the amount of the donor solvent in the above trivalent ate complex, including donor exchange the (solid-state) structure of the ate complex switched from intramolecular to that of an ion-separated compound of the general formula [Ce{N(SiHMe$_2$)$_2$}$_4$]$^-$[Li(do)$_n$]$^+$. The latter, when oxidized with 1,4-benzoquinone (bq), gave the desired [Ce{N(SiHMe$_2$)$_2$}$_4$] via an oxidative alkali-metal salt separation in a rapid and straightforward manner with only insoluble, easy-to-separate by-products (Scheme 1).

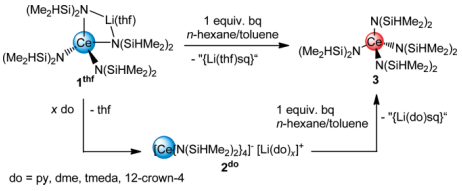

Scheme 1. Formation of [Ce{N(SiHMe$_2$)$_2$}$_4$] (**3**) via direct oxidation of ate complex [Ce{N(SiHMe$_2$)$_2$}$_4$Li(thf)] (**1^{thf}**) with 1,4-benzoquinone (bq) or by preceding donor exchange and subsequent oxidation of the formed solvent-separated ion pair [Ce{N(SiHMe$_2$)$_2$}$_4$][Li(do)$_n$] (**2do**) (sq = 1,4-benzosemiquinolato).

Results and Discussion

Ate complex [Ce{N(SiHMe$_2$)$_2$}$_4$Li(thf)] (**1^{thf}**) was obtained as published previously by our group.[8a] Treatment of **1^{thf}** with excess of different donor solvent molecules (pyridine, TMEDA, DME, 12-crown-4) and subsequent crystallization from either the donor solvent itself or from a mixture of it and *n*-hexane gave solvent-separated ion-pair complexes of the formula [Ce{N(SiHMe$_2$)$_2$}$_4$][Li(do)$_n$] (**2do**). The crystal structures of **2^{py}**, **2^{tmeda}** and **2$^{12\text{-}crown\text{-}4}$** display anionic Ce(III) centers tetra-

[a] *Institut für Anorganische Chemie, University of Tübingen, Auf der Morgenstelle 18, 72076 Tübingen, Germany*
E-mail: reiner.anwander@uni-tuebingen.de
http://uni-tuebingen.de/syncat-anwander
[‡] These authors contributed equally to this publication.
Supporting information and ORCID(s) from the author(s) for this article are available on the WWW under https://doi.org/10.1002/ejic.201901023.

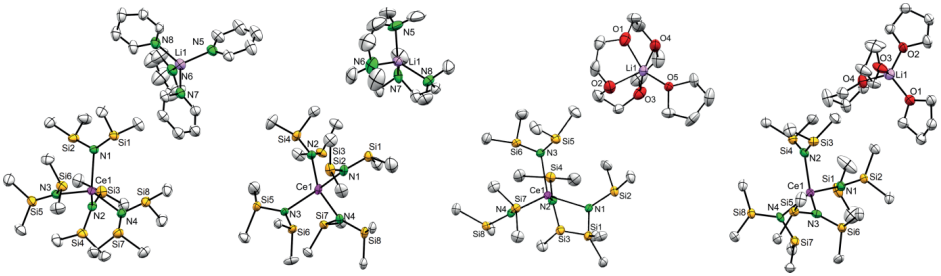

Figure 1. Crystal structures of $[Ce\{N(SiHMe_2)_2\}_4][Li(py)_4]$ **2^{py}** (left), $[Ce\{N(SiHMe_2)_2\}_4][Li(tmeda)_2]$ **2^{tmeda}** (center left), $[Ce\{N(SiHMe_2)_2\}_4][Li(12\text{-crown-4})(thf)]$ **2$^{12\text{-crown-4}}$** (center right) and $[Ce\{N(SiHMe_2)_2\}_4][Li(thf)_4]$ **2^{thf}** (right). Ellipsoids are shown at either the 50 % (**2^{py}**, **2$^{12\text{-crown-4}}$**, **2^{thf}**) or the 30 % (**2^{tmeda}**) probability level. Hydrogen atoms as well as disorder in the silylamido ligands (**2^{py}**, **2^{tmeda}**, **2^{thf}**) and donor solvent molecules (**2^{py}**, **2^{tmeda}**) are omitted for clarity.

hedrally coordinated by four $[N(SiHMe_2)_2]$ ligands. The lithium counterions are surrounded by either four molecules of pyridine, two molecules of TMEDA or one molecule of 12-crown-4 plus an additional molecule of THF (Figure 1).

As a result of the displacement of the lithium cation, the four Ce–N bonds are of equal length instead of two shortened and two elongated ones as found in the starting product **1^{thf}** (Table 1). As expected, the Ce–N bond lengths of the trivalent separated ion pairs **2^{py}** [2.397(4)-2.417(4) Å], **2^{tmeda}** [2.386(10)-2.438(6) Å] and **2$^{12\text{-crown-4}}$** [2.391(3)-2.436(3) Å] are elongated compared to the tetravalent target product $[Ce\{N(SiHMe_2)_2\}_4]$ (**3**) [2.238(1)-2.257(1) Å].[7] For further comparison, the separated ion pair $[Ce\{N(SiMe_3)_2\}_4][Na(thf)_4(Et_2O)]$ bearing the bulkier bis(trimethylsilyl) amido ligand exhibits slightly elongated Ce–N bond lengths in the range of 2.434(6)-2.448(6) Å.[11] As trivalent cerium is paramagnetic ($4f^1$), and due to solubility problems in common non-donating solvents (e.g. phase separation in toluene or benzene), the recorded ^{1}H NMR spectra were not very informative (Figure S4, Supporting Information). However, the chemical environment of lithium could be examined by ^{7}Li-NMR spectroscopy in a mixture of C_6D_6 and 1,2-difluorobenzene. The ^{7}Li-NMR spectra of the separated ion pairs **2^{py}**, **2^{tmeda}**, **2^{dme}** and **2$^{12\text{-crown-4}}$** revealed a singlet ranging from −1.44 to 2.45 ppm (Figure 2). In comparison and stark contrast, the intramolecular ate complex $[Ce\{N(SiHMe_2)_2\}_4Li(thf)]$ (**1^{thf}**) shows a broadened singlet at 84.04 ppm for the lithium center, reflecting the close proximity of the lithium to the paramagnetic Ce(III) center. Additionally, a signal at 1.10 ppm was

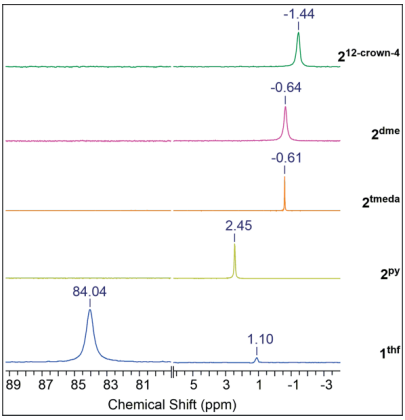

Figure 2. ^{7}Li NMR spectra of **1^{thf}** and **2do**.

Table 1. Bond lengths [Å] and angles [°] for **2^{py}**, **2^{tmeda}**, **2$^{12\text{-crown-4}}$**, **2^{thf}**, **1^{thf}**, and **3**

Bond	**2^{py}**	**2^{tmeda}**	**2$^{12\text{-crown-4}}$**	**2^{thf}**	**1^{thf}** [8a]	**3**[7]
Ce1–N1	2.398(4)	2.438(6)	2.412(3)	2.416(6)	2.388(5)	2.244(1)
Ce1–N2	2.397(4)	2.40(2)	2.408(3)	2.397(7)	2.386(4)	2.238(1)
Ce1–N3	2.404(4)	2.41(1)	2.391(3)	2.377(6)	2.523(4)	2.249(1)
Ce1–N4	2.417(4)	2.39(1)	2.436(3)	2.413(6)	2.532(5)	2.257(1)
Angle						
Ce1–N1–Si1	122.6(2)	129.0(3)	110.0(2)	123.0(3)	132.8(3)	108.68(5)
Ce1–N1–Si2	109.4(2)	107.2(4)	123.1(2)	105.7(3)	100.7(2)	122.41(6)
Ce1–N2–Si3	124.6(2)	122(1)	108.7(2)	109.9(3)	101.5(2)	125.73(6)
Ce1–N2–Si4	107.5(2)	110.1(8)	125.5(2)	120.7(4)	130.6(2)	106.60(5)
Ce1–N3–Si5	118.8(2)	129.4(6)	123.3(2)	111.1(3)	98.1(2)	105.64(5)
Ce1–N3–Si6	106.6(2)	106.2(6)	105.7(2)	121.3(3)	122.7(2)	124.74(6)
Ce1–N4–Si7	126.1(3)	104.1(4)	105.4(2)	102.8(3)	126.0(3)	126.08(6)
Ce1–N4–Si8	103.7(2)	132.3(5)	127.2(2)	130.8(3)	98.0(2)	106.23(5)

observed, indicating the presence of a solvent-separated ion-pair complex $[Ce\{N(SiHMe_2)_2\}_4][Li(thf)_x]$ in a ratio of 3:97. This small amount of ion-pair complex may be a result of the small hyperstoichiometric amount of THF present when using Soxhlet-extracted/activated $CeCl_3$ with statistically 1.04 molecules of THF as donor for each cerium center.

Therefore, intramolecular ate complex **1^{thf}** was treated with stoichiometric amounts of THF to enhance the formation of the ion-separated complex $[Ce\{N(SiHMe_2)_2\}_4][Li(thf)_x]$ (Figure S11, Supporting Information). Upon addition of five equivalents of THF, almost all of ate complex **1^{thf}** was consumed, whereas the signal for putative solvent-separated **2^{thf}** increased with the amount of THF added. Crystallization from a concentrated solution of **1^{thf}** in THF at –40 °C gave yellow crystals which were analyzed by X-ray diffraction confirming a compound of the composition $[Ce\{N(SiHMe_2)_2\}_4][Li(thf)_4]$ (**2^{thf}**). The crystal structure of **2^{thf}** shows a 4-coordinate cerium center with equally long Ce–N bonds [2.377(6)-2.416(6) Å] as found for the other solvent(do)-separated ion pairs **2do** (Figure 1).

The Si–H-stretch vibration is another sensitive spectroscopic probe of metal–$[N(SiHMe_2)_2]$ moieties.[12] While DRIFTS measurements of **1^{thf}** show two strong well-resolved absorption bands for the Si–H moieties at around 2000 cm^{-1}, the spectra of the ion pairs **2^{py}**, **2^{tmeda}**, **2^{dme}**, **2$^{12\text{-crown-4}}$**, and **2^{thf}** revealed one broad absorption band in this region supporting the formation of a highly symmetric environment around the cerium center (Figure 3). In the DRIFT spectrum of the oxidized species **3**, two distinct bands for the Si–H vibrations are visible again, which is generally attributed to the presence of β-H-agostic interactions.[7]

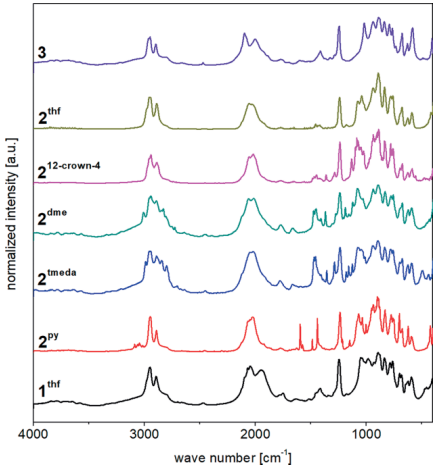

Figure 3. Stacked DRIFT spectra of **1^{thf}** (black trace), **2^{py}** (red trace), **2^{tmeda}** (blue trace), **2^{dme}** (green trace), **2$^{12\text{-crown-4}}$** (pink trace), **2^{thf}** (yellow trace), and **3** (purple trace).

Due to different problems encountered with the oxidation of trivalent $[Ce\{N(SiHMe_2)_2\}_3(thf)_2]$ with chlorinating oxidants (e.g., low yields with $PhICl_2$ or C_2Cl_6),[7] via potassium ate complex $[Ce\{N(SiHMe_2)_2\}_4K]$ (with Ph_3CCl)[8b] or labor-intensive oxidations of **1^{thf}** using C_2Cl_6[8a] or Ph_3CCl, previously reported synthesis routes seemed not as straightforward as desired for an efficient precursor. Hence, 1,4-benzoquinone was chosen as an oxidant for the different trivalent cerium precursors **2do**, aiming at $[Ce\{N(SiHMe_2)_2\}_4]$. Benzoquinone reduction in non-polar solvents forms only insoluble by-products and therefore workup procedures should be easy.[6e,13] The oxidation of **1^{thf}** with 1,4-benzoquinone was already examined previously,[6e,8a,8e,13] however, was reported to afford low yields. Notwithstanding, the oxidizability of the different Ce(III) complexes was re-investigated. Accordingly, **1^{thf}** and **2do** were treated with one equivalent of benzoquinone for 15 min in a mixture of toluene and *n*-hexane. The use of an equimolar amount of benzoquinone was essential for an efficient oxidation, which favors the formation of lithium 1,4-benzosemiquinolate as the insoluble by-product. After filtration of the reaction mixture, the soluble parts were evaporated to dryness under reduced pressure. ^{1}H NMR spectra of the crude products were recorded to compare the different Ce(III) species' performance as precursors (Figure 4). While all crude products contained minor impurities, the ^{1}H NMR spectrum of the oxidation product of **2^{py}** shows only a doublet at 0.34 ppm for the methyl and a septet at 6.01 ppm for the Si–H moieties. Another important indicator for assessing the oxidation efficiency is the yield of the product. Therefore, yields of the crude products were determined, showing that the products with less impurities had lower yields of 54–59 %. Products of the oxidation of **2^{tmeda}** and **2$^{12\text{-crown-4}}$** revealed higher yields for the crude product, however, required recrystallization to remove impurities. The higher yields in the latter cases might be due to a more efficient shielding of the Li cation from re-associ-

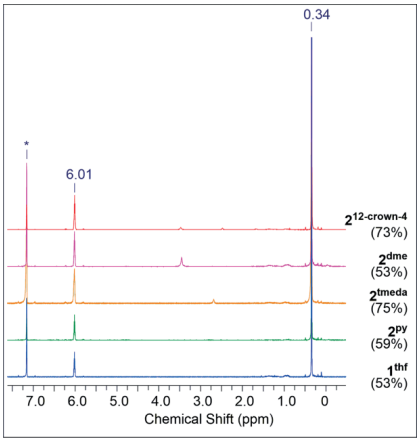

Figure 4. ^{1}H NMR spectra of the crude products of the oxidation reaction of **1^{thf}** and **2do** with 1,4-benzoquinone (yields are given in parentheses). Peaks at 0.34 and 6.01 ppm belong to $[Ce\{N(SiHMe_2)_2\}_4]$ (**3**). Solvent signal is marked with *.

ating with the anionic cerous fragment. Only **2^{dme}** showed low yields and purity which makes it the least useful precursor for [Ce{N(SiHMe$_2$)$_2$}$_4$] (**3**). The impact of ligand reorganization on Ce(III) oxidation has been thoroughly examined for Shibasaki's heterobimetallic BINOLate complexes [M$_3$(thf)$_x$Ce(binolate)-(thf)$_y$][14] by the Schelter group.[15] It was shown that the presence of distinct alkali-metal ions in the secondary coordination sphere control such ligand reorganization and hence tune the redox behavior (involving alkali-metal salt elimination).

Conclusions

The synthesis of homoleptic ceric silylamide [Ce{N(SiHMe$_2$)$_2$}$_4$] in non-donating solvents can be improved/optimized by carefully fine-tuning the donor coordination in the trivalent precursor [Ce{N(SiHMe$_2$)$_2$}$_4$Li(thf)]. Supplying extra donor molecules (do) transforms the intramolecular ate complex into a separated ion pair of the type [Ce{N(SiHMe$_2$)$_2$}$_4$][Li(do)$_n$] that can undergo straightforward oxidation with 1,4-benzoquinone to [Ce{N(SiHMe$_2$)$_2$}$_4$]. The purest oxidation product could be obtained by applying pyridine adduct [Ce{N(SiHMe$_2$)$_2$}$_4$][Li(py)$_4$], while tmeda and 12-crown-4 donor molecules gave higher yields but at the expense of higher amounts of impurities. Furthermore, ^{7}Li NMR spectroscopy features a nice tool to distinguish between intramolecular ate complexes and separated ion pairs in the presence of paramagnetic metal centers. We have thereby uncovered a new, less tedious route toward [Ce{N(SiHMe$_2$)$_2$}$_4$], hopefully facilitating future endeavors in metalorganic Ce(IV) chemistry.

Experimental Section

General Experimental Procedures and Instrumentation: All operations were performed under rigorous exclusion of air and moisture using a glovebox (MBraun MB150B-G-II and MBraun UNIlab pro ECO; <1 ppm O_2, <1 ppm H_2O) and standard Schlenk techniques under argon atmosphere. Solvents (toluene, *n*-hexane and THF) were purchased from Merck (formerly Sigma-Aldrich), pre-treated with Grubbs-type columns (M. Braun MB SPS-800), and stored inside a glovebox. 1,2-Difluorobenzene was purchased from Merck, dried over P_2O_5, distilled, and stored in a glovebox over molecular sieves (3 Å) for at least one week before use. C_6D_6 and [D_8]toluene were obtained from Euriso-top, dried with NaK alloy for at least 24 h, and filtered before use. Donor solvents (TMEDA, DME and pyridine) were purchased from Merck and dried with NaH, then distilled and stored in a glovebox. 12-Crown-4 was purchased from Merck, stored inside a glovebox, and used as received. 1,4-Benzoquinone was purchased from Merck, sublimed, and stored inside a glovebox. $CeCl_3$ was activated prior to use by Soxhlet extraction with THF, giving $CeCl_3(thf)_{1.04}$. [Ce(N(SiHMe$_2$)$_2$)$_4$Li(thf)] (**1^{thf}**) was synthesized according to published procedures.[7,8] NMR spectra were measured on a Bruker AV+400, a Bruker DRX-250 and a Bruker Avance III HD 300 spectrometer, were referenced to internal solvent residual signals and are reported relative to tetramethylsilane (^{1}H, ^{13}C).[16] ^{7}Li spectra are reported relative to LiCl. Due to the high air and moisture sensitivity of all compounds, all NMR spectra were recorded using NMR tubes with J.-Young-type valves. DRIFT spectra were recorded using a NICOLET 6700 FTIR spectrometer (Thermo SCIENTIFIC) diluted to 5 wt.-% with dried KBr powder as a dilution matrix. The sample was carefully homogenized with KBr in an agate mortar and transferred into a DRIFTS cell with KBr windows. The collected data were converted with the Kubelka–Munk refinement. Elemental analyses were carried out with an Elementar Vario MICRO Cube in the CHNS mode.

Syntheses

Synthesis of [Ce(N(SiHMe$_2$)$_2$)$_4$][Li(dme)$_3$] (2^{dme}): 1^{thf} (246.6 mg, 0.33 mmol) was dissolved in *n*-hexane, DME (90.1 mg, 1.00 mmol, 3.00 equiv.) was mixed with *n*-hexane and added dropwise whilst stirring. The solution was stirred for 15 min, then the solvent was removed in vacuo, providing **2^{dme}** (290.4 mg, 0.31 mmol, 93 %) as a yellow-orange powder. ^{7}Li NMR (C_6D_6/$C_6H_4F_2$, 299 K, 116.6 MHz): δ = –0.64 ppm; DRIFTS: $\tilde{\nu}$ = 3008 (w), 2942 (s), 2892 (m), 2849 (w), 2829 (w), 2807 (vw), 2726 (vw), 2060 (s), 2014 (s), 1769 (vw, br), 1665 (vw, br), 1475 (w), 1453 (m), 1410 (vw), 1369 (m), 1276 (vw), 1239 (s), 1207 (vw), 1191 (m), 1157 (w), 1123 (m), 1079 (vs), 1029 (w), 938 (s), 894 (vs), 889 (vs), 831 (s), 778 (m), 758 (m), 676 (m), 622 (w), 592 (m), 434 (vw), 427 (vw) cm^{-1}; elemental analysis calcd. (%) for $C_{28}H_{86}CeLiN_4O_6Si_8$: C 35.52, H 9.16, N 5.92; found C 35.41, H 9.27, N 5.99.

Synthesis of [Ce(N(SiHMe$_2$)$_2$)$_4$][Li(tmeda)$_2$] (2^{tmeda}): 1^{thf} (284.6 mg, 0.38 mmol) was dissolved in *n*-hexane, TMEDA (91.0 mg, 0.78 mmol, 2.05 equiv.) was mixed with *n*-hexane and added dropwise whilst stirring. The solution was stirred for 15 min, then the solvent was removed in vacuo, providing **2^{tmeda}** (336.0 mg, 0.37 mmol, 97 %) as a crystalline, greenish yellow material. Single crystals suitable for an X-ray structure analysis were obtained from a concentrated solution of **2^{tmeda}** in TMEDA and *n*-hexane at –35 °C. ^{7}Li NMR (C_6D_6/$C_6H_4F_2$, 299 K, 116.6 MHz): δ = –0.61 ppm; DRIFTS: $\tilde{\nu}$ = 2990 (m), 2954 (s), 2944 (s), 2891 (s), 2842 (m), 2800 (m), 2046 (s), 2017 (s), 1778 (w, br), 1664 (vw, br), 1470 (m), 1458 (s), 1409 (w), 1388 (vw), 1357 (m), 1288 (m), 1237 (s), 1182 (w), 1159 (m), 1127 (m), 1077 (s), 1068 (s), 1044 (s), 1013 (m), 942 (s), 895 (vs), 835 (s), 780 (s), 759 (s), 698 (w), 678 (m), 625 (m), 594 (m), 492 (w), 459 (vw), 437 (vw) cm^{-1}; elemental analysis calcd. (%) for $C_{28}H_{88}CeLiN_8Si_8$: C 37.01, H 9.76, N 12.33; found C 37.13, H 10.07, N 12.02.

Synthesis of [Ce(N(SiHMe$_2$)$_2$)$_4$][Li(py)$_4$] (2^{py}): 1^{thf} (249.6 mg, 0.33 mmol) was dissolved in *n*-hexane, pyridine (107.7 mg, 1.36 mmol, 4.08 equiv.) was mixed with *n*-hexane and added dropwise whilst stirring. The solution was stirred for 15 min, then the solvent was removed in vacuo, providing **2^{py}** (298.6 mg, 0.30 mmol, 90 %) as a crystalline, yellow-orange material. Single crystals suitable for an X-ray structure analysis were acquired from a concentrated solution of **2^{py}** in a mixture of pyridine and *n*-hexane at –35 °C. ^{7}Li NMR (C_6D_6/$C_6H_4F_2$, 299 K, 116.6 MHz): δ = 2.45 ppm; DRIFTS: $\tilde{\nu}$ = 3088 (w), 3059 (w), 3045 (w), 3016 (vw), 2949 (s), 2894 (m), 2035 (s, br), 1776 (w, br), 1628 (vw), 1597 (m), 1574 (w), 1488 (w), 1442 (m), 1243 (s), 1216 (w), 1151 (m), 1051 (s), 1037 (s), 1004 (m), 970 (vw), 931 (m), 893 (vs), 834 (s), 784 (m), 761 (s), 751 (m), 701 (s), 679 (m), 624 (m), 594 (m), 421 (m), 401 (w) cm^{-1}; elemental analysis calcd. (%) for $C_{36}H_{76}CeLiN_8Si_8$: C 43.55, H 7.72, N 11.29; found C 43.11, H 7.52, N 11.13.

Synthesis of [Ce(N(SiHMe$_2$)$_2$)$_4$][Li(12-crown-4)(thf)] (2$^{12\text{-crown-4}}$): 1^{thf} (50.0 mg, 0.067 mmol) was dissolved in *n*-hexane, 12-crown-4 (11.8 mg, 0.067 mmol, 1.00 equiv.) was mixed with *n*-hexane and added dropwise whilst stirring. The solution was stirred for 15 min, then the solvent was removed in vacuo, providing **2$^{12\text{-crown-4}}$** (57.7 mg, 0.062 mmol, 93 %) as a crystalline, yellow material. Single crystals suitable for an X-ray structure analysis were obtained from a concentrated solution of **2$^{12\text{-crown-4}}$** in *n*-hexane at –40 °C. ^{7}Li NMR (C_6D_6/$C_6H_4F_2$, 299 K, 116.6 MHz): δ = –1.44 ppm; DRIFTS: $\tilde{\nu}$ =

2941 (s), 2887 (m), 2018 (s), 1449 (w), 1363 (w), 1287 (w), 1239 (ws), 1133 (m), 1085 (ws), 1076 (s), 1024 (m), 938 (ws), 900 (ws), 889 (ws), 836 (ws), 781 (s), 771 (m), 758 (s), 676 (m), 625 (w), 588 (w) cm^{-1}; elemental analysis calcd. (%) for $C_{28}H_{80}CeLiN_4O_5Si_8$: C 36.37, H 8.72, N 6.06; found C 36.80, H 8.42, N 5.75.

Synthesis of $[Ce(N(SiHMe_2)_2)_4][Li(thf)_4]$ (2^{thf}): Single crystals of 2^{thf} suitable for an X-ray structure analysis were obtained from a saturated solution of 1^{thf} in THF by keeping it at –40 °C until crystals formed. ^7Li NMR ($C_6D_6/C_6H_4F_2$, 299 K, 116.6 MHz): δ = 1.10 ppm; DRIFTS: $\tilde{\nu}$ = 2949 (s), 2890 (s), 2056 (s), 2029 (s), 1242 (s), 1077 (s), 1042 (s), 938 (s), 892 (vs), 835 (s), 780 (s), 760 (s), 679 (m), 626 (w), 590 (m) cm^{-1}; elemental analysis calcd. (%) for $C_{32}H_{88}CeLiN_4O_4Si_8$: C 39.84, H 9.19, N 5.81; found C 39.40, H 8.97, N 5.89.

Oxidation of 1^{thf} with 1,4-benzoquinone: 1^{thf} (56.4 mg, 0.075 mmol) was dissolved in toluene, 1,4-benzoquinone (8.2 mg, 0.076 mmol) was dissolved in toluene and added dropwise to the solution of 1^{thf} whilst stirring. An immediate color change to black was observed. After stirring for 15 min, solid by-products were removed by centrifugation and filtration. After removal of the toluene in vacuo, the resulting product was washed three times with cold *n*-hexane and any precipitate again removed by centrifugation and filtration. Finally, *n*-hexane was removed in vacuo to yield **3** (27.1 mg, 53 %) as a dark red solid.

Oxidation of 2^{dme} with 1,4-benzoquinone: 2^{dme} (49.9 mg, 0.053 mmol) was dissolved in toluene, 1,4-benzoquinone (5.7 mg, 0.053 mmol) was dissolved in toluene and added dropwise to the solution of 2^{dme} whilst stirring. An immediate color change to black was observed. After stirring for 15 min, solid by-products were removed by centrifugation and filtration. After removal of the toluene in vacuo, the resulting product was washed three times with cold *n*-hexane and any precipitate again removed by centrifugation and filtration. Finally, *n*-hexane was removed in vacuo to yield **3** (18.9 mg, 53 %) as a dark red solid.

Oxidation of 2^{tmeda} with 1,4-benzoquinone: 2^{tmeda} (54.4 mg, 0.060 mmol) was dissolved in toluene, 1,4-benzoquinone (6.5 mg, 0.060 mmol) was dissolved in toluene and added dropwise to the solution of 2^{tmeda} whilst stirring. An immediate color change to black was observed. After stirring for 15 min, solid by-products were removed by centrifugation and filtration. After removal of the toluene in vacuo, the resulting product was washed three times with cold *n*-hexane and any precipitate again removed by centrifugation and filtration. Finally, *n*-hexane was removed in vacuo to yield **3** (30.3 mg, 75 %) as a dark red solid.

Oxidation of 2^{py} with 1,4-benzoquinone: 2^{py} (51.2 mg, 0.052 mmol) was dissolved in toluene, 1,4-benzoquinone (5.6 mg, 0.052 mmol) was dissolved in toluene and added dropwise to the solution of 2^{py} whilst stirring. An immediate color change to black was observed. After stirring for 15 min, solid by-products were removed by centrifugation and filtration. After removal of the toluene in vacuo, the resulting product was washed three times with cold *n*-hexane and any precipitate again removed by centrifugation and filtration. Finally, *n*-hexane was removed in vacuo to yield **3** (20.4 mg, 59 %) as a dark red solid.

Oxidation of $2^{12\text{-crown-4}}$ with 1,4-benzoquinone: $2^{12\text{-crown-4}}$ (50.0 mg, 0.054 mmol) was dissolved in toluene, 1,4-benzoquinone (5.8 mg, 0.054 mmol) was dissolved in toluene and added dropwise to the solution of $2^{12\text{-crown-4}}$ whilst stirring. An immediate color change to black was observed. After stirring for 15 min, solid by-products were removed by centrifugation and filtration. After removal of the toluene in vacuo, the resulting product was washed three times with cold *n*-hexane and any precipitate again removed by centrifugation and filtration. Finally, *n*-hexane was removed in vacuo to yield **3** (20.0 mg, 73 %) as a dark red solid.

Crystal Data Collection, Structure Solution, and Refinement

Crystals for X-ray crystallography were grown using saturated solutions in THF (2^{thf}), a mixture of TMEDA and *n*-hexane (2^{tmeda}), a mixture of pyridine and *n*-hexane (2^{py}) or *n*-hexane ($2^{12\text{-crown-4}}$). All compounds are sensitive toward moisture and oxygen, while single crystals start to melt at ambient temperature (except $2^{12\text{-crown-4}}$). At ambient temperature "melting" of the crystals occurred immediately. Suitable crystals for the diffraction experiments were handpicked in a glovebox, coated with Parabar 10312 and stored on microscope slides. Data collections were done on a *Bruker* APEX II Duo diffractometer by using QUAZAR optics and Mo-K_α (λ = 0.71073 Å). The data collection strategy was determined using COSMO[17] employing ω scans. Raw data were processed by APEX[18] and SAINT,[19] corrections for absorption effects were applied using SADABS.[20] The structures were solved by direct methods and refined against all data by full-matrix least-squares methods on F^2 using SHELXTL[21] and SHELXLE.[22] Disorder was found for 2^{py}, 2^{thf}, and 2^{tmeda}, and restraints (RIGU, SIMU, EADP) were given for refining the crystal structures. Plots were generated by using Mercury 3.19.1. Further details regarding the refinement and crystallographic data are listed in Table S1 and in the CIF files.

CCDC 1954721 (for 2^{py}), 1954722 (for $2^{12\text{-crown-4}}$), 1954723 (for 2^{tmeda}), and 1954724 (for 2^{thf}) contain the supplementary crystallographic data for this paper. These data can be obtained free of charge from The Cambridge Crystallographic Data Centre.

Supporting Information (see footnote on the first page of this article): NMR/DRIFT spectra.

Acknowledgments

We thank Dr. Daniel Werner for many fruitful discussions.

Keywords: Cerium · Redox chemistry · Silylamides · Solvent-separated ion pairs

[1] a) F. M. A. Sroor, F. T. Edelmann in *Tetravalent Cerium Chemistry*, (Ed. A. P. Izyumov, G.), Nova Science Publishers, Hauppauge, N. Y. **2012**, pp. 73–106; b) N. A. Piro, J. R. Robinson, P. J. Walsh, E. J. Schelter, *Coord. Chem. Rev.* **2014**, *260*, 21–36; c) R. Anwander, M. Dolg, F. T. Edelmann, *Chem. Soc. Rev.* **2017**, *46*, 6697-6709; d) Y.-M. So, W.-H. Leung, *Coord. Chem. Rev.* **2017**, *340*, 172–197; e) Y. Qiao, E. J. Schelter, *Acc. Chem. Res.* **2018**, *51*, 2926–2936.

[2] a) D. C. Bradley, A. K. Chatterjee, W. Wardlaw, *J. Chem. Soc.* **1956**, 2260–2264; b) D. C. Bradley, A. K. Chatterjee, W. Wardlaw, *J. Chem. Soc.* **1956**, 3469–3472; c) D. C. Bradley, A. K. Chatterjee, W. Wardlaw, *J. Chem. Soc.* **1957**, 2600–2604; d) A. Greco, S. Cesca, W. Bertolini, *J. Organomet. Chem.* **1976**, *113*, 321–330; e) G. B. Deacon, T. D. Tuong, D. G. Vince, *Polyhedron* **1983**, *2*, 969–970.

[3] For example, see: a) W. J. Evans, T. J. Deming, J. W. Ziller, *Organometallics* **1989**, *8*, 1581–1583; b) P. Toledano, F. Ribot, C. Sanchez, *Acta Crystallogr., Sect. C: Cryst. Struct. Commun.* **1990**, *46*, 1419–1422; c) E. Kurras, C, Kruger, *CSD Communication* **2004**; d) P. Dröse, A. R. Crozier, S. Lashkari, J. Gottfriedsen, S. Blaurock, C. G. Hrib, C. Maichle-Mössmer, C. Schädle, R. Anwander, F. T. Edelmann, *J. Am. Chem. Soc.* **2010**, *132*, 14046–14047; e) J. Schläfer, W. Tyrra, S. Mathur, *Inorg. Chem.* **2014**, *53*, 2751–2753; f) J. Friedrich, D. Schneider, L. Bock, C. Maichle-Mössmer, R. Anwander, *Inorg. Chem.* **2017**, *56*, 8114–8127.

[4] For example, see: a) P. S. Gradeff, F. G. Schreiber, K. C. Brooks, R. E. Sievers, *Inorg. Chem.* **1985**, *24*, 1110–1111; b) P. S. Gradeff, F. G. Schreiber, H. Mauermann, *J. Less-Common Met.* **1986**, *126*, 335–338; c) W. J. Evans, T. J. Deming, J. M. Olofson, J. W. Ziller, *Inorg. Chem.* **1989**, *28*, 4027–4034; d) V.

Nair, A. Deepthi, *Chem. Rev.* **2007**, *107*, 1862–1891; e) V. Nair, A. Deepthi, *Tetrahedron* **2009**, *65*, 10745–10755; f) A. R. Crozier, C. Schädle, C. Maichle-Mössmer, K. W. Törnroos, R. Anwander, *Dalton Trans.* **2013**, *42*, 5491–5499.
[5] T. Imamoto, Y. Koide, S. Hiyama, *Chem. Lett.* **1990**, *19*, 1445–1446.
[6] For example, see: a) P. S. Gradeff, H. Mauermann, F. G. Schreiber, *J. Less-Common Met.* **1989**, *149*, 87–94; b) L. G. Hubert-Pfalzgraf, N. El Khokh, J.-C. Daran, *Polyhedron* **1992**, *11*, 59–63; c) L. G. Hubert-Pfalzgraf, V. Abada, J. Vaissermann, *J. Chem. Soc., Dalton Trans.* **1998**, 3437–3442; d) S. Daniele, L. G. Hubert-Pfalzgraf, M. Perrin, *Polyhedron* **2002**, *21*, 1985–1990; e) P. L. Arnold, I. J. Casely, S. Zlatogorsky, C. Wilson, *Helv. Chim. Acta* **2009**, *92*, 2291–2303; f) E. M. Broderick, P. L. Diaconescu, *Inorg. Chem.* **2009**, *48*, 4701–4706; g) E. M. Broderick, P. S. Thuy-Boun, N. Guo, C. S. Vogel, J. Sutter, J. T. Miller, K. Meyer, P. L. Diaconescu, *Inorg. Chem.* **2011**, *50*, 2870–2877; h) P. Dröse, J. Gottfriedsen, C. G. Hrib, P. G. Jones, L. Hilfert, F. T. Edelmann, *Z. Anorg. Allg. Chem.* **2011**, *637*, 369–373; i) L. Li, F. Yuan, T. Li, Y. Zhou, M. Zhang, *Inorg. Chim. Acta* **2013**, *397*, 69–74; j) W. Huang, P. L. Diaconescu, *Inorg. Chem.* **2016**, *55*, 10013–10023; k) M. Paul, S. Shirase, Y. Morimoto, L. Mathey, B. Murugesapandian, S. Tanaka, S. Itoh, H. Tsurugi, K. Mashima, *Chem. Eur. J.* **2016**, *22*, 4008–4014.
[7] A. R. Crozier, A. M. Bienfait, C. Maichle-Mössmer, K. W. Törnroos, R. Anwander, *Chem. Commun.* **2013**, *49*, 87–89.
[8] a) D. Werner, G. B. Deacon, P. C. Junk, R. Anwander, *Chem. Eur. J.* **2014**, *20*, 4426–4438; b) U. J. Williams, D. Schneider, W. L. Dorfner, C. Maichle-Mössmer, P. J. Carroll, R. Anwander, E. J. Schelter, *Dalton Trans.* **2014**, *43*, 16197–16206; c) J. E. Kim, P. J. Carroll, E. J. Schelter, *Chem. Commun.* **2015**, *51*, 15047–15050; d) J. R. Levin, W. L. Dorfner, A. X. Dai, P. J. Carroll, E. J. Schelter, *Inorg. Chem.* **2016**, *55*, 12651–12659; e) D. Werner, G. B. Deacon, P. C. Junk, R. Anwander, *Dalton Trans.* **2017**, *46*, 6265–6277.
[9] D. Schneider, T. Spallek, C. Maichle-Mössmer, K. W. Törnroos, R. Anwander, *Chem. Commun.* **2014**, *50*, 14763–14766.
[10] P. B. Hitchcock, M. F. Lappert, A. V. Protchenko, *Chem. Commun.* **2006**, 3546–3548.
[11] W. J. Evans, D. S. Lee, D. B. Rego, J. M. Perotti, S. A. Kozimor, E. K. Moore, J. W. Ziller, *J. Am. Chem. Soc.* **2004**, *126*, 14574–14582.
[12] a) R. Anwander, O. Runte, J. Eppinger, G. Gerstberger, E. Herdtweck, M. Spiegler, *J. Chem. Soc., Dalton Trans.* **1998**, 847–858; b) I. Nagl, W. Scherer, M. Tafipolsky, R. Anwander, *Eur. J. Inorg. Chem.* **1999**, 1405–1407; c) J. Eppinger, M. Spiegler, W. Hieringer, W. A. Herrmann, R. Anwander, *J. Am. Chem. Soc.* **2000**, *122*, 3080–3096; d) C. Meermann, G. Gerstberger, M. Spiegler, K. W. Törnroos, R. Anwander, *Eur. J. Inorg. Chem.* **2008**, 2014–2023.
[13] For example, see: a) A. Sen, H. A. Stecher, A. L. Rheingold, *Inorg. Chem.* **1992**, *31*, 473–479; b) M. D. Walter, R. Fandos, R. A. Andersen, *New J. Chem.* **2006**, *30*, 1065; c) I. J. Casely, S. T. Liddle, A. J. Blake, C. Wilson, P. L. Arnold, *Chem. Commun.* **2007**, 5037–5039; d) M. D. Walter, C. H. Booth, W. W. Lukens, R. A. Andersen, *Organometallics* **2009**, *28*, 698–707; e) J. R. Robinson, C. H. Booth, P. J. Carroll, P. J. Walsh, E. J. Schelter, *Chem. Eur. J.* **2013**, *19*, 5996–6004; f) D. Schneider, N. Harmgarth, F. T. Edelmann, R. Anwander, *Chem. Eur. J.* **2017**, *23*, 12243–12252.
[14] H. Sasai, T. Suzuki, N. Itoh, K. Tanaka, T. Date, K. Okamura, M. Shibasaki, *J. Am. Chem. Soc.* **1993**, *115*, 10372–10373.
[15] a) J. R. Robinson, P. J. Carroll, P. J. Walsh, E. J. Schelter, *Angew. Chem. Int. Ed.* **2012**, *51*, 10159–10163; *Angew. Chem.* **2012**, *124*, 10306–10310; b) J. R. Robinson, Z. Gordon, C. H. Booth, P. J. Carroll, P. J. Walsh, E. J. Schelter, *J. Am. Chem. Soc.* **2013**, *135*, 19016–19024.
[16] G. R. Fulmer, A. J. M. Miller, N. H. Sherden, H. E. Gottlieb, A. Nudelman, B. M. Stoltz, J. E. Bercaw, K. I. Goldberg, *Organometallics* **2010**, *29*, 2176–2179.
[17] in *COSMO v. 1.61*, *Vol.* B. A. I., Madison, WI, **2012**.
[18] in *APEX 2 v. **2012**.10_0*, *Vol.* B. A. I., Madison, WI, **2012**.
[19] a) in *SAINT v. 8.34A*, *Vol.* B. A. I., Madison, WI, **2013**; b) in *SAINT v. 8.37A*, *Vol.* Bruker AXS Inc., Madison, WI, **2015**.
[20] L. Krause, R. Herbst-Irmer, G. M. Sheldrick, D. Stalke, *J. Appl. Crystallogr.* **2015**, *48*, 3–10.
[21] G. M. Sheldrick, *Acta Crystallogr., Sect. C: Struct. Chem.* **2015**, *71*, 3–8.
[22] C. B. Hübschle, G. M. Sheldrick, B. Dittrich, *J. Appl. Crystallogr.* **2011**, *44*, 1281–1284.

Received: September 20, 2019

Supporting Information

A Facile Route toward Ceric Silylamide $[Ce\{N(SiHMe_2)_2\}_4]$

Uwe Bayer, Lorenz Bock, Cäcilia Maichle-Mössmer, and Reiner Anwander*

ejic201901023-sup-0001-SupMat.pdf

Table of Contents

1. NMR Spectra S3

2. DRIFT Spectra S10

3. Crystallographic Data S13

1. NMR Spectra (solvent signals are marked with *)

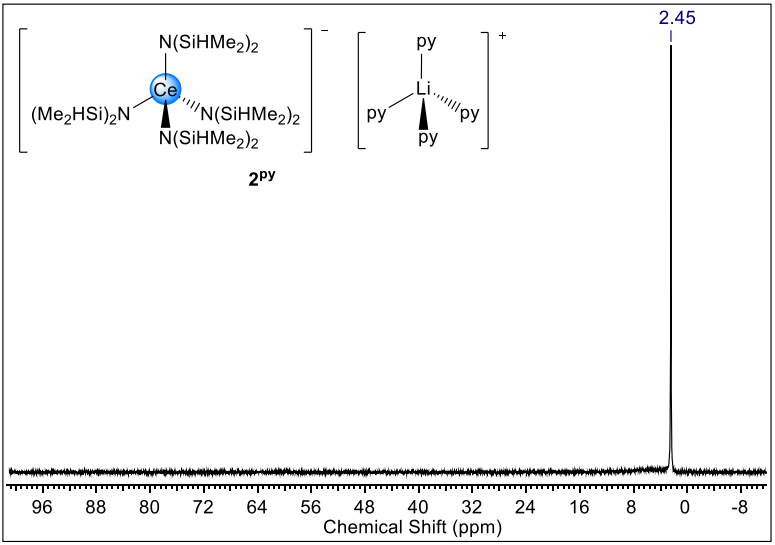

Figure S1. ^{7}Li NMR ($C_6D_6/C_6H_4F_2$, 299 K, 116.6 MHz) of $[Ce\{N(SiHMe_2)_2\}_4][Li(py)_4]$ (**2**^{py}).

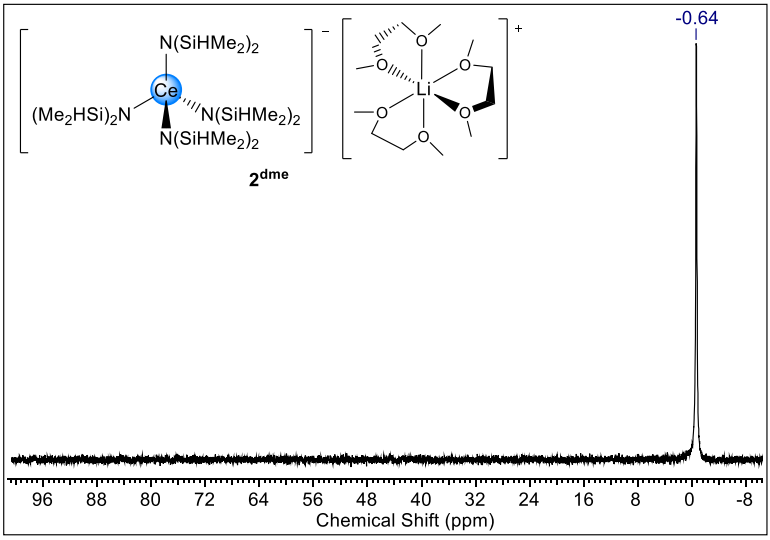

Figure S2. ^{7}Li NMR ($C_6D_6/C_6H_4F_2$, 299 K, 116.6 MHz) of $[Ce\{N(SiHMe_2)_2\}_4][Li(dme)_3]$ (**2**^{dme}).

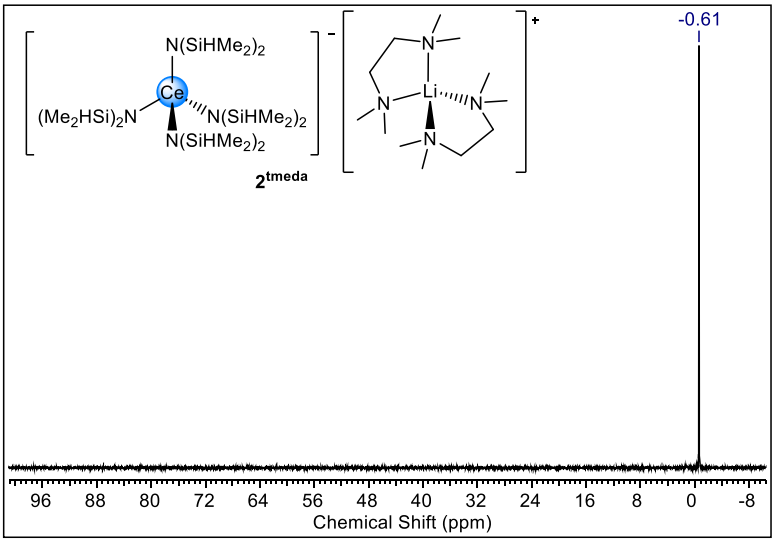

Figure S3. ^{7}Li NMR ($C_6D_6/C_6H_4F_2$, 299 K, 116.6 MHz) of $[Ce\{N(SiHMe_2)_2\}_4][Li(tmeda)_2]$ (**2**^{tmeda}).

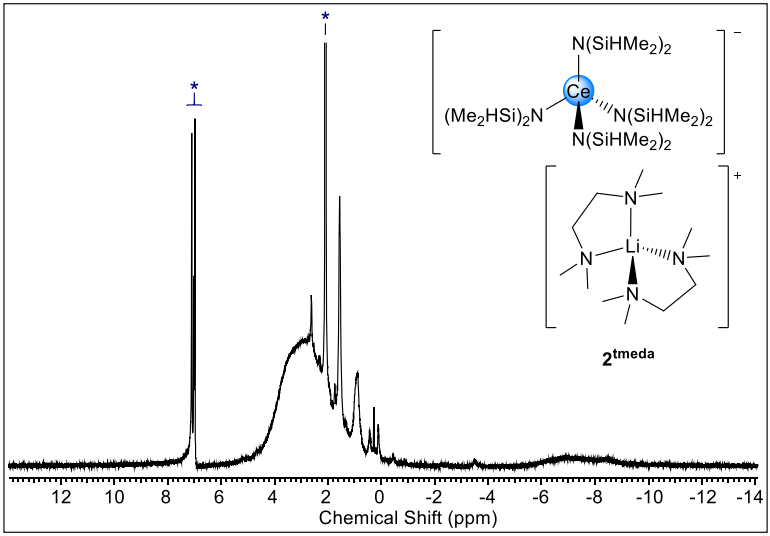

Figure S4. ^{1}H NMR (tol-d_8, 299 K, 250.1 MHz) of $[Ce\{N(SiHMe_2)_2\}_4][Li(tmeda)_2]$ (**2**^{tmeda}).

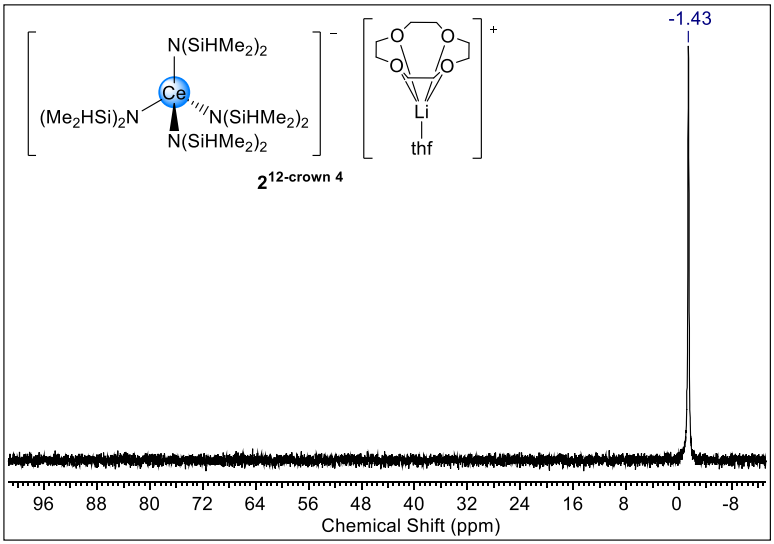

Figure S5. ^{7}Li NMR ($C_6D_6/C_6H_4F_2$, 299 K, 116.6 MHz) of [Ce{N(SiHMe$_2$)$_2$}$_4$][Li(12-crown-4)(thf)] (**2**$^{12\text{-crown-4}}$).

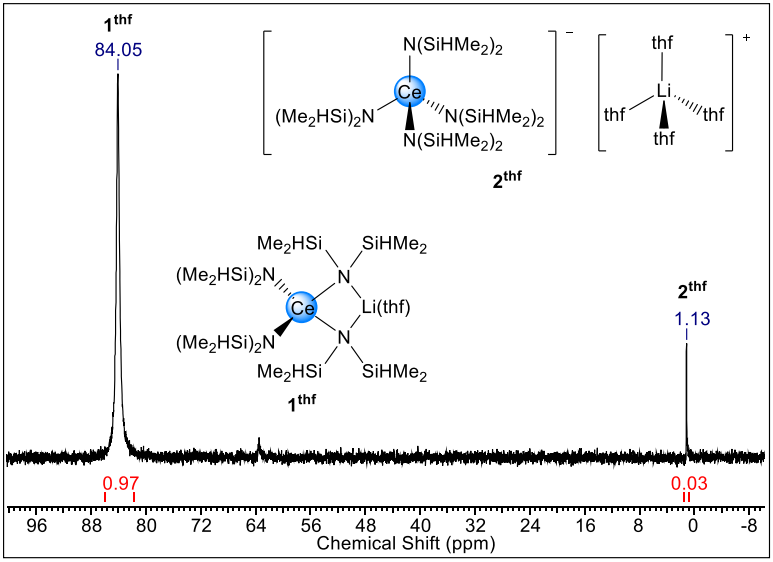

Figure S6. ^{7}Li NMR ($C_6D_6/C_6H_4F_2$, 299 K, 116.6 MHz) of [Ce{N(SiHMe$_2$)$_2$}$_4$Li(thf)] (**1**$^{\text{thf}}$).

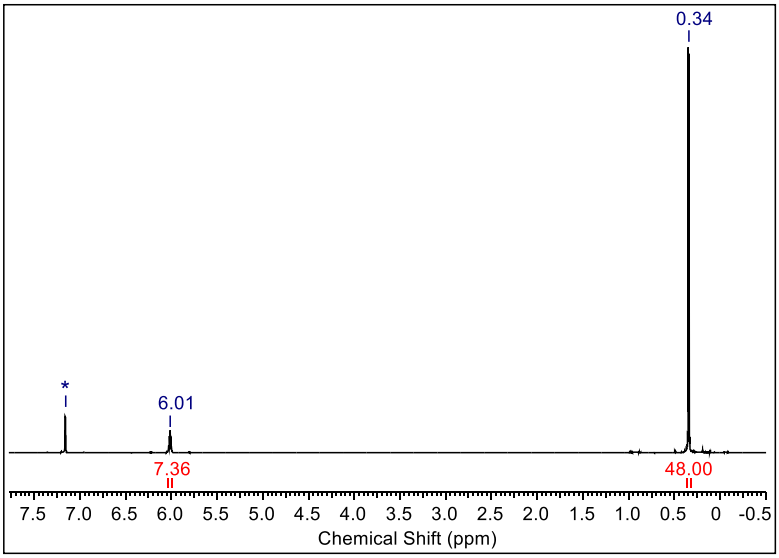

Figure S7. ^{1}H NMR (C_6D_6, 299 K, 400.1 MHz) of the crude product of the oxidation of [Ce{N(SiHMe$_2$)$_2$}$_4$][Li(py)$_4$] (**2^{py}**).

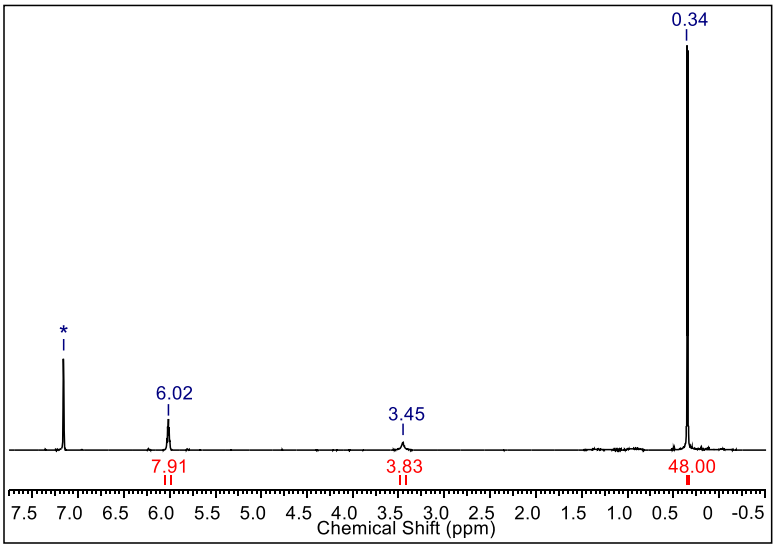

Figure S8. ^{1}H NMR (C_6D_6, 299 K, 400.1 MHz) of the crude product of the oxidation of [Ce{N(SiHMe$_2$)$_2$}$_4$][Li(dme)$_3$] (**2^{dme}**).

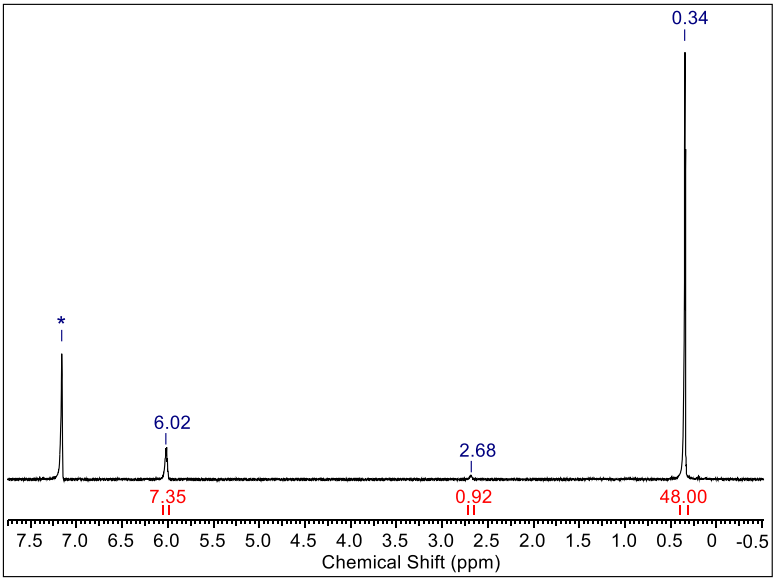

Figure S9. ^{1}H NMR (C_6D_6, 299 K, 400.1 MHz) of the crude product of the oxidation of [Ce{N(SiHMe$_2$)$_2$}$_4$][Li(tmeda)$_2$] (**2^{tmeda}**).

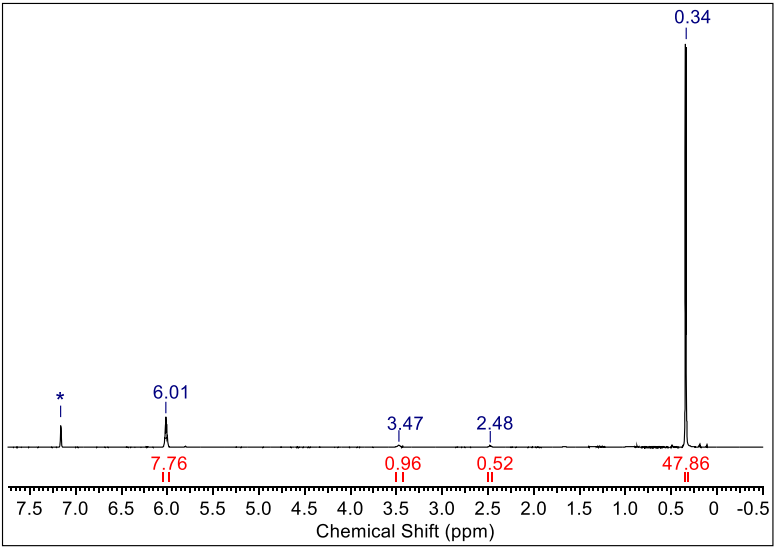

Figure S10. ^{1}H NMR (C_6D_6, 299 K, 400.1 MHz) of the crude product of the oxidation of [Ce{N(SiHMe$_2$)$_2$}$_4$][Li(12-crown-4)(thf)] (**2$^{12\text{-crown-4}}$**).

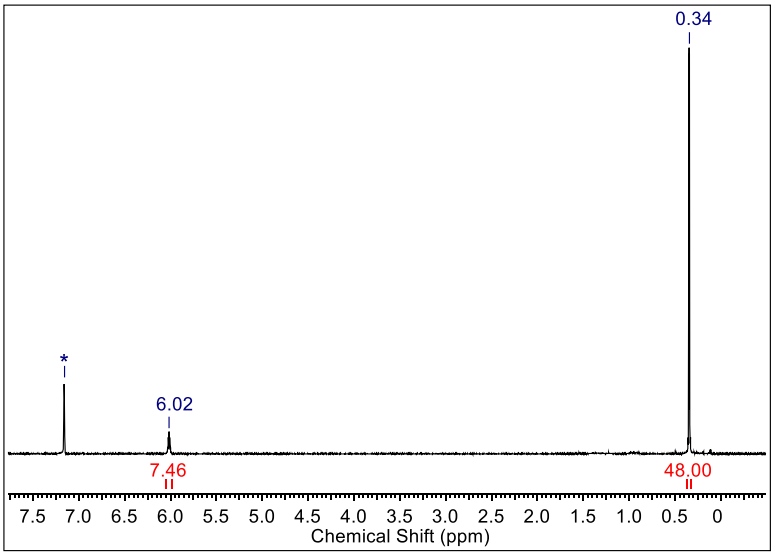

Figure S11. ^{1}H NMR (C_6D_6, 299 K, 400.1 MHz) of the crude product of the oxidation of [Ce{N(SiHMe$_2$)$_2$}$_4$Li(thf)] (**1^{thf}**).

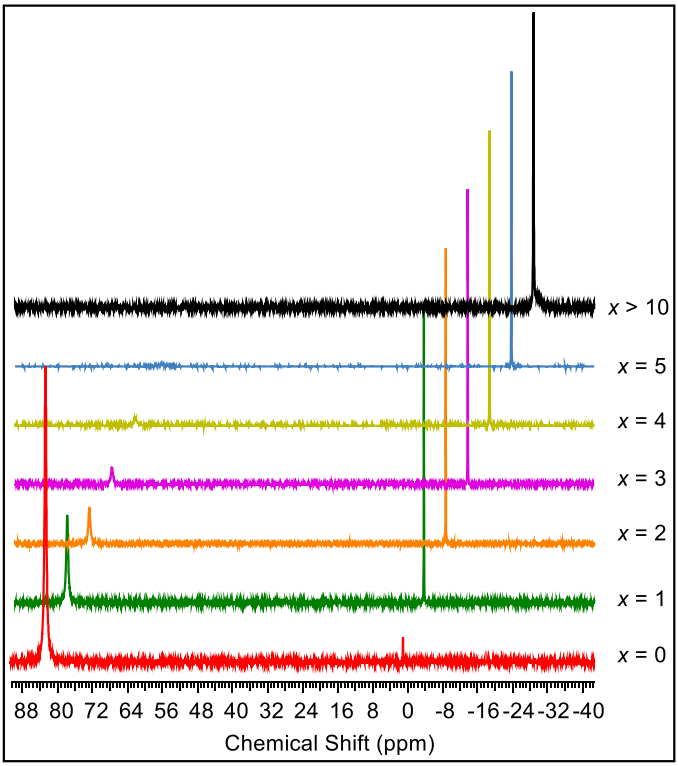

Figure S12. Stacked ^{7}Li NMR spectra of [Ce{N(SiHMe$_2$)$_2$}$_4$Li(thf)] (**1^{thf}**) with additional *x* equivalents of THF added.

2. DRIFT Spectra

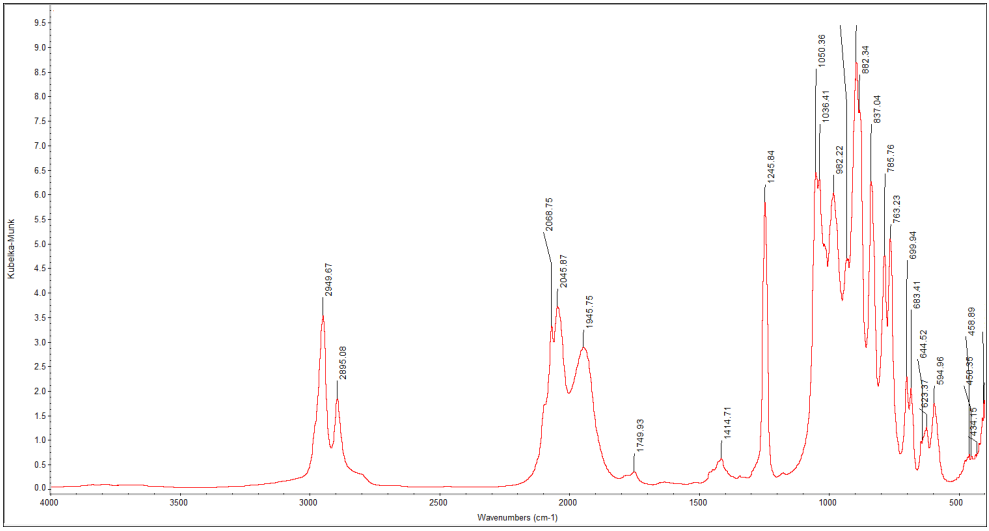

Figure S13. DRIFT spectrum of [Ce{N(SiHMe$_2$)$_2$}$_4$Li(thf)] (**1^{thf}**).

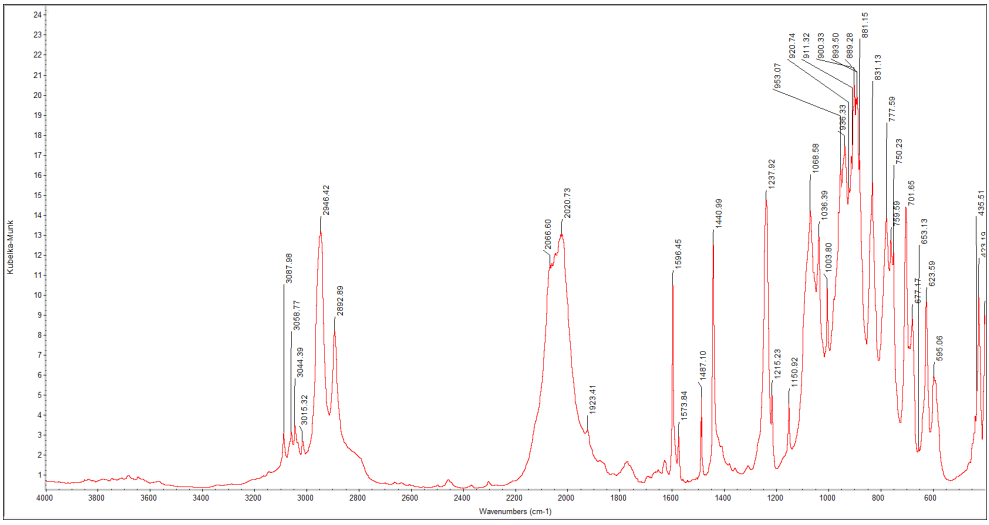

Figure S14. DRIFT spectrum of [Ce{N(SiHMe$_2$)$_2$}$_4$][Li(py)$_4$] (**2^{py}**).

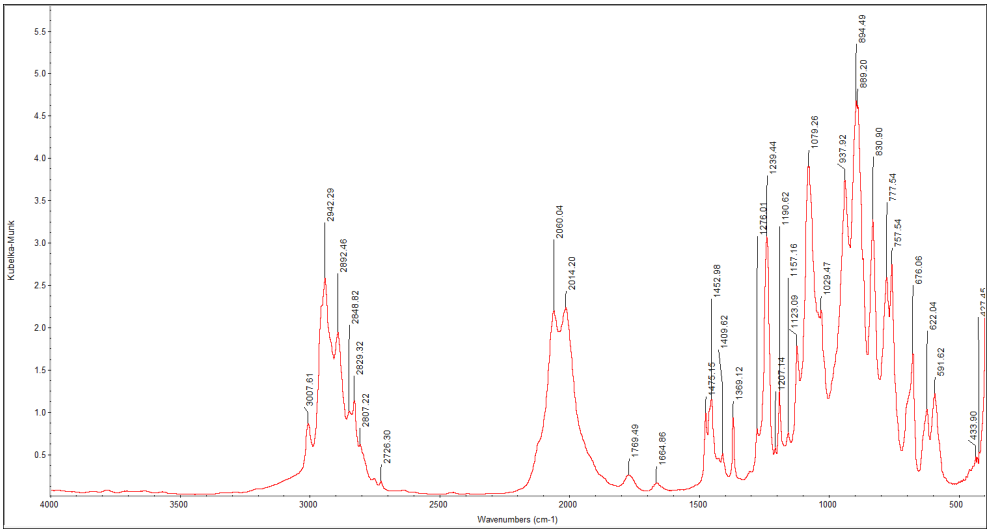

Figure S15. DRIFT spectrum of $[Ce\{N(SiHMe_2)_2\}_4][Li(dme)_3]$ (**2**^{dme}).

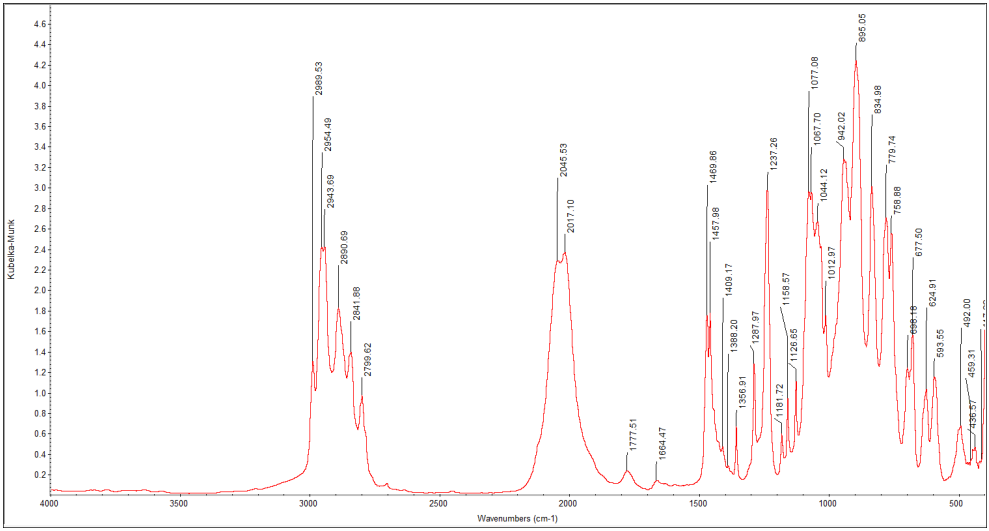

Figure S16. DRIFT spectrum of $[Ce\{N(SiHMe_2)_2\}_4][Li(tmeda)_2]$ (**2**^{tmeda}).

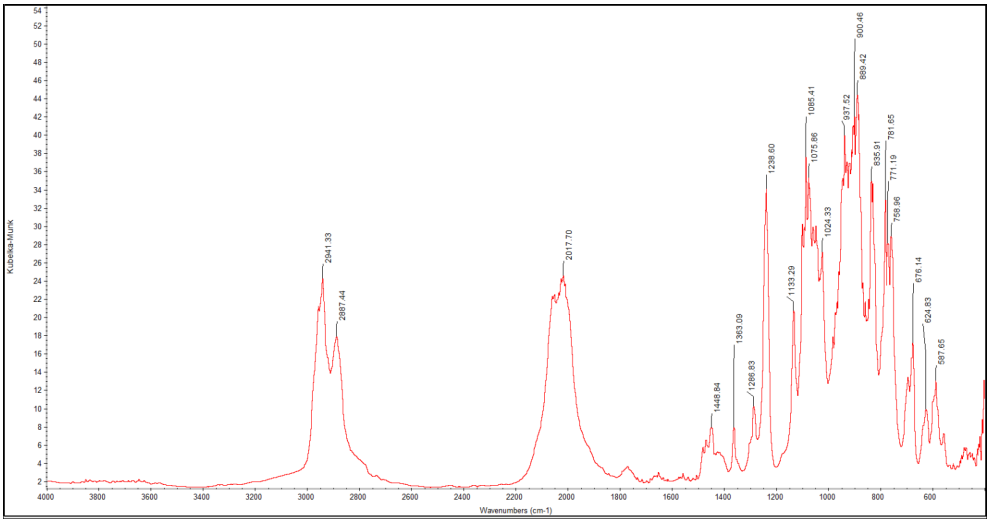

Figure S17. DRIFT spectrum of [Ce{N(SiHMe$_2$)$_2$}$_4$][Li(12-crown-4)(thf)] (**2$^{12\text{-crown-4}}$**).

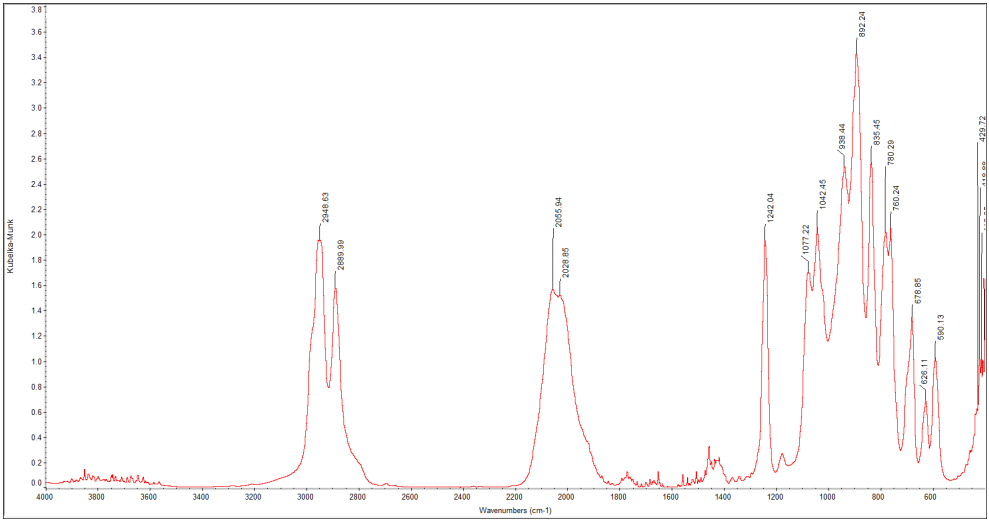

Figure S18. DRIFT spectrum of [Ce{N(SiHMe$_2$)$_2$}$_4$][Li(thf)$_4$] (**2^{thf}**).

3. Crystallographic Data

Table S1. Crystallographic data for compounds $\mathbf{2^{py}}$, $\mathbf{2^{tmeda}}$, $\mathbf{2^{12\text{-}crown\text{-}4}}$, and $\mathbf{2^{thf}}$

	$\mathbf{2^{py}}$	$\mathbf{2^{tmeda}}$	$\mathbf{2^{12\text{-}crown\text{-}4}}$	$\mathbf{2^{thf}}$
CCDC	1954721	1954723	1954722	1954724
formula	$C_{36}H_{76}CeLiN_8Si_8$	$C_{28}H_{88}CeLiN_8Si_8$	$C_{28}H_{80}CeLiN_4O_5Si_8$	
M [g·mol^{-1}]	992.82	908.84	924.74	964.84
λ [Å]	0.71073	0.71073	0.71073	0.71073
color	yellow	orange	colorless	yellow
crystal dimensions	0.127 x 0.116 x	0.346 x 0.132 x	0.155 x 0.121 x	0.221 x 0.151 x
[mm]	0.043	0.131	0.101	0.135
crystal system	Monoclinic	Monoclinic	Monoclinic	Triclinic
space group	P 2_1/c	P 2_1/c	P 2_1/c	P$\bar{1}$
a [Å]	14.5041(11)	16.2760(16)	19.025(4)	14.465(4)
b [Å]	16.1209(13)	14.9972(15)	11.663(2)	19.271(5)
c [Å]	24.568(2)	22.022(2)	23.592(5)	20.664(6)
α [°]	90	90	90	106.320(3)
β [°]	97.996(2)	96.301(2)	105.090(4)	94.712(3)
γ [°]	90	90	90	98.744(3)
V [Å^3]	5688.7(8)	5343.0(9)	5054.2(17)	5416(2)
Z	4	4	4	4
F(000)	2084	1940	1956	2052
T [K]	180(2)	100(2)	100(2)	100(2)
ρ_{calcd} [g·cm^{-3}]	1.159	1.130	1.215	1.183
μ[mm^{-1}]	0.999	1.057	1.123	1.050
Data / restraints / parameters	7924 / 556 / 580	13380 / 1524/ 714	10328 / 0 / 472	18575/996/1027
Goodness of fit	1.010	1.027	1.005	1.188
R_1 (I > 2σ (I))[a]	0.0422	0.0737	0.0409	0.0655
$_\omega R_2$ (all data)[b]	0.0982	0.2094	0.0971	0.1835

[a] $R_1 = \Sigma(||F0|-|Fc||)/\Sigma|F0|,F0> 4s(F0)$. $_\omega R_2 = \{\Sigma[w(F02-Fc2)2/\Sigma[w(F02)^2]]\}^{1/2}$

Paper II

ORGANOMETALLICS

pubs.acs.org/Organometallics Article

SOMC@Periodic Mesoporous Silica Nanoparticles: Meerwein–Ponndorf–Verley Reduction Promoted by Immobilized Rare-Earth-Metal Alkoxides

Lorenz Bock, Xuan Tran, Yucang Liang, Markus Kramer, Cäcilia Maichle-Mössmer, and Reiner Anwander*

Cite This: *Organometallics* 2020, 39, 1046–1058 Read Online

ACCESS | Metrics & More | Article Recommendations | Supporting Information

ABSTRACT: The Meerwein–Ponndorf–Verley (MPV) reduction is a reaction that offers a mild reduction of aldehydes and ketones to the corresponding alcohols. Although described as a catalytic reaction, its real-life applicability suffers from the necessity of using the standard catalyst $[Al(OiPr)_3]$ in stoichiometric amounts or even in excess. Rare-earth-metal-based catalysts are capable of performing in these reactions in a truly catalytic fashion. The ceric alkoxide $[Ce(OiPr)_4]_3$ has been synthesized via silylamine elimination from $Ce[N(SiHMe_2)_2]_4$ with isopropyl alcohol, its trimetallic solid-state structure has been determined by X-ray diffraction, and its performance in the MPV reduction of 4-*t*Bu-cyclohexanone has been examined and compared to that of cerous $[Ce(OCH_2tBu)_3]_4$. Spherical mesoporous silica nanoparticles with an MCM-41-type honeycomb pore symmetry, termed MSN-MCM-41 (particle size, ca. 250 nm diameter; pore size, 2.6 nm diameter), are employed for grafting the molecular precursors $Ce[N(SiHMe_2)_2]_4$, $[Ce(OiPr)_4]_3$, $Ce[N(SiMe_3)_2]_3$, and $La[N(SiMe_3)_2]_3$ according to the methods of surface organometallic chemistry (SOMC). The MPV reductions carried out with the homogeneous and heterogeneous catalysts reveal (a) a better performance of Ce(III) in comparison to Ce(IV), (b) better performance of $La[N(SiMe_3)_2]_3$@MSN-MCM-41 in comparison to $Ce[N(SiMe_3)_2]_3$@MSN-MCM-41 (high sensitivity of Ce(III)-grafted materials), and (c) reusability of the grafted catalyst systems. All hybrid materials were characterized by PXRD, N_2 physisorption, and $^1H/^{13}C/^{29}Si$ MAS NMR and FTIR spectroscopies as well as elemental analysis.

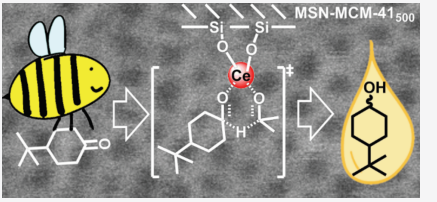

INTRODUCTION

Surface organometallic chemistry (SOMC) embraces the chemistry of organometallic complexes at the surface of suitable carrier materials, routinely resulting in metal–support chemical bonds.[1,2] The utilization of both discrete organometallics and reactive surface functional groups may generate robust hybrid materials with well-defined surface species. Optionally or ideally, the implementation of micro- or mesoporous materials can maximize the available surface area, with the performed reactions being confined to nanovessels, further influencing the reaction kinetics.[3,4] Here, mesoporous silicas have emerged as a class of versatile materials, combining a high intrapore specific surface area, a uniform pore size tunable over a wide range, the possibility of obtaining different pore geometries, a controllable population of reactive surface moieties, controllable particle morphology, and biological compatibility.[4,5]

Molecular catalysts immobilized in this way have several advantages in comparison to classical homogeneous or bulk heterogeneous catalysts: while they retain or even surpass the activity of homogeneous catalysts (every metal center is potentially catalytically active), deactivation and separation issues play a minor role.[1] At the same time the drawbacks of classical heterogeneous catalysts, i.e. the majority of the metal centers are inaccessibly located within the bulk of the catalytic material, are efficiently eluded.[2] Thus, SOMC-derived catalysts combine the high activity of well-defined homogeneous catalysts with the ease of separation and recyclability of heterogeneous catalysts. Furthermore, well-chosen SOMC protocols ensure site isolation of monometallic surface-grafted species, which minimizes the amount of intrinsically inactive metal centers formed via oligomerization (as routinely observed for homogeneous metalorganic catalysts).[1,2,4,6]

The Meerwein–Ponndorf–Verley (MPV) reduction, first developed in the 1920s, represents a reductive transformation of aldehydes and ketones to the corresponding alcohols in the presence of sacrificial alcohol.[7–9] The catalytically active site in this reaction is a Lewis acidic metal center, Al(III) in

Special Issue: Organometallic Chemistry at Various Length Scales

Received: November 21, 2019
Published: February 3, 2020

https://dx.doi.org/10.1021/acs.organomet.9b00794
Organometallics 2020, 39, 1046–1058

$[Al(OiPr)_3]$ in the originally described reaction, that, according to accepted theories (quantum chemical calculations), supports hydride transfer via a six-membered transition state (see Scheme 1).[10,11] While in principle this reaction affords a mild and efficient way to reduce aldehydes and ketones, widespread application has been hampered by the relative inactivity of $[Al(OiPr)_3]$, necessitating the use of "superstoichiometric amounts of catalyst".[12]

Scheme 1. Classical Aluminum Isopropoxide Promoted MPV Reduction and Its Reverse, the Oppenauer Oxidation

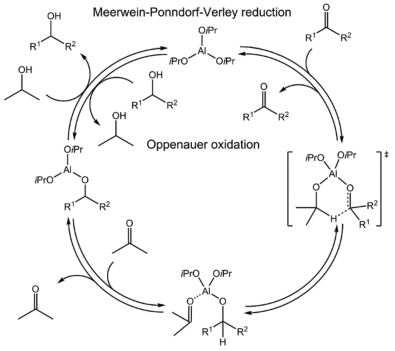

It has been shown in earlier works that the catalytic activity of the traditional MPV catalyst, $[Al(OiPr)_3]$, can be greatly improved with respect to established procedures, first by rigorously excluding oxygen and moisture and second by surface grafting on a suitable carrier material.[13] Apart from Al(III), a plethora of other metal centers has been shown to engage in catalytic MPV reductions, homogeneously[10,14−16] as well as heterogeneously.[17−19] Among these, rare-earth-metal derivatives stand out as particularly active catalysts,[14,16,20−24] which is attributed to their relatively high (Ln(III)-size dependent) Lewis acidity, tendency to form thermally stable alkoxide complexes, and ability to easily exchange alkoxy ligands.[10]

The application of SOLnC (surface organolanthanide chemistry) thus promises catalysts that should in theory be highly active, easy to separate, and recyclable. Indeed, the first investigations into this area undertaken over 20 years ago have produced extremely promising results.[25] Herein, we wish to further expand our understanding of the rare-earth-metal alkoxide-based MPV reduction, especially with regard to the Ce(III)/(IV) redox couple and the catalytic performance of several SOLnC-derived heterogeneous catalysts. The investigation of Ce(IV) alkoxide hybrid materials seemed a perfectly valid issue, given the successful application of silica-grafted Zr(IV) and Hf(IV) species in the catalytic MPV reduction.[26−28]

RESULTS AND DISCUSSION

Molecular Cerium Alkoxide Complexes. As isopropyl alcohol is usually the solvent and hydride source in the MPV reduction, as such displacing any alkoxy ligands present at the catalytically active metal center, cerium isopropoxides were envisaged as potential catalyst precursors. Previous to this work, the only known Ce(IV) isopropoxide was $[Ce(OiPr)_4(HOiPr)]_2$, first synthesized by Bradley et al.[29] and later structurally elucidated by Toledano et al. and Caulton et al.[30,31] It is noteworthy that for $[Ce(OiPr)_4(HOiPr)]_2$: (a) it was obtained from the ceric precursors $(C_5H_6N)_2CeCl_6$ and $(NH_4)_2Ce(NO_3)_6$ (= CAN),[30,32] (b) it undergoes photoreduction to the mixed-valent cluster $Ce_4O(OiPr)_{13}(HOiPr)$ upon visible irradiation,[33] (c) it undergoes facile thermal desolvation to form the ceric cluster $Ce_4O(OiPr)_{14}$,[34] and (d) the solid-state structure of dimeric $[Ce(OiPr)_4(HOiPr)]_2$ shows a phase transition at about −90 °C,[31] while the coordination sphere of the ceric centers is saturated by an additional alcohol donor molecule engaging in alcohol/alkoxide hydrogen bonding.[30,35] In attempts to synthesize ceric isopropoxide from $Ce[N(SiHMe_2)_2]_4$,[36] instead of the alcohol-coordinated dimer, the homoleptic trimer $[Ce(OiPr)_4]_3$ (**1**) was identified as the sole reaction product. It is noteworthy that dimeric $[Ce(OiPr)_4(HOiPr)]_2$ did neither form in the presence of five equiv of isopropyl alcohol nor when a significant excess of isopropyl alcohol was added. This behavior, and the pronounced difference in color between $Ce[N(SiHMe_2)_2]_4$ (dark red) and $[Ce(OiPr)_4]_3$ (yellow), simplified the reaction protocol to the extent that a solution of the silylamide precursor complex could be titrated with a mixture of isopropyl alcohol and *n*-hexane until no more color change was observable.

Ceric alkoxide **1** crystallizes as a trimer in the triclinic space group $P\bar{1}$ with four molecules in the unit cell. To our knowledge the $[Ce(OiPr)_4]_3$ trimers show an unprecedented variation of a structural motif well-known in metal alkoxide chemistry,[10] with two alkoxy ligands bridging the metal atoms in a μ_3 fashion (Figure 1). Moreover, three alkoxy ligands adopt a μ_2 coordination. The remaining isopropoxy ligands are bonded terminally to the cerium centers, with Ce3

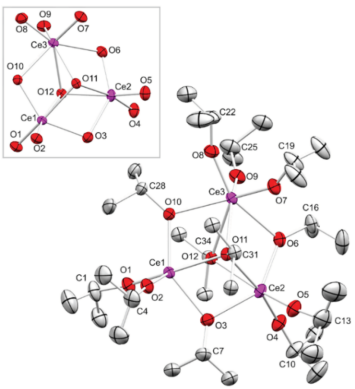

Figure 1. Crystal structure of one of the four independent molecules of $[Ce(OiPr)_4]_3$ in the unit cell. Ellipsoids are shown at the 50% level, and hydrogen atoms and disorders in the isopropyl groups are omitted for clarity. The inset shows the core of the structure without the C_3H_7 (*i*Pr) groups. For selected interatomic distances and angles, see Table 1.

https://dx.doi.org/10.1021/acs.organomet.9b00794
Organometallics 2020, 39, 1046−1058

accommodating three out of seven ligands. Thus, Ce3 exhibits a heptacoordination which breaks the C_3 symmetry usually present in these types of metal alkoxides,[10,37] as Ce1 and Ce2 are six-coordinate. Consequently, the Ce3−O(μ_2) bonds are significantly lengthened in comparison to the Ce1−O10 and Ce2−O6 bonds (Ce3−O6/O10 2.558(3)/2.497(3) Å, Ce1−O10 2.237(3) Å, Ce2−O6 2.184(3) Å), as are the Ce3−O(μ_3) bonds (Ce3−O11/12 2.517(3)/2.721(3) Å, Ce1−O11/12 2.480(3)/2.362(3) Å, Ce2−O11/12 2.446(3)/2.462(3) Å) (Table 1). The terminal and μ_2-bridging Ce−O bond lengths

Table 1. Selected Interatomic Distances (Å) and Bond Angles (deg) for 1

distance		angle	
Ce1−O1	2.061(3)	Ce1−O1−C1	165.7(3)
Ce1−O2	2.071(3)	Ce1−O2−C4	174.7(3)
Ce1−O3	2.337(3)	Ce1−O3−C7	129.6(8)
Ce1−O10	2.237(3)	Ce1−O10−C28	132.0(3)
Ce1−O11	2.480(3)	Ce1−O11−C31	123.8(2)
Ce1−O12	2.362(3)	Ce1−O12−C34	130.2(3)
Ce2−O3	2.357(3)	Ce2−O3−C7	127.1(7)
Ce2−O4	2.070(3)	Ce2−O4−C10	166.6(3)
Ce2−O5	2.06(1)	Ce2−O5−C13	169(1)
Ce2−O6	2.184(3)	Ce2−O6−C16	138.8(3)
Ce2−O11	2.446(3)	Ce2−O11−C31	121.7(2)
Ce2−O12	2.462(3)	Ce2−O12−C34	117.9(2)
Ce3−O6	2.558(3)	Ce3−O6−C16	117.2(3)
Ce3−O7	2.100(3)	Ce3−O7−C19	149.0(9)
Ce3−O8	2.087(3)	Ce3−O8−C22	159.0(3)
Ce3−O9	2.092(3)	Ce3−O9−C25	146.9(7)
Ce3−O10	2.497(3)	Ce3−O10−C28	123.7(3)
Ce3−O11	2.517(3)	Ce3−O11−C31	116.6(2)
Ce3−O12	2.721(3)	Ce3−O12−C34	116.8(2)

correspond well to the values reported by us for the terminal and bridging neopentoxy ligands in oligomeric noncyclic $[Ce(OCH_2tBu)_4]_3$.[38] The same structural motif, albeit with one less terminal alkoxy ligand and one μ_3-bridging oxo ligand, has been reported for ceric $[Ce_3(O)(OtBu)_{10}]$.[39,40] Solely *tert*-butoxy-containing $Ce_3(OtBu)_{11}$ shows mixed valences with two six-coordinate Ce(IV) centers and one six-coordinate Ce(III) center. The latter complex was first obtained by Arnold et al. as a decomposition product in the attempted synthesis of $Ce(OtBu)_4(thf)_2$,[37] where only a connectivity could be ascertained, and later again found via an attempted sublimation of dimeric $[Ce(OtBu)_4]_2$ by Mathur et al., where the structure could be fully elucidated.[41] A similar mixed-valent cluster with two Ce(IV) centers and one Ce(III) center, bearing one nitrato in addition to ten alkoxy ligands, had already been described in 2002 by Lappert et al.[42]

Even though **1** shows slightly elongated Ce3−O bonds similarly to the Ce(III) center in Mathur's *tert*-butoxide $Ce_3(OtBu)_{11}$, as well as distinct Ce3−$O_{terminal}$ bonds ranging from 2.497(3) to 2.721(3) Å and 2.087(3) to 2.100(3) Å, respectively, a mixed-valent complex with a coordinating free alcohol at Ce3 can be ruled out. For direct comparison, the terminal Ce−O bond lengths of the six-coordinate metal centers in $[Ce(OiPr)_4(HOiPr)]_2$ range from 2.083(9) to 2.188(6) Å, while the alcoholic Ce−O distance is elongated to 2.523(6) Å.[30] The absence of an alcohol adduct is further corroborated by the absence of an OH stretching vibration in the IR spectrum, the absence of paramagnetic signal broadening in the ^{1}H NMR spectrum (see Figure S15), and a magnetic susceptibility study showing compound **1** to be diamagnetic with μ_{eff} = 0.70 μ_B, determined by the Evans method (see the Experimental Section).

^{1}H-DOSY measurements with monomeric $Ce[N(SiHMe_2)_2]_4$ as an internal standard revealed that **1** does not abandon its trimeric structure upon dissolution in toluene even at ambient temperature. According to the Stokes−Einstein equation,[43] the diffusion coefficients of two species within the same sample are inversely proportional to their hydrodynamic radii. Thus, the calculated ratio of the molecular radius of the internal standard with the radii of the two possible species that could be adopted by **1** in solution (monomer or trimer, molecular radii determined from the solid-state structure for the trimer and from an energy-optimized structure (Chem3D) for the monomer) could be compared with the ratio of the diffusion coefficients determined from the diffusion measurement. The ratio of diffusion coefficients was determined as 1.13, being in good agreement with a trimeric structure for **1** in solution (ratio of molecular radii 1.15), while ruling out a monomeric structure (ratio of molecular radii 0.88) (see also Table 2 and pp S19−S20 in the Supporting Information).

Table 2. Molecular Radii and Ratios of the Two Possible $[Ce(OiPr)_4]_n$ Species and $Ce[N(SiHMe_2)_2]_4$

compound	r_{calcd}/Å[a]	r_{measd}/Å[b]	ratio vs $Ce[N(SiHMe_2)_2]_4$
$[Ce(OiPr)_4]_3$ (**1**)	6.35	6.35	1.15
$Ce(OiPr)_4$	4.85	n/a	0.88
$Ce[N(SiHMe_2)_2]_4$	5.5	5.5[33]	

[a]From energy-optimized structures (Chem3D). [b]From X-ray crystal structures.

Variable-temperature ^{1}H NMR experiments (see Figure S16) in the range +27 to −80 °C, however, could not resolve all three types of alkoxy ligands, indicating some mobility even at low temperatures. Only below −40 °C did both of the alkoxy proton signals decoalesce into two signals each with an integral ratio of 2:10, indicating that the seven terminal and three μ_2-bridging ligands still undergo fast exchange even at −80 °C, while the two μ_3-bridging ligands have lost their mobility.

While there are several reports in the literature about Ln(III) isopropoxides,[44−46] to the best of our knowledge, the only such structurally characterized compound that does not contain an oxo ligand is mixed-valent $[Eu_4(OiPr)_{10}(HOiPr)_3]\cdot 2iPrOH$, containing three donating *i*PrOH molecules as well as two molecules of *i*PrOH as lattice solvent.[47] Our own attempts at generating crystals of "$Ce(OiPr)_3$" suitable for an X-ray diffraction study join the ranks of earlier unsuccessful attempts. Upon addition of isopropyl alcohol to a bright yellow solution of $Ce[N(SiMe_3)_2]_3$, a popular precursor in Ce(III) chemistry,[48−50] instant precipitation of an insoluble, pale green solid occurred.

The latter was sparingly soluble at best in all tried solvents and solvent mixtures (*n*-hexane, cyclohexane, benzene, toluene, 1,2-difluorobenzene, acetonitrile, thf, dme, chloroform, isopropyl alcohol, methanol, acetone) and withstood all attempts at growing crystals suitable for an X-ray diffraction (XRD) study. Thus, it could only be tentatively identified by elemental analysis and DRIFT spectroscopy as $[Ce(OiPr)_3]_n$. Considering the tendency of all $Ln(OR)_n$-type compounds, especially

https://dx.doi.org/10.1021/acs.organomet.9b00794
Organometallics 2020, 39, 1046−1058

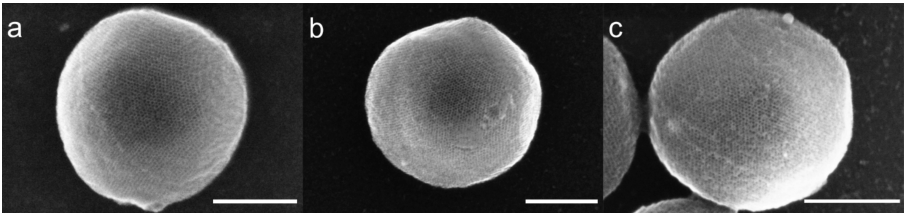

Figure 2. SEM micrographs of the parent material MSN-MCM-41-b (a) as well as La[N(SiMe$_3$)$_2$]$_3$@MSN-MCM-41$_{500}$-b (**H4**) before (b) and after (**H4a** (c)) use in catalysis. The scale bars correspond to 100 nm.

those bearing smaller alkoxy ligands, to form oligomers, a possible explanation for this might be that [Ce(O*i*Pr)$_3$]$_n$ forms a polymeric structure.

Support Materials. Mesoporous silica nanoparticles (MSN) with an MCM-41-type pore symmetry (two-dimensional, hexagonal array of cylindrical pores) were selected as a third-generation silica support material.[51−53] The monodisperse nanoparticulate composition of the support/host material was supposed to assist not only in a detailed understanding of the (pre)catalyst immobilization process but also with a meaningful interpretation of any diffusion-controlled heterogeneous catalysis/catalytic performance. Furthermore, the chosen support material features a highly regular pore size and arrangement, a narrow pore size distribution, and uniform particle morphology and is characterized by the ease and reproducibility of its synthesis.[51,52] A special focus was placed on the morphology and uniformity of the nanoparticles in order to reduce the amount of pore volume inaccessible to either the grafting of the metal-organic complexes or the molecules participating in the catalytic reaction, due to diffusion restraints. Since monodisperse MSN with large pore diameter are not easily available,[54] we targeted a pore size/diameter of ca. 2.6 nm. On the other hand, such a relatively small pore size might imply the occurrence of pore size and confinement effects. The MSN under study were synthesized according to a modified Stöber-type reaction, tailored to give the desired pore and particle sizes.[55] The successful independent synthesis of three batches of MSN-MCM-41-a/b/c was confirmed by powder X-ray diffraction (PXRD) measurements, where the material was deemed of sufficient quality if at least the reflections for the [100], [110], [200], and [210] reciprocal planes were detected (see Figure S5).

Nitrogen physisorption in combination with silylation experiments with HN(SiHMe$_2$)$_2$ were carried out to determine the number of free silanol groups on the surface of MSN-MCM-41-a/b/c after activation at 500 °C and <1 × 10^{-4} mbar,[56,57] while the IR spectra revealed the presence of isolated silanol groups at 3740 cm^{-1} (Figure 3).

The N$_2$-physisorption measurements of the activated samples MSN-MCM-41$_{500}$-a/b/c gave reversible type IV isotherms indicative of mesoporous MCM-41 support materials (see Figure 4 and Figures S7a−c and S8−S11). The specific surface area was calculated with the BET method,[58] ranging reproducibly around 1000−1200 m^2 g^{-1}. The pore size was determined via application of the BJH method[59] on the desorption branch of the isotherm and laid consistently around 2.6 nm (see Table 3). SEM measurements

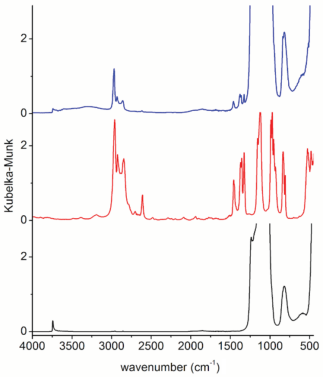

Figure 3. DRIFT spectra of parent material MSN-MCM-41$_{500}$-a (bottom, black), complex **1** (middle, red), and hybrid material [Ce(O*i*Pr)$_4$]$_3$@MSN-MCM-41$_{500}$-a (**H1**) (top, blue). In the last species, consumption of most of the Si−OH groups of the parent material (at 3740 cm^{-1}) and the appearance of vibrations originating from complex **1** are clearly visible.

were employed to determine the shape and size of the MSN, revealing a close to spherical appearance and a narrow monomodal size distribution of ca. 250 nm (see Figure S7d). Furthermore, the 2D-hexagonal MCM-41 pore structure was clearly visible in the SEM images (see Figure 2 and Figures S1−S4).

SOLnC@MSN-MCM-41. The metal-organic hybrid catalysts either were directly generated via alkoxide surface grafting or were generated sequentially via immobilization of a silylamide precursor and subsequent silylamido/isopropoxy surface ligand exchange (see Scheme 2).[2,60,61] The latter reaction sequence was performed either in a separate synthesis step involving a preisolated silylamide-grafted hybrid material or in situ during the catalytic reactions.

Grafting of ceric **1** was performed by combining the complex dissolved in *n*-hexane with the suspended silica particles with stirring, affording the hybrid material [Ce(O*i*Pr)$_4$]$_3$@MSN-MCM-41$_{500}$-a (**H1**). N$_2$-physisorption measurements of **H1** revealed a bimodal pore size distribution (see Figure 4), indicating that, after being grafted near the pore entrances, the relatively large trimeric [Ce(O*i*Pr)$_4$]$_3$ blocks diffusion of further precursor molecules into the pores, thus effectively

https://dx.doi.org/10.1021/acs.organomet.9b00794
Organometallics 2020, 39, 1046−1058

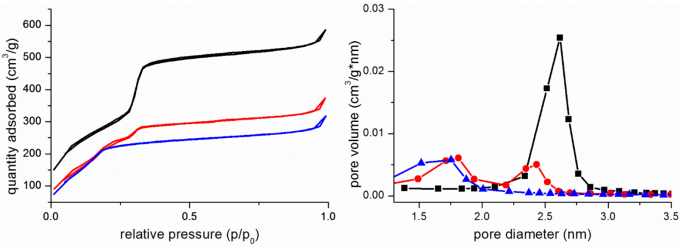

Figure 4. N_2-physisorption isotherms (left) and dV/dD pore size distributions (right) of parent material MSN-MCM-41$_{500}$-a (black) and hybrid materials [Ce(O*i*Pr)$_4$]$_3$@MSN-MCM-41$_{500}$-a (**H1**, red), and Ce[N(SiMe$_3$)$_2$]$_3$@MSN-MCM-41$_{500}$-a (**H3**, blue). While **H3** displays an isotherm and pore size distribution indicative of complete grafting on all available surface area, **H1** shows a bimodal pore size distribution with pores of size approximately that of the parent materials still present. This indicates that the pore diameter near the entrance of the pores gets reduced by initial grafting of the trimetallic alkoxide complex **1**, rendering larger parts of the remaining pores inaccessible for further precursor molecules.

Table 3. Characterization Data of All Parent and Hybrid Materials

material	a_{BET}[a] /m^2 g^{-1}	V_{pore}[b] /cm^3 g^{-1}	d_{pore}[c] /nm	$c_{surface\ SiOH}$[d] /mmol g^{-1}	wt% metal[e]
MSN-MCM-41-a	1062	0.72	2.6	1.11	n/a
[Ce(O*i*Pr)$_4$]$_3$@MSN-MCM-41$_{500}$-a (**H1**)	786	0.47	1.8	n/a	9.8
[Ce(O*i*Pr)$_4$]$_3$@MSN-MCM-41$_{500}$-a (**H1′**)[f]	791	0.48	1.8	n/a	
Ce[N(SiMe$_3$)$_2$]$_3$@MSN-MCM-41$_{500}$-a (**H3**)	824	0.41	1.8	n/a	10.8
HO*i*Pr@Ce[N(SiMe$_3$)$_2$]$_3$@MSN-MCM-41$_{500}$-a (**H3a**)[g]				n/a	11.3
MSN-MCM-41-b	1134	0.89	2.6	1.04	n/a
La[N(SiMe$_3$)$_2$]$_3$@MSN-MCM-41$_{500}$-b (**H4**)	903	0.54	2.0	n/a	10.2
HO*i*Pr@La[N(SiMe$_3$)$_2$]$_3$@MSN-MCM-41$_{500}$-b (**H4a**)	754	0.47	1.8	n/a	10.0
MSN-MCM-41-c	1107	0.77	2.6	1.11	n/a
Ce[N(SiHMe$_2$)$_2$]$_4$@MSN-MCM-41$_{500}$-c (**H2**)	758	0.43	1.7	n/a	5.0
HO*i*Pr@Ce[N(SiHMe$_2$)$_2$]$_4$@MSN-MCM-41$_{500}$-c (**H2a**)[f]				n/a	7.1

[a]BET surface area calculated between p/p_0 0.07 and 0.15. [b]BJH desorption cumulative pore volume between 1.5 and 4.5 nm. [c]Maximum pore diameter from the BJH desorption branch. [d]Calculated according to published procedures.[65] [e]Metal content determined by ICP-OES. [f]The hybrid material denoted **H1′** has been used in catalysis once before. [g]N_2-physisorption data could not be acquired due to volatile compounds stemming from catalysis experiments that were not removable from the pores without destroying surface-grafted complexes.

Scheme 2. Direct and Sequential Approaches toward Catalytically Active Hybrid Materials and Proposed Ceric Surface Species[a]

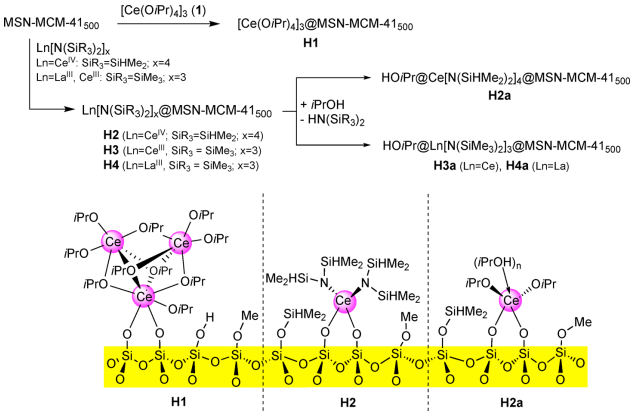

[a]Only bimodal ceric surface species are shown. For proposed surface species resulting from Ln(III) silylamide grafting see ref 25.

https://dx.doi.org/10.1021/acs.organomet.9b00794
Organometallics 2020, 39, 1046−1058

limiting the specific surface area available for grafting. The surface-grafted trimers proposed for **H1** (cf. Scheme 2) seem to tolerate the treatment with *i*PrOH at ambient temperature, since the N_2-physisorption isotherm retained a bimodal pore size distribution (see Figure S12). Also, the DRIFT spectra of material **H1** indicated that the band corresponding to free Si−OH groups remained virtually unchanged before and after treatment with *i*PrOH (see Figure S13). In order to counteract the formation of a trimetallic surface cluster complex and to achieve complete occupation of the available surface area, in a second approach the monomeric silylamide $Ce[N(SiHMe_2)_2]_4$ was grafted first onto MSN-MCM-41_{500}-c, giving rust-colored $Ce[N(SiHMe_2)_2]_4$@MSN-MCM-41_{500}-c (**H2**),[62] and postsynthetically treated with isopropyl alcohol to yield HO*i*Pr@$Ce[N(SiHMe_2)_2]_4$@MSN-MCM-41_{500}-c (**H2a**). For the hybrid material **H2**, the N_2-physisorption measurement only revealed a monomodal pore size distribution, showing that the entire pore surface was accessible for grafting (see Figure S10).

As the extremely low solubility of the putative homoleptic trivalent lanthanum and cerium isopropoxides ruled out any direct grafting experiments, the sequential approach via silylamide hybrid materials $Ce[N(SiMe_3)_2]_3$@MSN-MCM-41_{500}-a (**H3**) and $La[N(SiMe_3)_2]_3$@MSN-MCM-41_{500}-b (**H4**) and surface-mediated protonolysis with isopropyl alcohol was chosen to target HO*i*Pr@$Ce[N(SiMe_3)_2]_3$@MSN-MCM-41_{500}-a (**H3a**) and HO*i*Pr@$La[N(SiMe_3)_2]_3$@MSN-MCM-41_{500}-b (**H4a**). The successful grafting could be verified by DRIFT spectroscopy, where the spectrum of a hybrid material largely resembled a combination of the spectra of its parent material and the utilized organometallic precursor (see Figure 3 for material **H1**). The surface-mediated silylamido/alkoxy ligand exchange will involve the formation of exceedingly sterically unsaturated metal centers prone to adduct formation with alcohol molecules (Scheme 2). Since the same ligand exchange takes place in the catalytic experiments, this postsynthesis treatment was skipped as a separate step for materials **H3** and **H4**. Both materials were employed directly as precatalysts, which did not impede the catalytic activity. The silylamines $HN(SiMe_3)_2$ and $HN(SiHMe_2)_2$, respectively released as a result of the surface-mediated ligand exchange, could easily be identified by gas chromatography as a broad peak underlying the acetone peak, corroborating the successful protonolysis reaction. SEM imaging and PXRD measurements of the obtained hybrid materials **HX** confirmed that the MSN morphology and its periodic pore symmetry were essentially retained during the SOLnC procedure, while N_2-physisorption measurements confirmed that the immobilized catalyst was indeed located inside the pores, causing a reduction in the pore diameter and specific surface area as well as pore volume (see Table 3). Successful surface grafting was further corroborated by DRIFTS, showing a near-complete consumption of terminal Si−OH moieties and the appearance of bands corresponding to the grafted complexes (see Figure 3), and relatively high metal contents by ICP-OES analysis (Table 3). Strikingly, while **H1**, **H3**/**H3a**, and **H4**/**H4a** contain around 10 wt % metal, **H2**/**H2a** only have metal contents of around 5−7 wt %. This can be explained by a pronounced concomitant surface silylation in the case of $Ce[N(SiHMe_2)_2]_4$-grafted materials.[56] Since every protonolytic grafting reaction of $Ce[N(SiHMe_2)_2]_4$ with a Si−OH group liberates at least one molecule of $HN(SiHMe_2)_2$, it is reasonable to assume that these undergo grafting reactions themselves, which have been found to be far more efficient than in the case of the bulkier $HN(SiMe_3)_2$.[56] Every molecule of $HN(SiHMe_2)_2$ is able to silylate two Si−OH groups, thus significantly reducing available grafting sites for the original complex. This is corroborated by DRIFT spectroscopy, where the hybrid material $[Ce(OiPr)_4]_3$@MSN-MCM-41_{500}-a (**H1**) still shows a band relating to isolated Si−OH groups at 3740 cm^{-1}, while this band is much smaller for $Ce[N(SiHMe_2)_2]_4$@MSN-MCM-41_{500}-c (**H2**) (see Figure 5). After **H1** was treated with $HN(SiHMe_2)_2$, the Si−OH band in the DRIFT spectrum completely disappeared, showing that the remaining Si−OH groups that are inaccessible for $[Ce(OiPr)_4]_3$ are indeed still accessible for silylation by $HN(SiHMe_2)_2$.

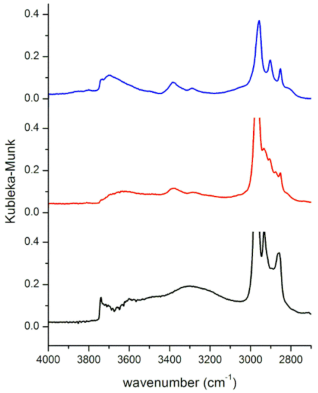

Figure 5. DRIFT spectra of $[Ce(OiPr)_4]_3$@MSN-MCM-41_{500}-a (**H1**) before (black, bottom) and after (red, middle) silylation with $HN(SiHMe_2)_2$ as well as of $Ce[N(SiHMe_2)_2]_4$@MSN-MCM-41_{500}-c (**H2**) (blue, top). The disappearance of the band originating from remaining free (noninteracting) Si−OH groups (at 3740 cm^{-1}) on the surface of the hybrid material after silylation is clearly visible. **H2** shows a strongly reduced band at 3740 cm^{-1} due to competitive silylation by $HN(SiHMe_2)_2$ liberated during protonolytic grafting of $Ce[N(SiHMe_2)_2]_4$.

A stable covalent linkage of the grafted species to the silica surface was examined by leaching experiments, evidencing the absence of traces of metal in the supernatant by ICP-OES analysis. The obtained heterogeneous catalysts could be stored at −35 °C for extended periods of time under an argon atmosphere, although precautions had to be taken with respect to the complete exclusion of even the most minute traces of oxygen in cases of all Ce(III)-based hybrid materials. The morphology of the grafted silica nanoparticles also remained unchanged upon use in MPV reductions or prolonged storage inside a glovebox.

N_2-physisorption experiments on the hybrid materials show markedly reduced specific surface areas (a_{BET}), pore volumes (V_{pore}), and pore diameters (d_{pore}) (see Table 3). However, since the grafting of the organometallic complexes on the surface of pores with rather small diameters reduces the pore diameter below the generally accepted threshold for mesoporous materials at 2 nm,[63] BET and BJH methods that are tailored for mesoporous materials might lose some accuracy, so that the values given in Table 3 can only indicate tendencies.

https://dx.doi.org/10.1021/acs.organomet.9b00794
Organometallics 2020, 39, 1046−1058

Apart from that, there were some problems with measuring N_2-physisorption data of some hybrid materials after they had been used in catalysis. Due to the sensitive nature of the surface-grafted complexes, degassing at elevated temperature was impossible, while by degassing at ambient temperature, volatile compounds within the pores could not be completely removed, preventing the acquisition of accurate N_2-physisorption isotherms.

The hybrid materials **H1**, **H2**, and **H2a** were further investigated by means of solid-state magic-angle spinning (MAS) NMR spectroscopy. The ^{1}H NMR spectrum of the parent materials (Figure 6a) revealed two peaks that can be attributed to the surface Si−OH groups (peak at 1.7 ppm) and to surface-grafted methoxy groups (peak at 3.3 ppm) originating from the solvent extraction step to remove the surfactant from the formed mesopores (see the Experimental Section).[64] These methoxy groups are also visible in the ^{13}C CPMAS NMR spectra (see Figure 7c−e) as a peak at ca. 50 ppm.

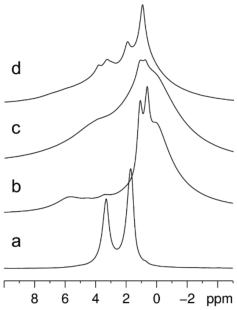

Figure 6. ^{1}H solid-state NMR spectra of MSN-MCM-41$_{500}$-a (a) and hybrid materials Ce[N(SiHMe$_2$)$_2$]$_4$@MSN-MCM-41$_{500}$-c (**H2**) (b), HO*i*Pr@Ce[N(SiHMe$_2$)$_2$]$_4$@MSN-MCM-41$_{500}$-c (**H2a**) (c), and [Ce(O*i*Pr)$_4$]$_3$@MSN-MCM-41$_{500}$-a (**H1**) (d). The spectrum of the parent material shows two resonances for Si−OH groups assignable to isolated Si−OH silanol groups (1.1 ppm) and Si−OCH$_3$ methoxy surface groups (3.3 ppm) from methanol grafting during the solvent-extraction process of the surfactant. Postsynthetic ligand exchange on **H2** to yield **H2a** can be followed by the disappearance of the SiH resonance at 5.6 ppm, even though the spectrum of **H2a** does not show sufficient resolution to allow comparison to the spectrum of **H1**.

The ^{1}H NMR spectrum of hybrid material **H1** indicates incomplete consumption of the isolated Si−O*H* groups by a dominant peak at 1.1 (cf. IR spectra, Figure 3). The exchange of the silylamido ligand in **H2** by isopropyl alcohol can be followed by the disappearance of the Si−*H* peak at 5.7 ppm in the spectrum of **H2a** (Figure 6).

The ^{13}C CPMAS spectra, on the other hand, show rather broad peaks for the distinct carbon atoms of the surface-grafted complexes: OCH(CH$_3$)$_2$ (67.1 ppm), OCH(CH$_3$)$_2$ (23.5 ppm), and SiH(CH$_3$)$_2$ (−2.0 ppm) (Figure 7). The ^{13}C CPMAS spectrum of silylamido/alkoxy-exchanged **H2a** still displays peaks attributable to SiHMe$_2$ moieties that most likely stem from surface silylation by HN(SiHMe$_2$)$_2$ liberated during grafting of Ce[N(SiHMe$_2$)$_2$]$_4$ (Figure 7d, also cf. Figure 3). The ^{13}C CPMAS NMR spectra along with the ^{13}C{^{1}H} solution-state spectra provide further insights into the grafting process: the solid-state spectrum of **H2** shows a strong resonance at −0.5 ppm that corresponds well to the resonance of the SiH*Me*$_2$ methyl groups of Ce[N(SiHMe$_2$)$_2$]$_4$ in C_6D_6 at 1.9 ppm.

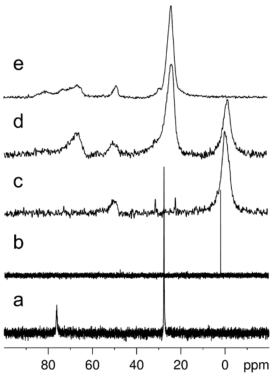

Figure 7. Solution-state ^{13}C{^{1}H} NMR spectra of [Ce(O*i*Pr)$_4$]$_3$ (a) and Ce[N(SiHMe$_2$)$_2$]$_4$ (b) as well as ^{13}C CPMAS NMR spectra of Ce[N(SiHMe$_2$)$_2$]$_4$@MSN-MCM-41$_{500}$-c (**H2**) (c), HO*i*Pr@Ce[N(SiHMe$_2$)$_2$]$_4$@MSN-MCM-41$_{500}$-c (**H2a**) (d), and [Ce(O*i*Pr)$_4$]$_3$@MSN-MCM-41$_{500}$-a (**H1**) (e). The spectra of all hybrid materials show a signal at 50 ppm for surface-grafted methoxy groups from the solvent-extraction process of the surfactant. The spectrum of **H2** shows the methyl resonance of the SiHMe$_2$ groups in the N(SiHMe$_2$)$_2$ ligands and surface-bound SiHMe$_2$ groups, while the spectrum of **H2b** shows the same resonance with reduced intensity from surface bound SiHMe$_2$ groups and additionally two resonances for the methyl and CH groups of the isopropoxy ligand. The spectrum of **H1** solely shows resonances for the isopropoxy ligands.

Upon treatment of **H2** with *i*PrOH to yield **H2a**, the resonance attributable to these methyl groups lost intensity but did not disappear entirely, corroborating the results from DRIFT and ^{1}H solid-state NMR spectroscopy with respect to the occurrence of a pronounced surface silylation. Furthermore, a set of resonances at 23.7 and 66.5 ppm is visible in the spectrum of **H2a**, corresponding to the methyl and methanetriyl groups of the isopropoxy ligand, thus further proving the successful ligand exchange of the silylamido ligand with *i*PrOH.

On application of ^{29}Si{^{1}H} HPDEC solid-state NMR spectroscopy (see Figure 8), it could be conclusively shown that the silylamido/alkoxy-ligand exchange (**H2** → **H2a**) was indeed successful. While the resonance corresponding to the silylamido ligand at −22.1 ppm entirely disappeared, the resonance attributable to the surface-grafted SiHMe$_2$ groups at 0.6 ppm remained.

Catalysis. As opposed to the established MPV reduction, where the "catalyst" is usually employed in stoichiometric or superstoichiometric amounts, all reactions under study were performed in a truly catalytic manner, usually with 5 mol% of metal, either homogeneously with a complex dissolved in isopropyl alcohol or heterogeneously with Ln(OR)$_n$@MSN-MCM-41$_{500}$ hybrid materials suspended in isopropyl alcohol. The catalytic reaction with [Al(O*i*Pr)$_3$] under otherwise

https://dx.doi.org/10.1021/acs.organomet.9b00794
Organometallics 2020, 39, 1046−1058

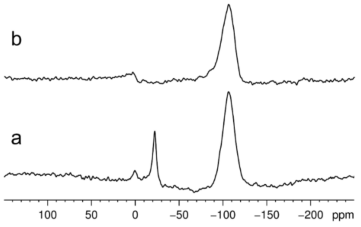

Figure 8. $^{29}Si\{^{1}H\}$ HPDEC solid-state NMR spectra of Ce[N-$(SiHMe_2)_2]_4$@MSN-MCM-41_{500}-c (**H2**) (a, bottom) and HO*i*Pr@$Ce[N(SiHMe_2)_2]_4$@MSN-MCM-41_{500}-c (**H2a**) (b, top). The resonance at −22.1 ppm corresponds to the $N(SiHMe_2)_2$ ligands ($Ce[N(SiHMe_2)_2]_4$ in C_6D_6: $\delta(^{29}Si)$ −22.8 ppm), while the resonance at 0.6 ppm corresponds to directly surface grafted $SiHMe_2$ groups and is still present in the spectrum of **H2a**, where the silylamido ligand has been exchanged by isopropoxy ligands. The large resonance at −107.5 ppm corresponds to the SiO_2 carrier material.

identical conditions was used as a benchmark system (Table 4, entry 1). The good results of this reaction after 24 h, even with only 5 mol% of $[Al(OiPr)_3]$, showed the importance of absolutely oxygen and moisture free conditions. Even though these conditions greatly improved the catalytic performance of $[Al(OiPr)_3]$, the comparison between this reaction and all rare-earth-metal-based reactions again underlined their vastly superior catalytic performance that has been demonstrated earlier.[25]

Catalytic activity in the Meerwein−Ponndorf−Verley reduction is generally attributed on one hand to the Lewis acidity of the metal center and on the other hand to its ability to rapidly exchange the alkoxy ligands.[14,66,67] As increasing one of these properties often counteracts the other one, it is of paramount importance for the catalytic performance to balance the two by choosing the most suitable rare-earth metal for the synthesis of the metal-organic catalysts or catalyst precursors, respectively.

Accordingly, the Ce(III/IV) redox couple makes it possible to change the electronic structure (Lewis acidity) and coordination environment (ligand exchange ability) without using different metals. Table 4 summarizes the catalytic performance of several homogeneous and heterogeneous catalysts. The results obtained with the cerium-based catalysts were promising (entries 4 and 6−10); however, it became clear that the Ce(III)-based catalysts outperformed the ceric catalysts at ambient temperature (e.g., **1** versus $[Ce(OCH_2tBu)_3]_4$),[68] most likely due to alkoxy ligand exchange being extremely slowed down at Ce(IV) centers.[69,70] A further drop in catalytic activity was observed for the ceric hybrid materials $[Ce(OiPr)_4]_3$@MSN-MCM-41_{500}-a (**H1**) and $Ce[N(SiHMe_2)_2]_4$@MSN-MCM-41_{500}-c (**H2**), even when the **H1** reactions were performed at 60 °C.

Because the heterogeneous cerous catalyst system $Ce[N(SiMe_3)_2]_3$@MSN-MCM-41_{500}-a (**H3**) was also exceedingly sensitive to any traces of oxygen or moisture (color change from nearly colorless to orange-brown of the heterogeneous catalysts within a few minutes at ambient temperature even inside the glovebox), the similarly sized redox-stable lanthanum was chosen as a replacement. And indeed, La(III) greatly increased the stability of the heterogeneous catalyst and consequently also led to a better catalytic performance, whether homogeneously or heterogeneously, and easier reusability of the hybrid materials as heterogeneous catalyst. Generally, homogeneous catalysts showed slightly better performance than their heterogeneous counterparts, which can be attributed to diffusion effects limiting the access of the substrate to the catalytically active metal centers. However, this slight disadvantage of the heterogeneous catalyst is easily offset by its greatly facilitated separation as well as reusability (see Table 4, entries 9, 10, and 11−13). Still, results in earlier studies conducted with $Nd[N(SiMe_3)_2]_3$ as a precatalyst on

Table 4. Catalytic Activities of Ln(III)-Based Catalysts in the MPV Reduction of 4-*t*Bu-cyclohexanone at Ambient Temperature

			conversion/% (*trans*:*cis*)	
entry	(pre)catalyst	mol% M	1 h	24 h
1	$Al(OiPr)_3$	5.1	<1	>99 (2.0)
2	MSN-MCM-41_{500}-c	n/a[a]	0	0
3	$[Ce(OiPr)_4]_3$ (**1**)	5.1	29 (1.9)	>99 (2.2)
4	$[Ce(OCH_2tBu)_3]_4$[b]	5.0	>99 (2.2)	n/a
5	$La[N(SiMe_3)_2]_3$	5.0	>99[c] (2.2)	n/a
6[d]	$[Ce(OiPr)_4]_3$@MSN-MCM-41_{500}-a (**H1**)	5.3	n/a	>99 (2.9)
7[d]	$[Ce(OiPr)_4]_3$@MSN-MCM-41_{500}-a (**H1′**)[e]	5.0	n/a	84 (3.1)
8	$Ce[N(SiHMe_2)_2]_4$@MSN-MCM-41_{500}-c (**H2**)	5.0	18 (3.4)	65 (3.7)
9	$Ce[N(SiMe_3)_2]_3$@MSN-MCM-41_{500}-a (**H3**)	5.0	84 (3.1)	>99 (3.0)
10	$Ce[N(SiMe_3)_2]_3$@MSN-MCM-41_{500}-a (**H3′**)[e]	5.0	70 (3.2)	>99 (3.1)
11	$La[N(SiMe_3)_2]_3$@MSN-MCM-41_{500}-b (**H4**)	5.0	97 (2.8)	>99 (3.0)
12	$La[N(SiMe_3)_2]_3$@MSN-MCM-41_{500}-b (**H4′**)[e]	5.0	70 (3.6)	>99 (3.1)
13	$La[N(SiMe_3)_2]_3$@MSN-MCM-41_{500}-b (**H4′′**)[e]	5.0	55 (3.2)	n/a[f]
14[g]	$Nd(OCtBu_3)_3$	1.4	95 (2.7)	>99 (2.6)
15[g]	$Nd[N(SiMe_3)_2]_3$@MCM-41_{100}[h]	1.9	90 (3.3)	>99 (3.3)

[a]Employed 96 mg, calculated as 5.3 mol % Si−OH. [b]$[Ce(OCH_2tBu)_3]_4$ was chosen as a cerous alkoxide due to its better solubility in comparison to $[Ce(OiPr)_3]_n$. [c]>99% already after 15 min. [d]Performed at 60 °C due to the low activity of the Ce(IV)-based catalyst. [e]Hybrid materials denoted **HX′** have been used in catalysis once before and those denoted **HX′′** two times. [f]83% conversion (*trans*:*cis* = 3.2) after 5 h. [g]Values taken from earlier reports.[25] [h]The parent material in this study was dehydroxylated at 100 °C and 10^{-3} mbar for 3 h.

https://dx.doi.org/10.1021/acs.organomet.9b00794
Organometallics 2020, 39, 1046−1058

MCM-41-type silica materials (pore size of the parent material 2.8 nm) dehydroxylated at 100 °C showed superior catalytic performance (see Table 4), with results similar to those for the lanthanum-based catalyst **H4** at less than half the amount of catalyst.

Since the MPV reduction of 4-*t*Bu-cyclohexanone can result in two possible products, namely *cis*- and *trans*-4-*t*Bu-cyclohexanol, the ratio between those two products is of further interest. Here, notable differences between homogeneous and heterogeneous catalysts were found, while the differences between distinct homogeneous and distinct heterogeneous catalysts are negligible (Table 4, ratios are given in parentheses following the conversion values). Thus, it can be inferred that the confinement of the catalytic reactions to the surface/pores of the support material has a favorable effect on the formation of the *trans* alcohol.

CONCLUSION

Mesoporous silica nanoparticles (MSN) with an MCM-41-type pore symmetry are suitable host materials for the synthesis of Ce(IV) and Ln(III) hybrid materials via surface organometallic chemistry (SOMC) of rare-earth-metal alkoxides and silylamides ($Ce[N(SiHMe_2)_2]_4$, $[Ce(OiPr)_4]_3$, $Ce[N(SiMe_3)_2]_3$, and $La[N(SiMe_3)_2]_3$). The MSN pore size of 2.6 nm (obtained from nitrogen physisorption) seems too small for exhaustive grafting of larger compounds, as revealed for the trimetallic ceric alkoxide $[Ce(OiPr)_4]_3$ (diameter ca. 1.3 nm, see Table 2). The Ln(III)-based catalysts, whether homogeneous or heterogeneous, outperformed the Ce(IV)-based catalysts in the Meerwein–Ponndorf–Verley reduction of 4-*t*Bu-cyclohexanone. This can be ascribed to a markedly slowed down ligand exchange at ceric centers. The reusable hybrid catalyst $La[N(SiMe_3)_2]_3$@MSN-MCM-41 performed best, since significant deterioration occurred for the respective Ce(III)-based material due to its high redox sensitivity. Importantly, the MSN particle size and morphology were retained after metal silylamide/alkoxide grafting, surface-mediated silylamido/alkoxy ligand exchange, and the catalytic reaction.

Furthermore, the previously unknown homoleptic ceric isopropoxide $[Ce(OiPr)_4]_3$ is accessible via silylamine elimination from $Ce[N(SiHMe_2)_2]_4$. Trimeric $[Ce(OiPr)_4]_3$ exhibits an unprecedented variation of the $[Ce_3(\mu_3\text{-}OiPr)_2(\mu_2\text{-}OiPr)_3]$ structural dicapped ring motif well-known in metal alkoxide chemistry.

EXPERIMENTAL SECTION

General Considerations. All operations regarding the organometallic precursors and the hybrid materials were performed under rigorous exclusion of moisture and air under an argon atmosphere, using standard Schlenk and glovebox (MBraun MB150B-G-II) techniques. Solvents were dried with Grubbs-type columns (MBraun MB SPS-800) and stored inside a glovebox. Deuterated solvents were purchased from Euriso-top (Cambridge Isotope Laboratories, Inc.), dried over NaK alloy for at least 24 h, and filtered before use. All other compounds were purchased from Merck KGaA or ABCR GmbH and used as received, except where noted otherwise. Isopropyl alcohol was dried by reacting it with elemental sodium (1 g/L), distilling it afterward, and storing it inside a glovebox over molecular sieves (3 Å). Solution-state NMR spectra were measured on a Bruker AV+400, Bruker DRX-250, and Bruker Avance III HD 300 spectrometers, referenced to internal solvent residual signals and reported relative to tetramethylsilane (^1H, ^{13}C).[71] Variable-temperature (VT) NMR experiments were measured on a Bruker AVII+500 spectrometer. All pulse gradient spin echo NMR measurements were performed on an Avance III HD spectrometer (Bruker) operating at 700.29 MHz for ^1H, using a TCI prodigy cryoprobe head equipped with a *z*-gradient unit. The gradient was calibrated using "doped water" (1% H_2O in D_2O with traces of $CuSO_4$), assuming a diffusion coefficient of 1.91×10^{-5} cm^2 s^{-1} for HDO. The diffusion measurements used a modified bipolar gradient pulse pair-stimulated echo sequence incorporating a longitudinal eddy current delay (BPP-LED). The gradient pulse length (δ) and the diffusion time (Δ) were kept at fixed values while the gradient strength was gradually increased. Typical values for δ and Δ were 2 and 50 ms, respectively. A longitudinal eddy current delay (T_e) of 5 ms was used. Sine-shaped gradient pulses were linearly varied between 1 and 52 G cm^{-1} (2–98%) in 32 steps, and at each step 32 scans were acquired. Five measurements per sample were performed at a constant sample temperature of 290 ± 0.1 K (Bruker Variable Temperature Unit BCU II). The data were analyzed with the T_1/T_2 relaxation module of Topspin 3.5. The signal areas were plotted against the gradient strength and the best fit was calculated using the Stejskal–Tanner equation

$$I_g = I_0 \exp[-4\pi^2\gamma^2\delta^2G^2(\Delta - \delta/3)]$$

(with D being the diffusion coefficient in cm^2 s^{-1}, γ the gyromagnetic ratio in Hz/G, G the gradient strength in G cm^{-1}, δ the gradient length in ms, Δ the interval between gradient pulses (diffusion time) in ms, I_g the signal area, and I_0 the signal intensity at G = 0%). Mean values for each sample are reported. Due to the high air and moisture sensitivity of all compounds, all solution-state NMR spectra were recorded using NMR tubes with J. Young-type valves. Solid-state NMR spectra were measured on a Bruker ASX 300 spectrometer (^1H, 300.13 MHz; ^{13}C, 75.47 MHz; ^{29}Si, 59.62 MHz) equipped with MAS (magic angle spinning) hardware at ambient temperature with samples packed in 3 mm ZrO_2 rotors at a rotation frequency of 5 or 8 kHz. DRIFT spectra were recorded using a NICOLET 6700 FTIR spectrometer (Thermo Fisher Scientific), and samples were diluted to 5 wt % with dried KBr powder as a dilution matrix. The sample was carefully homogenized with KBr in an agate mortar and transferred into a DRIFTS cell with KBr windows. The collected data were converted with the Kubelka–Munk refinement. Elemental analyses were carried out with an Elementar Vario MICRO Cube instrument in the CHNS mode. Scanning electron microscopy (SEM) images were taken with a Hitachi SU8030 microscope at an acceleration voltage of 30 kV. Samples were suspended in EtOH by sonication and brought onto semiconductor grade Si wafers, where the solvent was left to evaporate. X-ray diffraction quality crystals of compound **1** were grown from a saturated solution in 1,2-difluorobenzene at −35 °C. Data were collected on a Bruker APEX III DUO instrument with an IμS microfocus sealed tube and QUAZAR optics for Mo Kα (λ = 0.71073 Å) radiation. The data collection strategy was determined using COSMO[72] employing ω scans. Raw data were processed using APEX[73] and SAINT,[74,75] and corrections for absorption effects were applied using SADABS.[76] The structure was solved with direct methods and refined against all data with full-matrix least-squares methods on F^2 using SHELXTL[77] and ShelXle.[78] Disorder models were calculated using DSR, a program for refining structures in ShelXl.[79] All graphics were created using Mercury[80] and POV-Ray.[81] Further details of the refinement and crystallographic data are given in Table S3 and in the CIF files. CCDC deposition number 1964539 contains all supplementary crystallographic data for compound **1** and can be obtained free of charge from The Cambridge Crystallographic Data Centre via www.ccdc.cam.ac.uk/structures/.

Powder X-ray diffraction analyses were carried out on a Bruker D8 ADVANCE instrument in the step/scan mode using Cu K_α radiation (λ = 1.5406 Å). The small-angle diffractograms were recorded in the range of 2θ = 0.5–10.01° with a step size of 0.008°/step and a scan speed of 2 s/step. N_2-physisorption measurements were performed on an ASAP2020 volumetric adsorption apparatus (Micromeritics Instrument Corp.) at 77 K ($a_m(N_2,77\ K)$ = 0.162 nm^2). The samples were degassed at <7.5 × 10^{-6} mbar prior to analysis, in the case of the

https://dx.doi.org/10.1021/acs.organomet.9b00794
Organometallics 2020, 39, 1046–1058

pure silica materials at 523 K for 4 h and in the case of the hybrid materials at 313 K for 12 h to avoid degradation of the grafted organometallics. The Brunauer−Emmett−Teller (BET) specific surface area was calculated from the nitrogen adsorption branch of the isotherm in the relative pressure range of 0.07−0.15 for the pure SiO_2 materials and the hybrid materials.[58] Pore size distributions (dV/dD) were calculated from the nitrogen desorption branch using the Barrett−Joyner−Halenda (BJH) method.[59]

Materials. All silica support materials were synthesized according to a modified Stöber method,[55,56] adapted from Lin et al.[82] The amounts of all starting materials for all MSN-MCM-41$_{500}$ materials are given in Table 5. In a typical synthesis, CTAB was dissolved in demineralized H_2O in a polypropylene (PP) bottle (Nalgene/Thermo Fisher Scientific). After a completely homogeneous solution was obtained, 2 M NaOH was added, the temperature was adjusted to 338 K, and the solution was stirred for ca. 1 h to achieve thermal equilibrium. The stirring (triangular-prismatic stir bar, length ca. 4 cm) was adjusted to 500 min^{-1} before tetraethyl orthosilicate (TEOS) was added dropwise during 4 min. Upon complete addition, the solution turned white and turbid. The suspension was stirred for 1:45 h before stirring and heating were stopped, and it was cooled naturally to ambient temperature. The solid material was separated by centrifugation (sigma 3-30KS, sigma Laborzentrifugen GmbH) at 21000 min^{-1} (41415g) and washed three times each with MeOH and H_2O before being dried overnight at 333 K. Template residues were removed by extraction in MeOH/HCl. To this end, the dried MSN-MCM-41$_{as\text{-}made}$ samples were suspended in a mixture of MeOH (160 mL) and concentrated HCl (37%, 5 mL) and heated to reflux for 24 h, before the separation and washing process was repeated. After drying at 333 K overnight again, the resulting MSN-MCM-41$_{extracted}$ sample were activated at 753 K and <1 × 10^{-4} mbar for 12 h to yield MSN-MCM-41$_{500}$.

Table 5. Amounts of Starting Materials Used in the Syntheses of MSN-MCM-41$_{500}$[a]

	MSN-MCM-41-a	MSN-MCM-41-b	MSN-MCM-41-c
CTAB	2.014/5.526	2.002/5.493	2.007/5.507
H_2O	960.023/53.28 mol	960.01/53.27 mol	960.07/53.28 mol
NaOH (2 M)	8.0 mL/16.0	8.0 mL/16.0	8.0 mL/16.0
TEOS	10.014/48.1	9.4/44.8	9.34/44.8

[a]Listed as g/mmol if not stated otherwise.

MSN-MCM-41$_{500}$-a. A 1.501 g amount (24.98 mmol, 52%) of MSN-MCM-41$_{500}$-a was obtained as a white powder. Anal. Found: C, 0.78; H, 0.44; N, 0.06. a_{BET} 1062 m^2 g^{-1}, V_{pore} 0.72 cm^3 g^{-1}, d_{pore} 2.6 nm. Surface Si−OH groups 1.11 mmol g^{-1}. DRIFTS: $\tilde{\nu}$ 3743 (w), 1238 (m), 1075 (vs), 820 (m), 448 (s) cm^{-1}.

MSN-MCM-41$_{500}$-b. A 1.640 g amount (27.28 mmol, 61%) of MSN-MCM-41$_{500}$-b was obtained as a white powder. Anal. Found: C, 1.14; H, 0.48; N, 0.22. a_{BET} 1134 m^2 g^{-1}, V_{pore} 0.89 cm^3 g^{-1}, d_{pore} 2.6 nm. Surface Si−OH groups 1.04 mmol g^{-1}. DRIFTS: $\tilde{\nu}$ 3743 (w), 1238 (m), 1058 (vs), 825 (m), 440 (s) cm^{-1}.

MSN-MCM-41$_{500}$-c. A 1.563 g amount (26.0 mmol, 58%) of MSN-MCM-41$_{500}$-c was obtained as a white powder. Anal. Found: C, 0.86; H, 0.41; N, 0.28. a_{BET} 1107 m^2 g^{-1}, V_{pore} 0.77 cm^3 g^{-1}, d_{pore} 2.6 nm. Surface Si−OH groups 1.11 mmol g^{-1}. DRIFTS $\tilde{\nu}$ 3743 (w), 1237 (m), 1070 (vs), 819 (m), 442 (s) cm^{-1}.

Organometallic Precursors. The syntheses of Ce[N(SiMe$_3$)$_2$]$_3$, La[N(SiMe$_3$)$_2$]$_3$, Ce[N(SiHMe$_2$)$_2$]$_4$, and [Ce(OCH$_2$$t$Bu)$_4$]$_3$ are described in detail elsewhere.[33,35,83,84]

[Ce(OiPr)$_4$]$_3$ (1). Ce[N(SiHMe$_2$)$_2$]$_4$ (291.3 mg, 0.435 mmol) was dissolved in n-hexane (5 mL), and iPrOH (105.5 mg, 1.755 mmol, 4.03 equiv) was equally mixed with n-hexane (5 mL). The iPrOH solution was then added dropwise to the Ce[N(SiHMe$_2$)$_2$]$_4$ solution. Upon complete addition, a color change from deep red to translucent yellow could be observed. Alternatively, the iPrOH was used in slight excess (6−8 equiv) and the iPrOH/n-hexane mixture was added to the Ce[N(SiHMe$_2$)$_2$]$_4$ solution until a color change could no longer be observed. The mixture was stirred for 15 min, and then the solvent was removed in vacuo. The resulting crude product was recrystallized from $C_6H_4F_2$ to yield 159.8 mg (0.141 mmol, 98%) of [Ce(OiPr)$_4$]$_3$ as blocky, yellow crystals. ^{1}H NMR (C_6D_6, 400.16 MHz, 299 K): δ 5.25 (sept, 12 H, OCHMe$_2$, J = 6.05 Hz), 1.53 (d, 72 H, OCHMe_2, J = 6.04 Hz) ppm. ^{13}C NMR (C_6D_6, 100.6 MHz, 298 K): δ 76.60 (OCHMe$_2$), 28.12 (OCHMe_2) ppm. DRIFTS: $\tilde{\nu}$ 2961 (vs), 2926 (s), 2847 (s), 2612 (m), 1458 (m), 1358 (s), 1327 (s), 1124 (vs), 989 (s), 973 (vs), 954 (s), 836 (s), 809 (m), 528 (s), 482 (s), 444 (s) cm^{-1}. Anal. Calcd for $C_{36}H_{84}Ce_3O_{12}$ (1129.41 g mol^{-1}): C, 38.29; H, 7.50. Found: C, 38.75; H, 7.45. Evans (C_6D_6, 400.16 MHz, 299 K): χ_{mol} = 7.72 × 10^{-4} emu mol^{-1}, $\chi_{mol}T$ = 0.23 emu K mol^{-1}, μ_{eff} = 0.70 μ_B, Δ = 3.8 Hz, c = 0.0148 mol L^{-1}.

[Ce(OiPr)$_3$]$_n$. Ce[N(SiMe$_3$)$_2$]$_3$ (137.4 mg, 0.221 mmol) was dissolved in n-hexane (5 mL), and an excess of iPrOH (10 drops, ca. 100 mg, ca. 1.7 mmol, ca. 8 equiv) was added. The mixture was briefly shaken, and a discoloration of the yellow solution along with the formation of a slightly greenish white precipitate could be observed. Solvents and liberated HN(SiMe$_3$)$_2$ were removed in vacuo to yield 58.5 mg of [Ce(OiPr)$_3$]$_n$ (0.184 mmol, 83%) as a slightly off-white powder. DRIFTS: $\tilde{\nu}$ 2959 (s), 2924 (w), 2859 (w), 2817 (w), 2695 (vw), 2609 (vw), 1460 (w), 1375 (w), 1357 (w), 1331 (w), 1158 (s), 1130 (s), 991 (m), 966 (vs), 824 (m), 518 (m), 487 (w), 445 (w) cm^{-1}. Anal. Calcd for $C_9H_{21}CeO_3$ (317.38 g mol^{-1}): C, 34.06; H, 6.67. Found: C, 33.66; H, 6.36. 6.36. For comparison, the routinely observed formation of the oxo cluster Ln$_5$O(OiPr)$_{13}$ would correspond to $C_{39}H_{91}Ce_5O_{14}$ (1484.73 g mol^{-1}): Ce, 31.55; H, 6.18.

Grafting Reactions. See also the Supporting Information. As an exemplary grafting procedure, the synthesis of the hybrid material [Ce(OiPr)$_4$]$_3$@MCM-41$_{500}$-MSN (**H1**) is given here. The activated silica material (MSN-MCM-41$_{500}$-a, 400.4 mg, ca. 0.44 mmol of SiOH) was suspended in n-hexane and the organometallic precursor ([Ce(OiPr)$_4$]$_3$, 159.7 mg, 0.141 mmol, 0.42 mmol of Ce), dissolved in n-hexane, was added. After the mixture was stirred overnight, the solid hybrid material was separated from the supernatant by centrifugation and washed with n-hexane three times before residual solvent was removed in vacuo to yield [Ce(OiPr)$_4$]$_3$@MCM-41$_{500}$-MSN (**H1**) as a light brown powder. The supernatant was checked for remaining precursor complex by ^{1}H NMR (or ICP-OES), and the grafting experiment was deemed successful (consumption of all accessible Si−OH groups) since there was still precursor present. The remaining organometallic precursor complex could easily be reclaimed by filtration and subsequent evaporation of the supernatant. Anal. Found: Ce, 9.8 (ICP-OES) C, 10.52; H, 2.15. a_{BET} 786 m^2 g^{-1}, V_{pore} 0.47 cm^3 g^{-1}, d_{pore} 1.8 nm. DRIFTS: $\tilde{\nu}$ 2969 (w), 2932 (vw), 2859 (vw), 1462 (vw), 1379 (vw), 1327 (vw), 1238 (m), 1065 (vs), 821 (m), 449 (s) cm^{-1}.

Catalysis. All operations regarding the catalytic MPV reduction were performed under rigorous exclusion of air and moisture using Schlenk (Table 4, entries 6 and 7) and glovebox techniques (MBraun MB150B-G-II). All solvents and liquid chemicals were carefully predried and degassed using appropriate methods[85] and stored over molecular sieves (3 Å) in a glovebox. To the iPrOH used as a solvent and hydride source was added ca. 5 mg/mL of n-dodecane as an internal standard for GC measurements. Solid chemicals that were packed under an Ar atmosphere were stored in a glovebox and used as received; others were degassed in vacuo and transferred into a glovebox under an Ar atmosphere. For a typical catalytic experiment, the catalyst was dissolved or, in the case of heterogeneous catalysts, suspended in 5 mL of iPrOH, while the substrate, 4-tBu-cyclohexanone, was dissolved in 4 mL of iPrOH. The substrate solution was then added with stirring to the catalyst solution or suspension, and the vessel was washed once with 1 mL of iPrOH which was also added. GC samples of ca. 0.1 mL each were taken with a syringe at set time intervals (usually 15 min, 1 h, 2 h, 3 h, and, where required, 24 h), and in the case of heterogeneous catalysts, the solids were removed by centrifugation and decanting of the solution. The GC samples were immediately measured. Where temperatures other than ambient temperature were employed, the reactions were performed outside the glovebox under Schlenk technique conditions in 25 mL

https://dx.doi.org/10.1021/acs.organomet.9b00794
Organometallics 2020, 39, 1046−1058

Schlenk flasks and heated with an oil bath; samples for GC were taken via a septum with syringes.

■ ASSOCIATED CONTENT

Supporting Information

The Supporting Information is available free of charge at https://pubs.acs.org/doi/10.1021/acs.organomet.9b00794.

Experimental details of grafting reactions, SEM images, PXRD diagrams, N_2-physisorption isotherms, size distribution histograms, NMR spectra, details of the diffusion measurements, and crystallographic data (PDF)

Accession Codes

CCDC 1964539 contains the supplementary crystallographic data for this paper. These data can be obtained free of charge via www.ccdc.cam.ac.uk/data_request/cif, or by emailing data_request@ccdc.cam.ac.uk, or by contacting The Cambridge Crystallographic Data Centre, 12 Union Road, Cambridge CB2 1EZ, UK; fax: +44 1223 336033.

■ AUTHOR INFORMATION

Corresponding Author

Reiner Anwander − *Institut für Anorganische Chemie, Universität Tübingen, 72076 Tübingen, Germany;* orcid.org/0000-0002-1543-3787; Email: reiner.anwander@uni-tuebingen.de

Authors

Lorenz Bock − *Institut für Anorganische Chemie, Universität Tübingen, 72076 Tübingen, Germany*

Xuan Tran − *Institut für Anorganische Chemie, Universität Tübingen, 72076 Tübingen, Germany*

Yucang Liang − *Institut für Anorganische Chemie, Universität Tübingen, 72076 Tübingen, Germany*

Markus Kramer − *Institut für Organische Chemie, Universität Tübingen, 72076 Tübingen, Germany*

Cäcilia Maichle-Mössmer − *Institut für Anorganische Chemie, Universität Tübingen, 72076 Tübingen, Germany;* orcid.org/0000-0001-7638-1610

Complete contact information is available at: https://pubs.acs.org/10.1021/acs.organomet.9b00794

Notes

The authors declare no competing financial interest.

■ ACKNOWLEDGMENTS

We thank Elke Nadler for the acquisition of all SEM images.

■ REFERENCES

(1) Samantaray, M. K.; Pump, E.; Bendjeriou-Sedjerari, A.; D'Elia, V.; Pelletier, J. D. A.; Guidotti, M.; Psaro, R.; Basset, J. M. Surface organometallic chemistry in heterogeneous catalysis. *Chem. Soc. Rev.* **2018**, *47*, 8403−8437.

(2) Copéret, C.; Héroguel, F., Recent Advances in Surface Organometallic Chemistry. In *Applied Homogeneous Catalysis with Organometallic Compounds: A Comprehensive Handbook in Four Vols.*, 3rd ed.; Cornils, B., Herrmann, W. A., Beller, M., Paciello, R., Eds.; Wiley-VCH: Weinheim, 2017; pp 1069−1084.

(3) Basset, J. M.; Choplin, A. Surface organometallic chemistry: A new approach to heterogeneous Catalysis? *J. Mol. Catal.* **1983**, *21*, 95−108.

(4) Anwander, R. SOMC@PMS. Surface Organometallic Chemistry at Periodic Mesoporous Silica. *Chem. Mater.* **2001**, *13*, 4419−4438.

(5) Kim, T.-W.; Chung, P.-W.; Lin, V. S. Y. Facile Synthesis of Monodisperse Spherical MCM-48 Mesoporous Silica Nanoparticles with Controlled Particle Size. *Chem. Mater.* **2010**, *22*, 5093−5104.

(6) *Modern Surface Organometallic Chemistry*; Basset, J.-M., Psaro, R., Roberto, D., Ugo, R., Eds.; Wiley-VCH: Weinheim, 2009.

(7) Meerwein, H.; Schmidt, R. Ein neues Verfahren zur Reduktion von Aldehyden und Ketonen. *Liebigs Ann. Chem.* **1925**, *444*, 221−238.

(8) Verley, A. Sur l'échange des groupements fonctionelles entre deux molécules. Passage de la fonction alcool à la fonction aldéhyde et inversement. *Bull. Soc. Chim. Fr.* **1925**, *37*, 537−542.

(9) Ponndorf, W. Der reversible Austausch der Oxydationsstufen zwischen Aldehyden oder Ketonen einerseits und primären oder sekundären Alkoholen anderseits. *Angew. Chem.* **1926**, *39*, 138−143.

(10) Bradley, D. C.; Mehrotra, R. C.; Rothwell, I. P.; Singh, A. *Alkoxo and Aryloxo Derivatives of Metals*; Academic Press: London, San Diego, 2001.

(11) Cohen, R.; Graves, C. R.; Nguyen, S. T.; Martin, J. M.; Ratner, M. A. The mechanism of aluminum-catalyzed Meerwein-Schmidt-Ponndorf-Verley reduction of carbonyls to alcohols. *J. Am. Chem. Soc.* **2004**, *126*, 14796−803.

(12) Wilds, A. L. Reduction with Aluminum Alkoxides. *Org. React.* **2011**, *2*, 178−223.

(13) Anwander, R.; Gerstberger, G.; Palm, C.; Groeger, O.; Engelhardt, G. Enhanced catalytic activity of MCM-41-grafted aluminium isopropoxide in MPV reductions. *Chem. Commun.* **1998**, 1811−1812.

(14) de Graauw, C. F.; Peters, J. A.; van Bekkum, H.; Huskens, J. Meerwein-Ponndorf-Verley Reductions and Oppenauer Oxidations: An Integrated Approach. *Synthesis* **1994**, *1994*, 1007−1017.

(15) Cha, J. S. Recent Developments In Meerwein-Ponndorf-Verley and Related Reactions for the Reduction of Organic Functional Groups Using Aluminum, Boron, and Other Metal Reagents: A Review. *Org. Process Res. Dev.* **2006**, *10*, 1032−1053.

(16) Huskens, J.; de Graauw, C. F.; Peters, J. A.; van Bekkum, H. Chiral induction in lanthanide(III)-alkoxide-catalysed Meerwein-Ponndorf-Verley reductions. *Recl. Trav. Chim. Pays-Bas* **1994**, *113*, 488−491.

(17) Ruiz, J. R.; Jiménez-Sanchidrián, C. Heterogeneous Catalysis in the Meerwein-Ponndorf-Verley Reduction of Carbonyl Compounds. *Curr. Org. Chem.* **2007**, *11*, 1113−1125.

(18) Uysal, B.; Oksal, B. S. Catalytic activity of SBA-15-grafted indium tri-isopropoxide in chemoselective MPV reductions. *J. Porous Mater.* **2015**, *22*, 1053−1064.

(19) Uysal, B.; Oksal, B. S.; Karatas, E. New $In(O^iPr)_3$-MCM-41 heterogeneous catalyst in MPV reductions of unsaturated carbonyl compounds: effect of mesoporous silica SBA-15 and MCM-41 as supporting surfaces on catalytic activity of $In(O^iPr)_3$. *J. Inclusion Phenom. Macrocyclic Chem.* **2017**, *87*, 85−94.

(20) Namy, J. L.; Souppe, J.; Collin, J.; Kagan, H. B. New preparations of lanthanide alkoxides and their catalytical activity in Meerwein-Ponndorf-Verley-Oppenauer reactions. *J. Org. Chem.* **1984**, *49*, 2045−2049.

(21) Okano, T.; Matsuoka, M.; Konishi, H.; Kiji, J. Meerwein-Ponndorf-Verley Reduction of Ketones and Aldehydes Catalyzed by Lanthanide Tri-2-propoxides. *Chem. Lett.* **1987**, *16*, 181−184.

(22) Evans, D. A.; Nelson, S. G.; Gagne, M. R.; Muci, A. R. A chiral samarium-based catalyst for the asymmetric Meerwein-Ponndorf-Verley reduction. *J. Am. Chem. Soc.* **1993**, *115*, 9800−9801.

(23) Nakano, Y.; Sakaguchi, S.; Ishii, Y. Meerwein−Ponndorf−Verley-type reductive acetylation of carbonyl compounds to acetates by lanthanide complexes in the presence of isopropenyl acetate. *Tetrahedron Lett.* **2000**, *41*, 1565−1569.

(24) Fukuzawa, S.; Nakano, N.; Saitoh, T. Reduction of Carbonyl Compounds by Lanthanide Metal/2-Propanol: In-situ Generation of Samarium Isopropyloxide for Stereoselective Meerwein-Ponndorf-Verley Reduction. *Eur. J. Org. Chem.* **2004**, *2004*, 2863−2867.

(25) Anwander, R.; Palm, C. Meerwein-Ponndorf-Verley reductions mediated by lanthanide-alkoxide-functionalized mesoporous silicates. *Stud. Surf. Sci. Catal.* **1998**, *117*, 413−420.
(26) Leyrit, P.; McGill, C.; Quignard, F.; Choplin, A. A novel heterogeneous molecular catalyst for the Meerwein−Ponndorf−Verley and Oppenauer reactions. *J. Mol. Catal. A: Chem.* **1996**, *112*, 395−400.
(27) Quignard, F.; Graziani, O.; Choplin, A. Group 4 alkyl complexes as precursors of silica anchored molecular catalysts for the reduction of ketones by hydrogen transfer. *Appl. Catal., A* **1999**, *182*, 29−40.
(28) Zhu, Y.; Jaenicke, S.; Chuah, G. K. Supported zirconium propoxide − a versatile heterogeneous catalyst for the Meerwein−Ponndorf−Verley reduction. *J. Catal.* **2003**, *218*, 396−404.
(29) Bradley, D. C.; Chatterjee, A. K.; Wardlaw, W. Primary alkoxides of quadrivalent cerium and thorium. *J. Chem. Soc.* **1956**, 2260−2264.
(30) Toledano, P.; Ribot, F.; Sanchez, C. Structure du bis(2-propanol)-bis-μ-(2-propanolato)-hexakis(2-propanolato)dicérium-(IV). *Acta Crystallogr., Sect. C: Cryst. Struct. Commun.* **1990**, *46*, 1419−1422.
(31) Huggins, B. A.; Ellis, P. D.; Gradeff, P. S.; Vaartstra, B. A.; Yunlu, K.; Huffman, J. C.; Caulton, K. G. Nature of the phase change in solid bis(isopropyl alcohol)octakis(isopropoxo)dicerium, as determined by variable-temperature X-ray diffraction and deuterium NMR spectroscopy. *Inorg. Chem.* **1991**, *30*, 1720−1722.
(32) Bradley, D. C.; Chatterjee, A. K.; Wardlaw, W. 671. Structural chemistry of the alkoxides. Part VII. Secondary alkoxides of quadrivalent cerium and thorium. *J. Chem. Soc.* **1956**, 3469−3472.
(33) Yunlu, K.; Gradeff, P. S.; Edelstein, N.; Kot, W.; Shalimoff, G.; Streib, W. E.; Vaartstra, B. A.; Caulton, K. G. Photoreduction of cerium(IV) in $Ce_2(O^iPr)_8(^iPrOH)_2$. Characterization and structure of $Ce_4O(O^iPr)_{13}(^iPrOH)$. *Inorg. Chem.* **1991**, *30*, 2317−2321.
(34) Sirio, C.; Hubert-Pfalzgraf, L. G.; Bois, C. Facile thermal desolvation of $Ce_2(OPr^i)_8(Pr^iOH)_2$: Characterization and molecular structure of $Ce_4(\mu_4\text{-}O)(\mu_3\text{-}OPr^i)(\mu\text{-}OPr^i)_4(OPr^i)_8$. *Polyhedron* **1997**, *16*, 1129−1136.
(35) Vaartstra, B. A.; Huffman, J. C.; Gradeff, P. S.; Hubert-Pfalzgraf, L. G.; Daran, J.-C.; Parraud, S.; Yunlu, K.; Caulton, K. G. Alcohol adducts of alkoxides: intramolecular hydrogen bonding as a general structural feature. *Inorg. Chem.* **1990**, *29*, 3126−3131.
(36) Crozier, A. R.; Bienfait, A. M.; Maichle-Mössmer, C.; Törnroos, K. W.; Anwander, R. A homoleptic tetravalent cerium silylamide. *Chem. Commun.* **2013**, *49*, 87−89.
(37) Arnold, P. L.; Casely, I. J.; Zlatogorsky, S.; Wilson, C. Organometallic Cerium Complexes from Tetravalent Coordination Complexes. *Helv. Chim. Acta* **2009**, *92*, 2291−2303.
(38) Friedrich, J.; Schneider, D.; Bock, L.; Maichle-Mössmer, C.; Anwander, R. Cerium(IV) Neopentoxide Complexes. *Inorg. Chem.* **2017**, *56*, 8114−8127.
(39) Evans, W. J.; Deming, T. J.; Olofson, J. M.; Ziller, J. W. Synthetic and structural studies of a series of soluble cerium(IV) alkoxide and alkoxide nitrate complexes. *Inorg. Chem.* **1989**, *28*, 4027−4034.
(40) Aspinall, H. C.; Bacsa, J.; Jones, A. C.; Wrench, J. S.; Black, K.; Chalker, P. R.; King, P. J.; Marshall, P.; Werner, M.; Davies, H. O.; Odedra, R. Ce(IV) complexes with donor-functionalized alkoxide ligands: improved precursors for chemical vapor deposition of CeO_2. *Inorg. Chem.* **2011**, *50*, 11644−11652.
(41) Schläfer, J.; Tyrra, W.; Mathur, S. Octakis(*tert*-butoxo)-dicerium(IV) $[Ce_2(O^tBu)_8]$: synthesis, characterization, decomposition, and reactivity. *Inorg. Chem.* **2014**, *53*, 2751−2753.
(42) Gun'ko, Y. K.; Elliott, S. D.; Hitchcock, P. B.; Lappert, M. F. First mixed valence cerium−organic trinuclear cluster $[Ce_3(OBu^t)_{10}NO_3]$ as a possible molecular switch: synthesis, structure and density functional calculations. *J. Chem. Soc., Dalton Trans.* **2002**, 1852−1856.
(43) Einstein, A. Über die von der molekularkinetischen Theorie der Wärme geforderte Bewegung von in ruhenden Flüssigkeiten suspendierten Teilchen. *Ann. Phys.* **1905**, *322*, 549−560.
(44) Kritikos, M.; Moustiakimov, M.; Wijk, M.; Westin, G. Synthesis, structure and characterisation of $Ln_3O(OPr^i)_{13}$ with Ln = Nd, Gd or Er. *J. Chem. Soc., Dalton Trans.* **2001**, 1931−1938.
(45) Blagg, R. J.; Tuna, F.; McInnes, E. J.; Winpenny, R. E. Pentametallic lanthanide-alkoxide square-based pyramids: high energy barrier for thermal relaxation in a holmium single molecule magnet. *Chem. Commun.* **2011**, *47*, 10587−9.
(46) Suslova, E. V.; Troyanov, S. I.; Turova, N. Y. Lanthanum alkoxides. Crystal structure of $[La_6(\mu_6\text{-}Cl)(\mu_3\text{-}OPr^i)_2(\mu\text{-}OPr^i)_9(OPr^i)_6]$. *Russ. J. Inorg. Chem.* **2015**, *60*, 1384−1389.
(47) Westin, G.; Moustiakimov, M.; Kritikos, M. Synthesis, characterization, and properties of three europium 2-propoxides: $[Eu_4(OPr^i)_{10}(HOPr^i)_3]$*2HOPr^i, $Eu_5O(OPr^i)_{13}$, and $EuAl_3(OPr^i)_{12}$. *Inorg. Chem.* **2002**, *41*, 3249−58.
(48) Zabula, A. V.; Qiao, Y.; Kosanovich, A. J.; Cheisson, T.; Manor, B. C.; Carroll, P. J.; Ozerov, O. V.; Schelter, E. J. Structure, Electronics and Reactivity of Ce(PNP) Complexes. *Chem. - Eur. J.* **2017**, *23*, 17923−17934.
(49) Palumbo, C. T.; Halter, D. P.; Voora, V. K.; Chen, G. P.; Chan, A. K.; Fieser, M. E.; Ziller, J. W.; Hieringer, W.; Furche, F.; Meyer, K.; Evans, W. J. Metal versus Ligand Reduction in Ln(3+) Complexes of a Mesitylene-Anchored Tris(Aryloxide) Ligand. *Inorg. Chem.* **2018**, *57*, 2823−2833.
(50) Werner, D.; Bayer, U.; Rad, N. E.; Junk, P. C.; Deacon, G. B.; Anwander, R. Unique and contrasting structures of homoleptic lanthanum(iii) and cerium(iii) 3,5-dimethylpyrazolates. *Dalton Trans.* **2018**, *47*, 5952−5955.
(51) Huh, S.; Wiench, J. W.; Yoo, J.-C.; Pruski, M.; Lin, V. S.-Y. Organic Functionalization and Morphology Control of Mesoporous Silicas via a Co-Condensation Synthesis Method. *Chem. Mater.* **2003**, *15*, 4247−4256.
(52) Lai, C. Y.; Trewyn, B. G.; Jeftinija, D. M.; Jeftinija, K.; Xu, S.; Jeftinija, S.; Lin, V. S. A mesoporous silica nanosphere-based carrier system with chemically removable CdS nanoparticle caps for stimuli-responsive controlled release of neurotransmitters and drug molecules. *J. Am. Chem. Soc.* **2003**, *125*, 4451−4459.
(53) Liang, Y.; Anwander, R. Nanostructured catalysts via metal amide-promoted smart grafting. *Dalton Trans.* **2013**, *42*, 12521−12545.
(54) Rosenholm, J. M.; Sahlgren, C.; Lindén, M. Towards multifunctional, targeted drug delivery systems using mesoporous silica nanoparticles–opportunities & challenges. *Nanoscale* **2010**, *2*, 1870−1883.
(55) Büchel, G.; Unger, K. K.; Matsumoto, A.; Tsutsumi, K. A Novel Pathway for Synthesis of Submicrometer-Size Solid Core/Mesoporous Shell Silica Spheres. *Adv. Mater.* **1998**, *10*, 1036−1038.
(56) Anwander, R.; Nagl, I.; Widenmeyer, M.; Engelhardt, G.; Groeger, O.; Palm, C.; Röser, T. Surface Characterization and Functionalization of MCM-41 Silicas via Silazane Silylation. *J. Phys. Chem. B* **2000**, *104*, 3532−3544.
(57) Deschner, T.; Liang, Y.; Anwander, R. Silylation Efficiency of Chlorsilanes, Alkoxysilanes, and Monosilazanes on Periodic Mesoporous Silica. *J. Phys. Chem. C* **2010**, *114*, 22603−22609.
(58) Brunauer, S.; Emmett, P. H.; Teller, E. Adsorption of Gases in Multimolecular Layers. *J. Am. Chem. Soc.* **1938**, *60*, 309−319.
(59) Barrett, E. P.; Joyner, L. G.; Halenda, P. P. The Determination of Pore Volume and Area Distributions in Porous Substances. I. Computations from Nitrogen Isotherms. *J. Am. Chem. Soc.* **1951**, *73*, 373−380.
(60) Liang, Y.; Erichsen, E. S.; Anwander, R. Functionalization of large-pore periodic mesoporous silicas: metal silylamide and isopropoxide molecular grafting and secondary surface ligand exchange. *Dalton Trans.* **2013**, *42*, 6922−6935.
(61) Sonström, A.; Schneider, D.; Maichle-Mössmer, C.; Anwander, R. Titanium(IV) Catecholate-Grafted Mesoporous Silica KIT-6:

https://dx.doi.org/10.1021/acs.organomet.9b00794
Organometallics 2020, 39, 1046−1058

Probing Sequential and Convergent Immobilization Approaches. *Eur. J. Inorg. Chem.* **2019**, 682−692.
(62) Crozier, A. R.; Schädle, C.; Maichle-Mössmer, C.; Törnroos, K. W.; Anwander, R. Synthesis and grafting of CAN-derived tetravalent cerium alkoxide silylamide precursors onto mesoporous silica MCM-41. *Dalton Trans.* **2013**, *42*, 5491−9.
(63) Storck, S.; Bretinger, H.; Maier, W. F. Characterization of micro- and mesoporous solids by physisorption methods and pore-size analysis. *Appl. Catal., A* **1998**, *174*, 137−146.
(64) Hara, K.; Akahane, S.; Wiench, J. W.; Burgin, B. R.; Ishito, N.; Lin, V.-S. Y.; Fukuoka, A.; Pruski, M. Selective and Efficient Silylation of Mesoporous Silica: A Quantitative Assessment of Synthetic Strategies by Solid-State NMR. *J. Phys. Chem. C* **2012**, *116*, 7083−7090.
(65) König, S. *Manganese, Chromium, and Cobalt Surface-Functionalized Cubic Mesoporous Silica KIT-6 and MCM-48*; Diploma Thesis, Eberhard-Karls Universität, Tübingen, 2009.
(66) Laue, T.; Plagens, A. *Named Organic Reactions*, 2nd ed.; Wiley: Chichester, 2005.
(67) Kobayashi, S.; Nagayama, S.; Busujima, T. Lewis Acid Catalysts Stable in Water. Correlation between Catalytic Activity in Water and Hydrolysis Constants and Exchange Rate Constants for Substitution of Inner-Sphere Water Ligands. *J. Am. Chem. Soc.* **1998**, *120*, 8287−8288.
(68) Boyle, T. J.; Tribby, L. J.; Bunge, S. D. Synthesis and Structural Characterization of a Series of Carboxylic Acid Modified Cerium(III) Alkoxides. *Eur. J. Inorg. Chem.* **2006**, 4553−4563.
(69) Paul, M.; Shirase, S.; Morimoto, Y.; Mathey, L.; Murugesapandian, B.; Tanaka, S.; Itoh, S.; Tsurugi, H.; Mashima, K. Cerium-Complex-Catalyzed Oxidation of Arylmethanols under Atmospheric Pressure of Dioxygen and Its Mechanism through a Side-On μ-Peroxo Dicerium(IV) Complex. *Chem. - Eur. J.* **2016**, *22*, 4008−4014.
(70) Shirase, S.; Shinohara, K.; Tsurugi, H.; Mashima, K. Oxidation of Alcohols to Carbonyl Compounds Catalyzed by Oxo-Bridged Dinuclear Cerium Complexes with Pentadentate Schiff-Base Ligands under a Dioxygen Atmosphere. *ACS Catal.* **2018**, *8*, 6939−6947.
(71) Fulmer, G. R.; Miller, A. J. M.; Sherden, N. H.; Gottlieb, H. E.; Nudelman, A.; Stoltz, B. M.; Bercaw, J. E.; Goldberg, K. I. NMR Chemical Shifts of Trace Impurities: Common Laboratory Solvents, Organics, and Gases in Deuterated Solvents Relevant to the Organometallic Chemist. *Organometallics* **2010**, *29*, 2176−2179.
(72) *COSMO v. 1.61*; Bruker AXS Inc.: Madison, WI, 2012.
(73) *APEX 2 v. 2012.10_0*; Bruker AXS Inc.: Madison, WI, 2012.
(74) *SAINT v. 8.34A*; Bruker AXS Inc.: Madison, WI, 2013.
(75) *SAINT v. 8.37A*; Bruker AXS Inc.: Madison, WI, 2015.
(76) Krause, L.; Herbst-Irmer, R.; Sheldrick, G. M.; Stalke, D. Comparison of silver and molybdenum microfocus X-ray sources for single-crystal structure determination. *J. Appl. Crystallogr.* **2015**, *48*, 3−10.
(77) Sheldrick, G. M. Crystal structure refinement with SHELXL. *Acta Crystallogr., Sect. C: Struct. Chem.* **2015**, *71*, 3−8.
(78) Hübschle, C. B.; Sheldrick, G. M.; Dittrich, B. ShelXle: a Qt graphical user interface for SHELXL. *J. Appl. Crystallogr.* **2011**, *44*, 1281−1284.
(79) Kratzert, D.; Holstein, J. J.; Krossing, I. DSR: enhanced modelling and refinement of disordered structures with SHELXL. *J. Appl. Crystallogr.* **2015**, *48*, 933−938.
(80) *Mercury CSD 3.10.2*; The Cambridge Crystallographic Data Centre: Cambridge, U.K., 2001.
(81) *Persistence of Vision Raytracer (Version 3.7)*; Persistence of Vision Pty. Ltd.: Williamstown, Victoria, Australia, 2004.
(82) Radu, D. R.; Lai, C. Y.; Jeftinija, K.; Rowe, E. W.; Jeftinija, S.; Lin, V. S. A polyamidoamine dendrimer-capped mesoporous silica nanosphere-based gene transfection reagent. *J. Am. Chem. Soc.* **2004**, *126*, 13216−7.
(83) Bradley, D. C.; Ghotra, J. S.; Hart, F. A. Low co-ordination numbers in lanthanide and actinide compounds. Part I. The preparation and characterization of tris{bis(trimethylsilyl)-amido}-lanthanides. *J. Chem. Soc., Dalton Trans.* **1973**, 1021.
(84) Bayer, U.; Bock, L.; Maichle-Mössmer, C.; Anwander, R. A Facile Route toward Ceric Silylamide $[Ce\{N(SiHMe_2)_2\}_4]$. *Eur. J. Inorg. Chem.* **2020**, 101−106.
(85) Armarego, W. L. F.; Chai, C. L. L. *Purification of Laboratory Chemicals*; Elsevier Science: Burlington, MA, 2003.

https://dx.doi.org/10.1021/acs.organomet.9b00794
Organometallics 2020, 39, 1046−1058

Supporting Information

SOMC @ Periodic Mesoporous Silica Nanoparticles: Meerwein-Ponndorf-Verley Reduction Promoted by Immobilized Rare-Earth-Metal Alkoxides

Lorenz Bock,[†] Xuan Tran,[†] Yucang Liang,[†] Markus Kramer[‡], Cäcilia Maichle-Mössmer,[†] and Reiner Anwander[†]*

[†]Institut für Anorganische Chemie, Universität Tübingen, Auf der Morgenstelle 18, 72076 Tübingen, Germany

[‡]Institut für Organische Chemie, Universität Tübingen, Auf der Morgenstelle 18, 72076 Tübingen, Germany

Table of Contents

Experimental details of hybrid material synthesis	S3
SEM images of parent and hybrid materials	S4-S7
Powder X-ray diffractograms of parent and hybrid materials	S8-S9
N_2-physisorption isotherms of parent and hybrid materials	S10-S13
DRIFT spectra	S13
^{13}C CP/MAS spectrum of *i*PrOH@MCM-41$_{500}$-a	S14
^{1}H NMR spectrum of [Ce(O*i*Pr)$_4$]$_3$	S15
^{1}H VT NMR spectra of [Ce(O*i*Pr)$_4$]$_3$	S16
^{1}H-PGSE measurement of [Ce(O*i*Pr)$_4$]$_3$	S17-S18
Crystallographic data for [Ce(O*i*Pr)$_4$]$_3$	S19
References	S19

Experimental Details of Hybrid Materials H2-H4a

Ce[N(SiHMe$_2$)$_2$]$_4$@MSN-MCM-41$_{500}$-c (H2). To a suspension of MCM-41$_{500}$-MSN (**MSN-MCM-41$_{500}$-c**, 494.6 mg, ca. 0.55 mmol SiOH) in *n*-hexane (5 ml), a solution of Ce[N(SiHMe$_2$)$_2$]$_4$ (234.7 mg, 0.35 mmol) in *n*-hexane (5 ml) was added under stirring. After stirring overnight, the supernatant was removed by centrifugation and the solid material washed three times with *n*-hexane, until the supernatant was clear and showed no more traces of Ce[N(SiHMe$_2$)$_2$]$_4$ in the ^{1}H NMR spectrum. Residual *n*-hexane was removed *in vacuo* to yield **H2** as a rust colored powder. DRIFTS: $\tilde{\nu}$ = 2957 (w), 2903 (vw), 2852 (vw), 2143 (vw, b), 1419 (vw), 1237 (m), 1062 (vs), 901 (m), 838 (m), 798 (m), 678 (w), 589 (w), 462 (m), 458 (m), 451 (m) cm^{-1}.

HO*i*Pr@Ce[N(SiHMe$_2$)$_2$]$_4$@MSN-MCM-41$_{500}$-c (H2a). H2a was reclaimed from a catalytic reaction of 4-*t*Bu-cyclohexanone with **H2** in *i*PrOH (10.0 ml) by centrifugation, subsequently washed three times with *n*-hexane and dried *in vacuo*. DRIFTS: $\tilde{\nu}$ = 2973 (w), 2145 (vw), 1467 (vw), 1374 (vw), 1235 (m), 1079 (vs), 904 (w), 805 (w), 474 (m), 445 (m), 410 (m) cm^{-1}.

Ce[N(SiMe$_3$)$_2$]$_3$@MSN-MCM-41$_{500}$-a (H3). To a suspension of MCM-41$_{500}$-MSN (**MSN-MCM-41$_{500}$-a**, 552.2 mg, ca. 0.61 mmol SiOH) in *n*-hexane (5 ml), a solution of Ce[N(SiMe$_3$)$_2$]$_3$ (913.3 mg, 1.47 mmol) in *n*-hexane (5 ml) was added under stirring. After stirring overnight, the supernatant was removed by centrifugation and the solid material washed three times with *n*-hexane, until the supernatant was clear and showed no more traces of Ce[N(SiMe$_3$)$_2$]$_3$ in the ^{1}H NMR spectrum. Residual *n*-hexane was removed *in vacuo* to yield **H3** as a slightly yellow powder. DRIFTS: $\tilde{\nu}$ = 2954 (w), 2899 (vw), 1239 (m), 1063 (vs), 841 (m), 654 (w), 606 (w), 458 (m), 443 (s) cm^{-1}.

HO*i*Pr@Ce[N(SiMe$_3$)$_2$]$_3$@MSN-MCM-41$_{500}$-a (H3a). H3a was reclaimed from a catalytic reaction of 4-*t*Bu-cyclohexanone with **H3** in *i*PrOH (10.0 ml) by centrifugation, subsequently washed three times with *n*-hexane and dried *in vacuo*. DRIFTS: $\tilde{\nu}$ = 2974 (w), 1467 (vw), 1375 (vw), 1234 (m), 1073 (vs), 812 (w), 461 (s), 442 (s), 434 (m) cm^{-1}.

La[N(SiMe$_3$)$_2$]$_3$@MSN-MCM-41$_{500}$-b (H4). To a suspension of MCM-41$_{500}$-MSN (**MSN-MCM-41$_{500}$-b**, 499.2 mg, ca. 0.52 mmol SiOH) in *n*-hexane (5 ml), a solution of La[N(SiMe$_3$)$_2$]$_3$ (378.0 mg, 0.61 mmol) in *n*-hexane (5 ml) was added under stirring. After stirring overnight, the supernatant was removed by centrifugation and the solid material washed three times with *n*-hexane, until the supernatant was clear and showed no more traces of La[N(SiMe$_3$)$_2$]$_3$ in the ^{1}H NMR spectrum. Residual *n*-hexane was removed *in vacuo* to yield **H4** as an off-white powder. DRIFTS: $\tilde{\nu}$ = 2952 (w), 2898 (vw), 2853 (vw), 1240 (m), 1051 (vs), 834 (m), 660 (w), 592 (w), 460 (m), 450 (m), 431 (m) cm^{-1}.

HO*i*Pr@La[N(SiMe$_3$)$_2$]$_3$@MSN-MCM-41$_{500}$-b (H4a). H4a was reclaimed from a catalytic reaction of 4-*t*Bu-cyclohexanone with **H4** in PrOH (10.0 ml) by centrifugation, subsequently washed three times with *n*-hexane and dried *in vacuo*. DRIFTS: $\tilde{\nu}$ = 2974 (w), 1467 (vw), 1387 (vw), 1234 (m), 1070 (vs), 814 (w), 461 (m), 446 (m), 438 (m) cm^{-1}.

SEM Images of Parent and Hybrid Materials

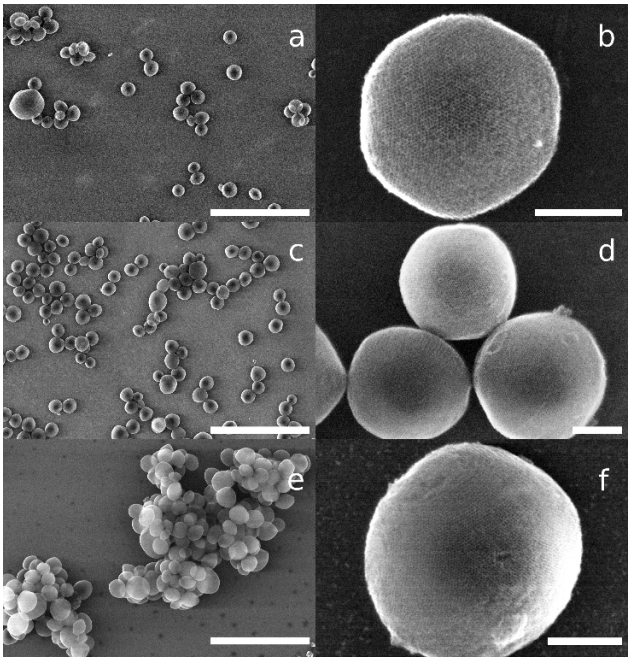

Figure S1. SEM micrographs of all MCM-41_{500} nanoparticulate parent materials. **a** and **b** show the parent material for **H1**, **H3** and **H3a** (MSN-MCM-41_{500}-a), **c** and **d** for **H4** and **H4a** (MSN-MCM-41_{500}-b) and **e** and **f** for **H2** and **H2a** (MSN-MCM-41_{500}-c). The scale bars in **a**, **c** and **e** correspond to a length of 2 µm, those in **b**, **d** and **f** of 100 nm.

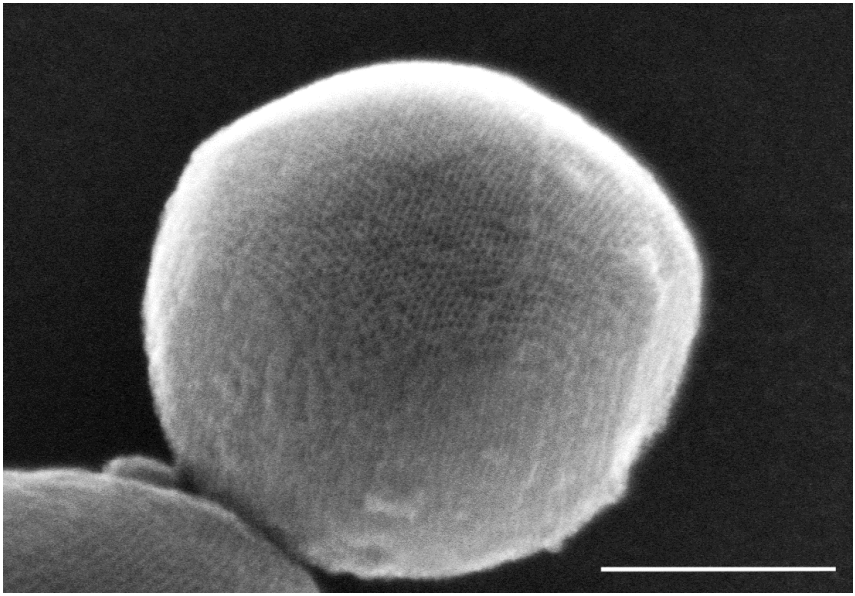

Figure S2. SEM image of one tilted particle of MSN-MCM-41_{500}-b. The transition from the pore entrances (top half of the particle) to the sides of the channel-like pores is clearly visible. The scale bar corresponds to 100 nm.

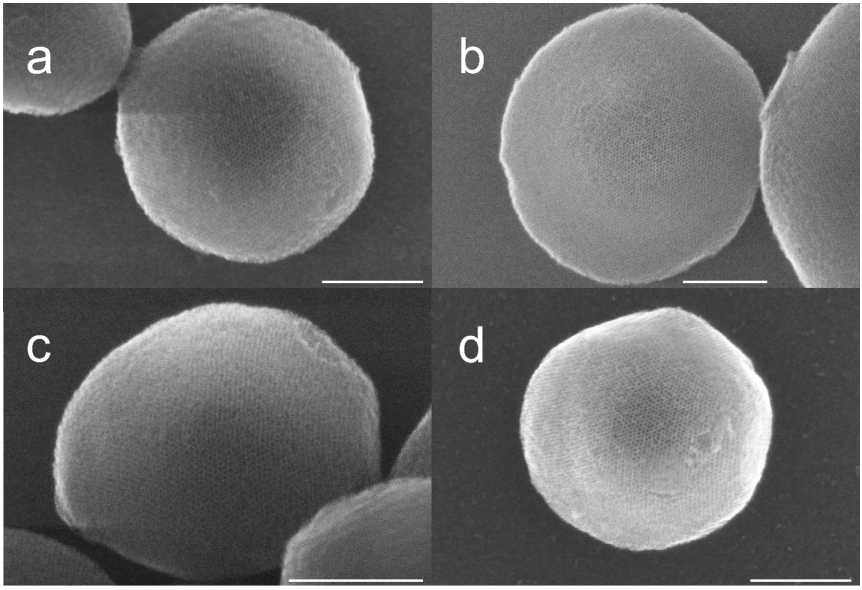

Figure S3. SEM images of hybrid materials $[Ce(O\textit{i}Pr)_4]_3$@MSN-MCM-41_{500}-a (**H1**, a), $Ce[N(SiHMe_2)_2]_4$@MSN-MCM-41_{500}-c (**H2**, b), $Ce[N(SiMe_3)_2]_3$@MSN-MCM-41_{500}-a (**H3**, c) and $La[N(SiMe_3)_2]_3$@MSN-MCM-41_{500}-b (**H4**, d). The scale bars correspond to 100 nm.

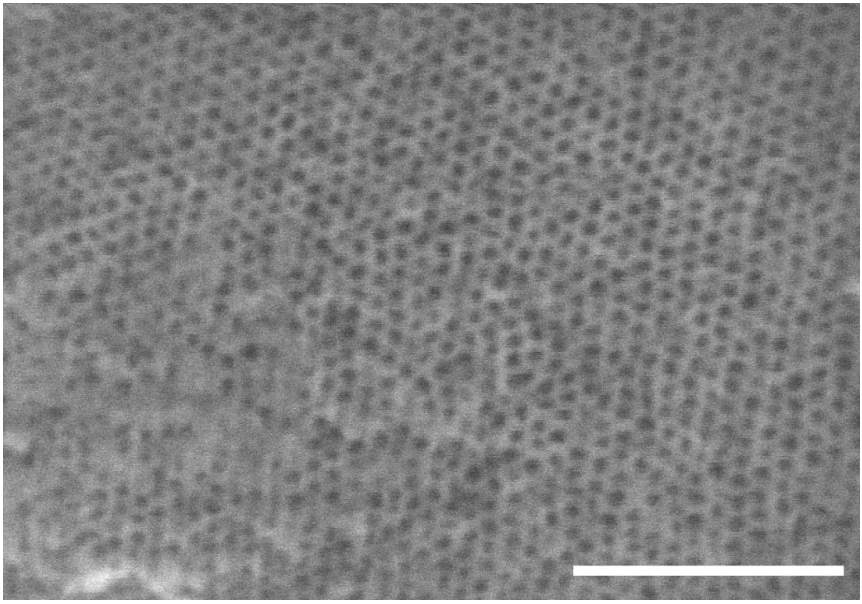

Figure S4. Close up SEM image of a particle of hybrid material La[N(SiMe$_3$)$_2$]$_3$@MSN-MCM-41$_{500}$-b (**H4**). The scale bar corresponds to 50 nm.

Powder X-Ray Diffractograms

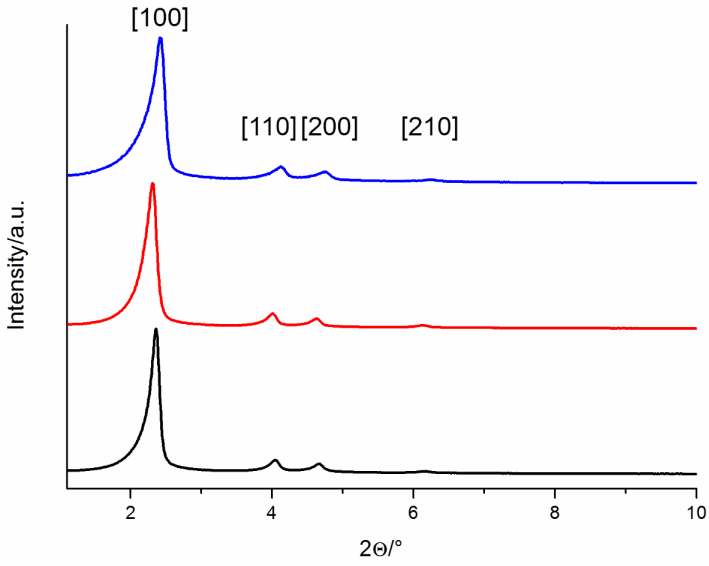

Figure S5. Powder X-ray diffractograms of the three parent materials MSN-MCM-41_{500}-a (black trace, bottom), MSN-MCM-41_{500}-b (red trace, middle) and MSN-MCM-41_{500}-c (blue trace, top). The periodic mesoporous structure is confirmed by the visibility of the [100], [110], [200] and [210] reflections.

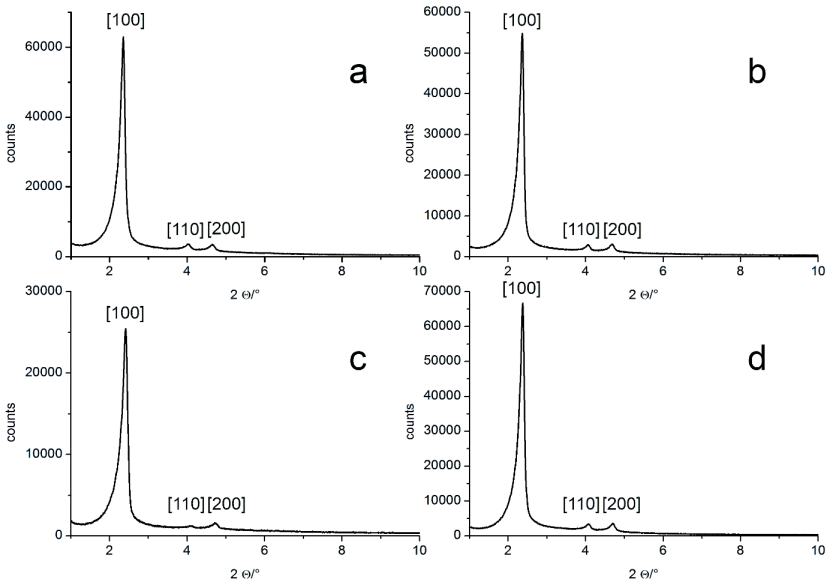

Figure S6. Powder X-ray diffractograms of the hybrid materials $[Ce(O\mathit{i}Pr)_4]_3$@MSN-MCM-41_{500}-a (**H1**, a), $Ce[N(SiHMe_2)_2]_4$@MSN-MCM-41_{500}-c (**H2**, b), $Ce[N(SiMe_3)_2]_3$@MSN-MCM-41_{500}-a (**H3**, c) and $La[N(SiMe_3)_2]_3$@MSN-MCM-41_{500}-b (**H4**, d). It can be seen that the periodic mesoporous MCM-41 type structure is kept largely intact during grafting.

N_2 Physisorption

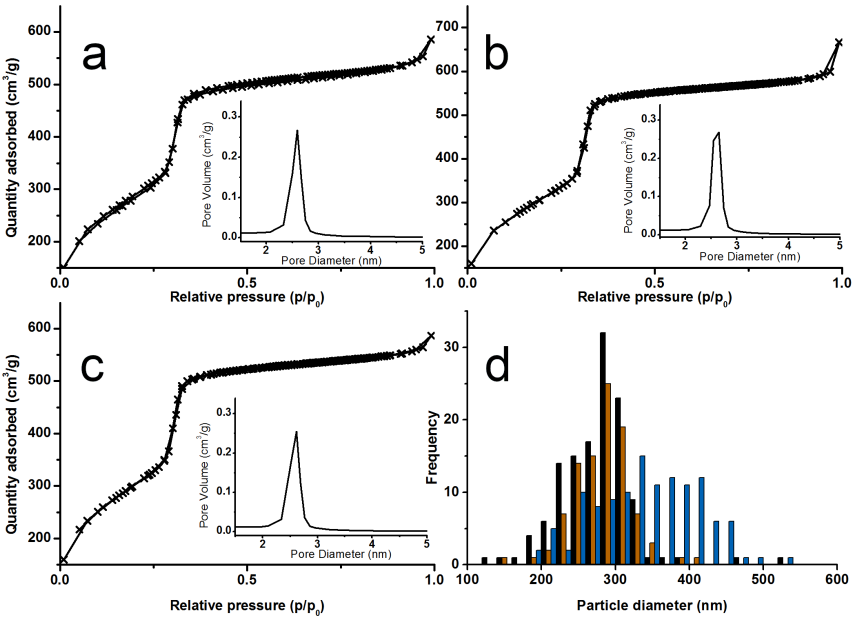

Figure S7. N_2-physisorption isotherms and pore size distributions of parent materials MSN-MCM-41_{500}-a (a), MSN-MCM-41_{500}-b (b) and MSN-MCM-41_{500}-c (c), as well as particle size distribution for all three materials (d; MSN-MCM-41_{500}-a: black, MSN-MCM-41_{500}-b: brown, MSN-MCM-41_{500}-c: blue).

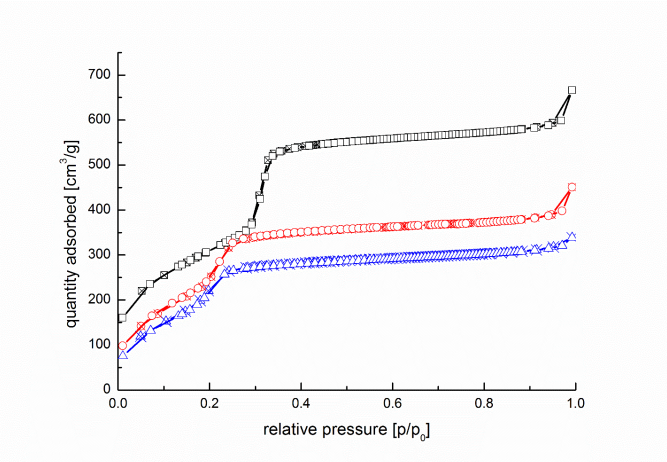

Figure S8. N_2-physisorption isotherms of parent material MSN-MCM-41$_{500}$-b (top, black squares) and hybrid materials La[N(SiMe$_3$)$_2$]$_3$@MSN-MCM-41$_{500}$-b (**H4**, middle, red circles) and HO*i*Pr@La[N(SiMe$_3$)$_2$]$_3$@MSN-MCM-41$_{500}$-b (**H4a**, bottom, blue triangles).

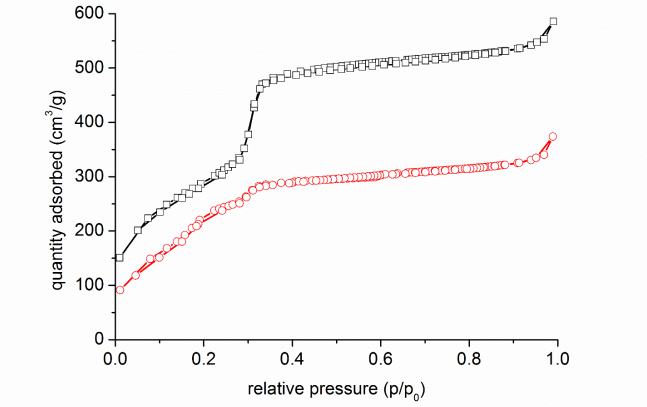

Figure S9. N_2-physisorption isotherms of parent material MSN-MCM-41$_{500}$-a (top, black squares) and hybrid material [Ce(O*i*Pr)$_4$]$_3$@MSN-MCM-41$_{500}$-a (**H1**, bottom, red circles).

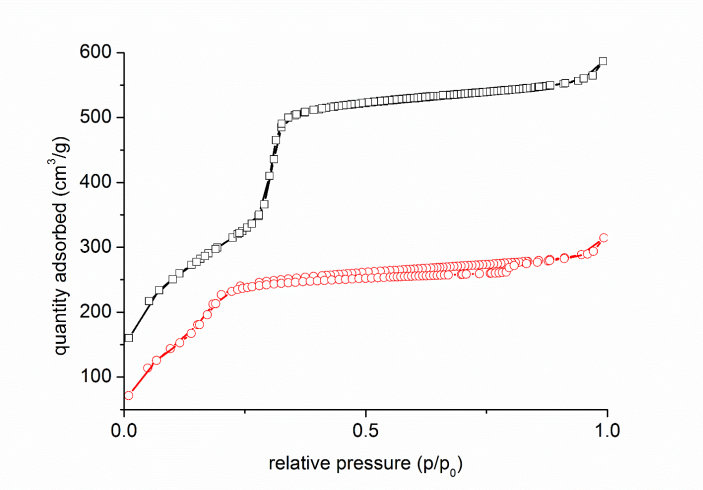

Figure S10. N_2-physisorption isotherms of parent material MSN-MCM-41_{500}-c (top, black squares) and hybrid material $Ce[N(SiHMe_2)_2]_4$@MSN-MCM-41_{500}-c (**H2**, bottom, red circles).

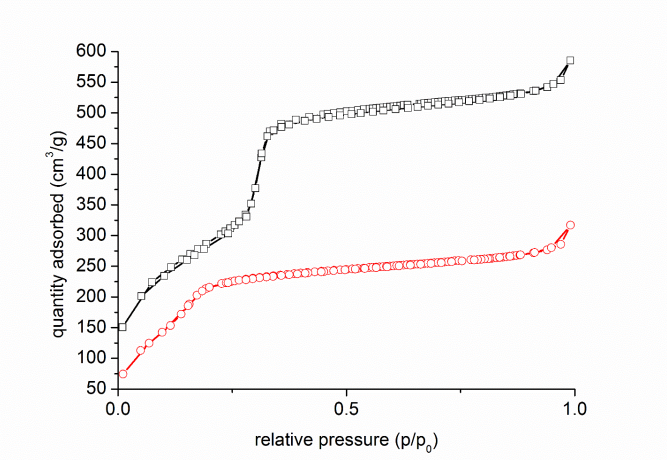

Figure S11. N_2-physisorption isotherms of parent material MSN-MCM-41_{500}-a (top, black squares) and hybrid material $Ce[N(SiMe_3)_2]_3$@MSN-MCM-41_{500}-a (**H3**, bottom, red circles).

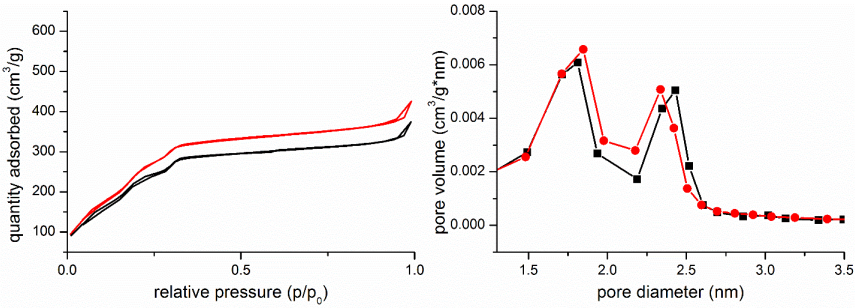

Figure S12. N_2-physisorption isotherms (left) and pore size distributions (right) of hybrid material **H1** before (black) and after (red) treatment with *i*PrOH at ambient temperature.

DRIFT Spectroscopy

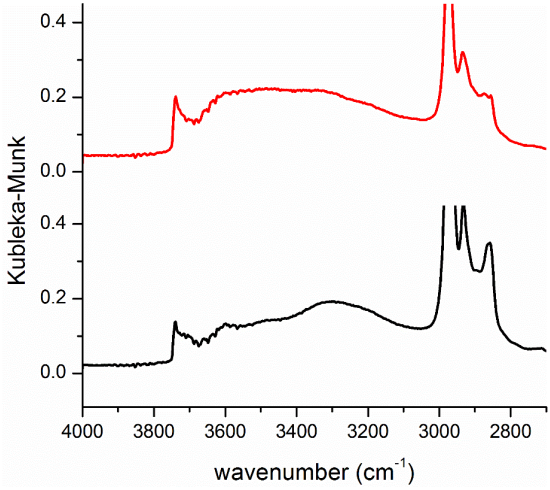

Figure S13. DRIFT spectra of hybrid material **H1** before (black, bottom) and after (red, top) treatment with *i*PrOH. The similarity of the band at 3740 cm^{-1}, corresponding to free Si-OH groups on the surface of the material, does not indicates any significant surface alkylation with *i*PrOH at ambient temperature.

NMR Spectroscopy

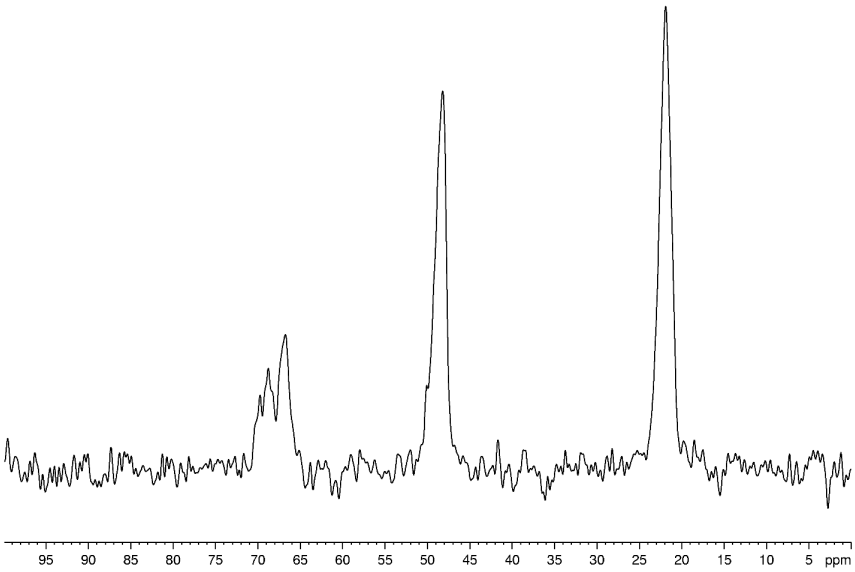

Figure S14. ^{13}C CP/MAS spectrum (75.48 MHz, MAS at 8 kHz) of *i*PrOH@MCM-41_{500}-a (performed at ambient temperature). The resonances at 22 ppm and 68 ppm correspond to the CH_3 and CH groups of *i*PrOH, respectively, the resonance at 48 ppm to surface grafted methoxy groups (see also Figure 7).

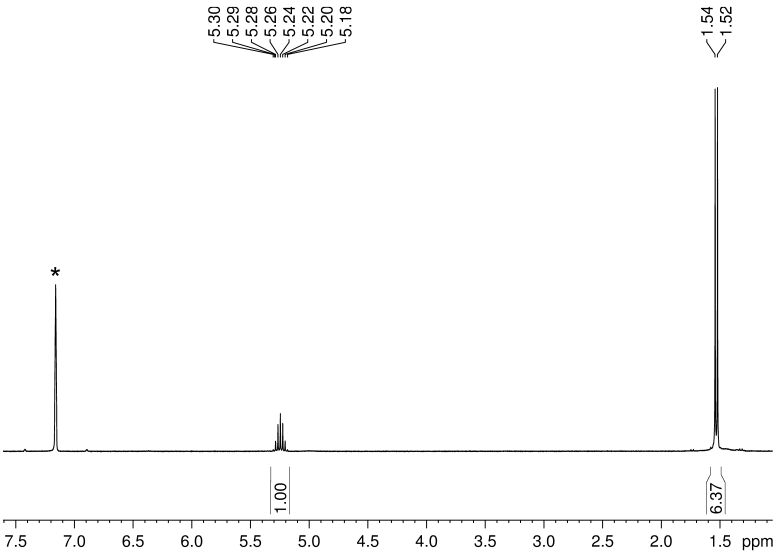

Figure S15. ^{1}H NMR spectrum of [Ce(O*i*Pr)$_4$]$_3$ (**1**) (C_6D_6, 300.13 MHz, 299 K). An asterisk marks the solvent residual signal.

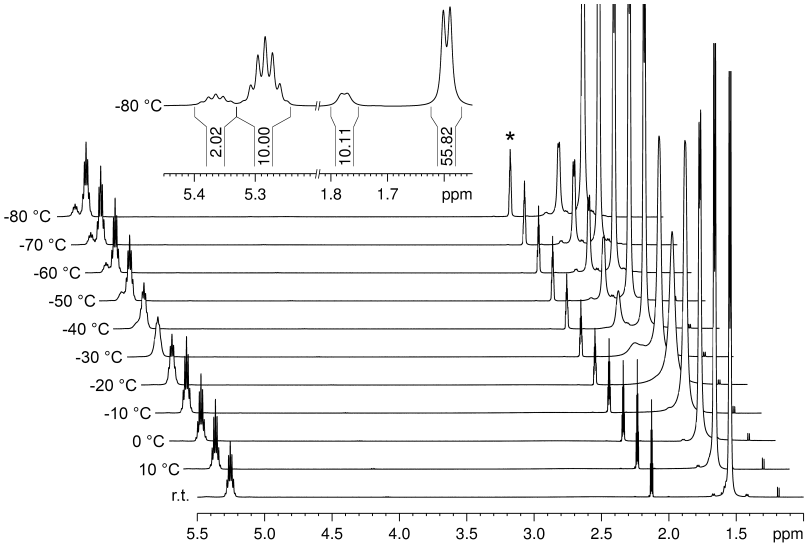

Figure S16. Variable temperature ^{1}H NMR of [Ce(O*i*Pr)$_4$]$_3$ (**1**) between room temperature and -80 °C (toluene-d8, 500.13 MHz). The inset shows the integrals of the decoalesced signals of the isopropyl groups at -80 °C with a ratio of 10:2, corresponding to the μ_2-bridging and terminal isopropoxy ligands (7+3=10) and the μ_3-bridging ones (2). An asterisk marks the residual signal of the methyl group from toluene-d8.

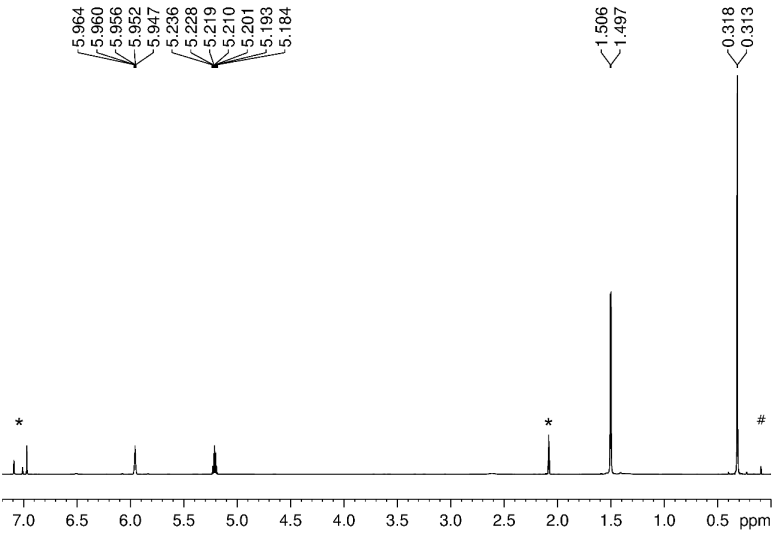

Figure S17. ^{1}H NMR spectrum (toluene-d8, 700.29 MHz, 299 K) of $[Ce(O\textit{i}Pr)_4]_3$ (**1**) and $Ce[N(SiHMe_2)_2]_4$ as internal standard. The peaks at 5.21 and 1.50 ppm correspond to the former (see Figure S5), those at 5.96 and 0.32 ppm to the latter.[1] Asterisks denote solvent residual signals, a number sign an impurity.

Table S1. Calculated and Measured Molecular Radii for All Possible Species in the ^{1}H-Detected Pulsed Field Gradient Spin Echo (PGSE) Experiments

Compound	r_{calc}/Å	$r_{measured}$/Å
$[Ce(O\textit{i}Pr)_4]_3$	6.35	6.35
$Ce(O\textit{i}Pr)_4$	4.85	n/a
$Ce[N(SiHMe_2)_2]_4$	5.5	5.5[1]

In order to determine whether **1** was present as a monomer or a trimer in solution at ambient temperature, a ^{1}H detected PGSE experiment was undertaken to determine the diffusion coefficient *D*. As *D* alone does not easily allow inference of the hydrodynamic radius or the molecular weight of the investigated species, the experiment was carried out with an internal standard, the structure and monomeric nature of which was known. Thus, employing the Stokes-Einstein-equation the ratio of hydrodynamic radii is inversely proportional to the ratio of the *D*-values.

From structural data and, in the case of the monomer $Ce(O\textit{i}Pr)_4$, energy-optimized structural simulation data, the molecular radii of all involved structures were measured and the ratios could be compared to the ratios of *D*-values obtained from the diffusion measurements.

Table S2. *D*-Constants Derived from ^{1}H-Detected PGSE Experiments

Signal (ppm)	Proton	*D*-constant/m^2·s^{-1}
5.96	Si*H*Me$_2$	9.8·10^{-10}
5.21	OC*H*Me$_2$	8.7·10^{-10}
1.50	OCH*Me$_2$*	8.7·10^{-10}
0.32	SiH*Me$_2$*	9.8·10^{-10}

Table S1 gives the values for the molecular radii calculated from energy optimized structural simulations and, where available, from X-ray structural data. The good agreement between the two in the cases where both are available lends significant credibility to the value for the monomeric Ce(O*i*Pr)$_4$, where structural data is not available. Table S2 gives the *D*-constants derived from five ^{1}H-detected PGSE experiments of the same sample at different times.

Based on the Stokes-Einstein relation

$$D = \frac{k_B \cdot T}{6\pi \cdot \eta \cdot r_H}$$

the diffusion coefficients of two different species in the same sample (with T and η identical) are inversely proportional:

$$\frac{D_{ref}}{D_{mono-/trimer}} = \frac{r_H(mono-/trimer)}{r_H(ref)}$$

With the diffusion coefficients from table S3, this gives a ratio of

$$\frac{D_{ref}}{D_{mono-/trimer}} = \frac{9.8}{8.7} = 1.13$$

Assuming a monomeric structure Ce(O*i*Pr)$_4$, the ratio of molecular radii would give

$$\frac{r_{mol}(monomer)}{r_{mol}(ref)} = \frac{4.85}{5.5} = 0.88$$

while a trimeric structure [Ce(O*i*Pr)$_4$]$_3$ would give

$$\frac{r_{mol}(trimer)}{r_{mol}(ref)} = \frac{6.35}{5.5} = 1.15$$

thus clearly indicating [Ce(O*i*Pr)$_4$]$_3$ as the structure of homoleptic Ce(IV) isopropanolate in aprotic, non donating solvents.

[1] A. R. Crozier, A. M. Bienfait, C. Maichle-Mössmer, K. W. Törnroos and R. Anwander, *Chem. Commun.* **2013**, *49*, 87-89.

Crystallography

Table S3. Crystallographic Data for $[Ce(O^iPr)_4]_3$ (1)

CCDC	1964539
Formula	$C_{144}H_{336}Ce_{12}O_{48}$
M ($g \cdot mol^{-1}$)	4517.55
Crystal System	triclinic
Space Group	P -1
a (Å)	19.0877(8)
b (Å)	24.2255(9)
c(Å)	25.7603(10)
α (°)	64.3140(10)
β (°)	69.9190(10)
γ (°)	73.8380(10)
V ($Å^3$)	9963.4(7)
Z	2
T (K)	99(2)
ρ_{calcd} ($g \cdot cm^{-3}$)	1.506
μ (mm^{-1})	2.743
F (000)	4560.0
Θ range (°)	2.249 – 28.485
total reflns	379402
unique reflns	47527
Rint	0.0818
observed reflns (I>2σ)	35319
Data/restraints/parameters	47527/2406/2222
R1/wR2 (I>2σ)	0.0629/0.0986
R1/wR2 (all data)	0.0395/0.0852
GOF	1.010
largest diff. peak and hole ($e \cdot Å^{-3}$)	2.322 and -1.405

$R1 = \Sigma(||F_o|-|F_c||)/\Sigma|F_o|, F_o > 4\sigma(F_o)$. $wR2 = \{\Sigma[w(F_o^2-F_c^2)^2/\Sigma[w(F_o^2)^2]\}^{1/2}$

References

[1] A. R. Crozier, A. M. Bienfait, C. Maichle-Mössmer, K. W. Törnroos and R. Anwander, *Chem. Commun.* **2013**, *49*, 87-89.